

Technical Report

Title: *Laboratory Geomechanical Strength
Testing of DGR-1 & DGR-2 Core*

Document ID: TR-07-03


Authors: B. Gorski, T. Anderson and T. Conlon
CANMET Mining and Mineral Sciences
Laboratories, Natural Resources Canada

Revision: 3

Date: February 3, 2009

DGR Site Characterization Document
Intera Engineering Project 06-219



Intera Engineering DGR Site Characterization Document		
Title:	Laboratory Geomechanical Strength Testing of DGR-1 & DGR-2 Core	
Document ID:	TR-07-03	
Revision Number:	3	Date: February 3, 2009
Author(s):	B. Gorski, T. Anderson and B. Conlon CANMET Mining and Mineral Sciences Laboratories Natural Resources Canada	
Technical Review:	Dougal McCreath, Kenneth Raven, Tom Lam (OPG)	
QA Review:	John Avis	
Approved by:	 Kenneth Raven	

Document Revision History		
Revision	Effective Date	Description of Changes
0	October 3, 2007	Initial Release
1	November 9, 2007	Additions to Table A-8, Appendix D and Table F-4 reflecting supplementary direct shear testing of 3 Cobourg Fm samples Addition of Section 7 on Data Quality and Use
2	April 15, 2008	Conversion from Technical Memorandum to Technical Report
3	February 3, 2009	Formation depths and Tables F-1 to F-4 adjusted to conform with results of November 2008 core workshop

TABLE OF CONTENTS

1 INTRODUCTION 1

2 STANDARD OPERATING PROCEDURES 1

3 SPECIMENS 1

4 TEST APPARATUS AND PROCEDURES 2

 4.1 Zero Pressure Velocity Tests 2

 4.2 Uniaxial Compression Strength Tests 2

 4.3 Acoustic Emission (AE) Tests 2

 4.4 Brazilian Tensile Strength Tests 3

 4.5 Direct Shear Strength Tests 3

5 ANALYSIS OF DATA 4

 5.1 Zero Pressure Velocity Tests 4

 5.2 Uniaxial Compression Strength Tests 4

 5.3 Acoustic Emission (AE) Tests 7

 5.4 Brazilian Tensile Strength Tests 7

 5.5 Direct Shear Strength Tests 7

6 RESULTS AND CONCLUSIONS 8

7 DATA QUALITY AND USE 9

8 DISCLAIMER 9

9 REFERENCES 9

LIST OF APPENDICES

APPENDIX A Data and Calculation Tables

Tables:

A-1. Dimensions and densities of DGR-1 uniaxial specimens 12

A-2. Dimensions and densities of DGR-2 uniaxial specimens 13

A-3. Dynamic elastic constants of DGR-1 specimens 14

A-4. Dynamic elastic constants of DGR-2 specimens 15

A-5. Static elastic constants of DGR-1 specimens 16

A-6. Static elastic constants of DGR-2 specimens 17

A-7. Brazilian test data for DGR-2 specimens 18

A-8. Shear test data for DGR-2 specimens 19

APPENDIX B Stress-Strain Curves of Uniaxial Tests

Figures:

B-1. Specimen DGR-1, 27.30 m.....22
B-2. Specimen DGR-1, 29.38 m.....22
B-3. Specimen DGR-1, 70.84 m.....23
B-4. Specimen DGR-1, 108.62 m.....24
B-5. Specimen DGR-1, 160.93 m.....25
B-6. Specimen DGR-1, 171.14 m.....26
B-7. Specimen DGR-1, 183.60 m.....27
B-8. Specimen DGR-1, 206.55 m.....28
B-9. Specimen DGR-1, 266.20 m.....29
B-10. Specimen DGR-1, 286.69 m.....30
B-11. Specimen DGR-1, 314.88 m.....31
B-12. Specimen DGR-1, 367.06 m.....32
B-13. Specimen DGR-1, 386.55 m.....33
B-14. Specimen DGR-1, 415.16 m.....34
B-15. Specimen DGR-1, 438.10 m.....35
B-16. Specimen DGR-1, 455.22 m.....36
B-17. Specimen DGR-1, 460.41 m.....37
B-18. Specimen DGR-2, 457.21 m.....38
B-19. Specimen DGR-2, 474.71 m.....39
B-20. Specimen DGR-2, 491.32 m.....40
B-21. Specimen DGR-2, 502.78 m.....41
B-22. Specimen DGR-2, 519.61 m.....42
B-23. Specimen DGR-2, 533.94 m.....43
B-24. Specimen DGR-2, 580.99 m.....44
B-25. Specimen DGR-2, 586.35 m.....45
B-26. Specimen DGR-2, 587.51 m.....46
B-27. Specimen DGR-2, 606.50 m.....47
B-28. Specimen DGR-2, 646.42 m.....48
B-29. Specimen DGR-2, 654.97 m.....49
B-30. Specimen DGR-2, 655.32 m.....50
B-31. Specimen DGR-2, 660.68 m.....51
B-32. Specimen DGR-2, 661.61 m.....52
B-33. Specimen DGR-2, 666.79 m.....53
B-34. Specimen DGR-2, 668.46 m.....54
B-35. Specimen DGR-2, 673.26 m.....55
B-36. Specimen DGR-2, 674.11 m.....56
B-37. Specimen DGR-2, 676.45 m.....57
B-38. Specimen DGR-2, 679.83 m.....58
B-39. Specimen DGR-2, 683.02 m.....59
B-40. Specimen DGR-2, 688.22 m.....60
B-41. Specimen DGR-2, 694.11 m.....61
B-42. Specimen DGR-2, 695.15 m.....62
B-43. Specimen DGR-2, 702.69 m.....63
B-44. Specimen DGR-2, 704.47 m.....64
B-45. Specimen DGR-2, 710.29 m.....65
B-46. Specimen DGR-2, 719.38 m.....66
B-47. Specimen DGR-2, 737.16 m.....67

APPENDIX C Failed Uniaxial Specimens and AE Source Locations

Figures:

C-1. Specimen DGR-1, 27.30 m.....69
C-2. Specimen DGR-1, 29.38 m.....70
C-3. Specimen DGR-1, 70.84 m.....71

C-4. Specimen DGR-1, 108.62 m.....	72
C-5. Specimen DGR-1, 160.93 m.....	73
C-6. Specimen DGR-1, 171.14 m.....	74
C-7. Specimen DGR-1, 183.60 m.....	75
C-8. Specimen DGR-1, 206.55 m.....	76
C-9. Specimen DGR-1, 266.20 m.....	77
C-10. Specimen DGR-1, 286.69 m.....	78
C-11. Specimen DGR-1, 314.88 m.....	79
C-12. Specimen DGR-1, 367.06 m.....	80
C-13. Specimen DGR-1, 386.55 m.....	81
C-14. Specimen DGR-1, 415.16 m.....	82
C-15. Specimen DGR-1, 438.10 m.....	83
C-16. Specimen DGR-1, 455.22 m.....	84
C-17. Specimen DGR-1, 460.41 m.....	85
C-18. Specimen DGR-2, 457.21 m.....	86
C-19. Specimen DGR-2, 474.71 m.....	87
C-20. Specimen DGR-2, 491.32 m.....	88
C-21. Specimen DGR-2, 502.78 m.....	89
C-22. Specimen DGR-2, 519.61 m.....	90
C-23. Specimen DGR-2, 533.94 m.....	91
C-24. Specimen DGR-2, 580.99 m.....	92
C-25. Specimen DGR-2, 586.35 m.....	93
C-26. Specimen DGR-2, 587.51 m.....	94
C-27. Specimen DGR-2, 606.50 m.....	95
C-28. Specimen DGR-2, 646.42 m.....	96
C-29. Specimen DGR-2, 654.97 m.....	97
C-30. Specimen DGR-2, 655.32 m.....	98
C-31. Specimen DGR-2, 660.68 m.....	99
C-32. Specimen DGR-2, 661.61 m.....	100
C-33. Specimen DGR-2, 666.79 m.....	101
C-34. Specimen DGR-2, 668.46 m.....	102
C-35. Specimen DGR-2, 673.26 m.....	103
C-36. Specimen DGR-2, 674.11 m.....	104
C-37. Specimen DGR-2, 676.45 m.....	105
C-38. Specimen DGR-2, 679.83 m.....	106
C-39. Specimen DGR-2, 683.02 m.....	107
C-40. Specimen DGR-2, 688.22 m.....	108
C-41. Specimen DGR-2, 694.11 m.....	109
C-42. Specimen DGR-2, 695.15 m.....	110
C-43. Specimen DGR-2, 702.69 m.....	111
C-44. Specimen DGR-2, 704.47 m.....	112
C-45. Specimen DGR-2, 710.29 m.....	113
C-46. Specimen DGR-2, 719.38 m.....	114
C-47. Specimen DGR-2, 737.16 m.....	115

APPENDIX D Plots of Shear Stress vs. Displacement and Shear Stress vs. Normal Stress

Figures:

D-1. Specimen DGR-2, 613.37 m.....	117
D-2. Specimen DGR-2, 616.59 m.....	118
D-3. Specimen DGR-2, 646.72 m.....	119
D-4. Specimen DGR-2, 692.00 m.....	120
D-5. Specimen DGR-2, 697.86 m.....	121
D-6. Specimen DGR-2, 702.23 m.....	122
D-7. Specimen DGR-2, 705.86 m.....	123
D-8. Specimen DGR-2, 708.57 m.....	124
D-9. Specimen DGR-2, 664.94 m.....	125

D-10. Specimen DGR-2, 673.06 m.....	126
D-11. Specimen DGR-2, 684.00 m.....	127

APPENDIX E Failed Brazilian Specimens

Figure:

E-1. Tested Brazilian Specimens	129
---------------------------------------	-----

APPENDIX F Geological Descriptions and Geological Formation of Intera DGR Specimens

Tables:

F-1. Geological formations and descriptions of DGR-1 uniaxial specimens	131
F-2. Geological formations and descriptions of DGR-2 uniaxial specimens	132
F-3. Geological formations and descriptions of DGR-2 Brazilian specimens.....	133
F-4. Geological formations and descriptions of DGR-2 shear specimens	133

1 Introduction

Ontario Power Generation (OPG) is proposing to construct a Low and Intermediate Level Radioactive Waste Deep Geologic Repository (DGR). The proposal calls for the DGR to be located at a depth of about 660 m within the sedimentary bedrock beneath the Bruce site near Kincardine, Ontario. OPG has retained Intera Engineering Ltd., Ottawa, Ontario to develop and implement a DGR Site Characterisation Plan (SCP). Phase 1 of the SCP represents the initial geoscientific investigation undertaken to confirm the suitability of the Bruce site. The Bruce site overburden is underlain by near flat lying Palaeozoic age dolostone, shale and limestone sedimentary rock to an estimated depth of about 860 m where Precambrian granite basement is encountered.

Natural Resources Canada (NRCan) through the CANMET Mining and Mineral Sciences Laboratories (CANMET-MMSL) was contracted by Intera to provide laboratory geomechanical services. The objective of this contracted work was to conduct mechanical tests on shale, limestone and dolostone rock core originating from boreholes DGR-1 and DGR-2. Uniaxial compression tests comprised the bulk of the testing program. Supplemental Brazilian and shear tests were included during the program. This report describes the test apparatus and procedures and presents the results of the testing program.

Work described in this Technical Report (TR) was completed in accordance with Intera Test Plan TP-07-04 – Geomechanical Lab Testing of DGR-1 & DGR-2 Core (Intera Engineering Ltd., 2007a), prepared following the general requirements of the DGR Project Quality Plan (Intera Engineering Ltd., 2007b).

2 Standard Operating Procedures

The test program was carried out at the CANMET-MMSL's Rock Mechanics test facility located in Bells Corners. The Rock Mechanics test facility is managed by the Ground Control Program. The test facility is an ISO 17025 (International Standards Organization) accredited testing laboratory. Standard Operating Procedures (SOPs) that form part of the facility's accredited test procedures were selected for this project. The Standard Operating Procedures used for this test program were:

SOP-T 2100	Specimen Preparation, Standardization and Dimensional Tolerance Verification,
SOP-T 2101	Installing Bonded Resistance Strain Gauges,
SOP-T 2103	Compressional P-Wave Velocity Test,
SOP-T 2104	Brazilian Tensile Strength Test,
SOP-T 2112	Uniaxial Compressive Strength Test with Servo Computer Control Press,
SOP-T 2113	Uniaxial Elastic Moduli and Poisson's Ratio Test with Servo Computer Control Press, and
SOP-T 2121(draft)	Direct Shear Test with Constant Normal Load.

3 Specimens

The 75 mm diameter specimens originated from boreholes DGR-1 and DGR-2. The total number of specimens received and tested comprised: 47 uniaxial compressive strength tests; 20 Brazilian strength tests; and 11 shear strength tests.

The procedure for the preparation of a cylindrical specimen conforms to the ASTM D4543 standard (ASTM D4543, 2007) and CANMET-MMSL SOP-T 2100. The wet specimens were jacketed with heat-shrink tubing prior to sample preparation, to minimize the loss or gain of water. The end surfaces of specimens were ground flat to within 0.025 mm, parallel to each other to within 0.025 mm, and perpendicular to the longitudinal axis of the specimen to within 0.25 degrees as determined using a gauge plate and dial gauge.

Specimen lengths were determined to the nearest 0.025 mm by averaging the length measured at four points 90 degrees to each other. Specimen diameters were measured to the nearest 0.025 mm by averaging three measurements taken at the upper, middle and lower sections of the specimens. The average diameter was used for calculating the cross-sectional area. The volumes of the specimens were calculated from the average length and diameter measurements. The weights of the specimens were determined to the nearest 0.01 g and the densities of the specimens were computed to the nearest 0.001 Mg/m³. The borehole, depth, dimensions and bulk density of each tested specimen, are listed in Tables A-1, A-2, A-7 and A-8.

Strain gauges were applied on the uniaxial test specimens for the measurement of deformations. The gauge lengths were at least ten times the largest grain in the specimens. Two diametrically opposed axial strain gauges were bonded at mid height of the specimens and were connected in series to form a single active gauge. Similarly, two diametrically opposed circumferential strain gauges were mounted at 90 degrees to the axial gauges.

Wet specimens required that gauges be installed with three applications of adhesives and coating. A segment of the heat-shrink tubing was first removed from the gauge area. The area was then dried and the adhesive was applied to fill surface irregularities and seal pores. The gauging area was then abraded to remove extra glue on the rock surface, and the strain gauge was installed. After lead attachment, a thick coat was applied on and completely covered the gauge and solder joints for moisture protection. During the curing of the adhesives and coating, the specimens were covered by wet paper and stored in an environmental chamber to minimize the loss of moisture from the specimen. The procedure to apply strain gauges to a specimen conformed to SOP-T 2101 and ASTM E1237 standard (ASTM E1237, 2003).

4 Test Apparatus and Procedures

4.1 Zero Pressure Velocity Tests

Zero pressure P-wave and S-wave velocities were measured for all the uniaxial specimens prior to testing. The testing apparatus comprised a pulse generator, power amplifier, pulsing and sensing heads (transmitter and receiver) and oscilloscope. The P-wave and S-wave velocities were measured in accordance with SOP-T2103, and ASTM standard D 2845, (ASTM D2845, 2005).

4.2 Uniaxial Compression Strength Tests

Uniaxial compressive strength tests were conducted in a computer controlled, servo-hydraulic compression machine, consisting of a 2.22 MN rated load cell, load frame, hydraulic power supply, digital controller and test software. Three linear variable differential transformers (LVDTs) were arrayed around the specimen at 120 degree intervals for the measurement of axial deformations. A circumferential extensometer was used to measure specimen circumferential deformation.

The uniaxial test specimens were loaded in stress control to imminent failure at a rate of 0.75 MPa/s (ASTM D7012, 2007). Uniaxial data were scanned every second and stored digitally in engineering units. Time, load, axial strain and diametric strain were recorded during uniaxial tests. After testing, the specimens were photographed.

4.3 Acoustic Emission (AE) Tests

Acoustic emission tests were incorporated into the uniaxial compression tests. The AE system consisted of 12 transducer channels, 16 bit, 10 MHz, 40 dB preamplification, 60 dB gain, high and low pass filters and source location software.

Two outer arrays of 3 piezoelectric transducers each were attached to the surface of the specimens. Arrays for DGR-1 specimens were located 2 centimetres in from the ends of the specimen. Arrays for DGR-2 specimens were located in 1/3rd the length of the specimens. The transducers were spaced 120 degrees from each other for each array. The bottom array 1 consisted of transducers 1, 2 and 3 and the upper array 2 consisted of transducers 4, 5 and 6. The transducers were numbered clockwise looking down the specimen. Specimen references to top, bottom and down refer to the specimen orientation as retrieved from the borehole. Transducer 1 was orientated over the black line scribed on the specimen by Intera personnel. Transducer 4 on array 2 was rotated 60 degrees clockwise away from transducer 1 on array 1.

Acoustic emissions were recorded before, during and after each uniaxial compressive strength test. Time, counts, magnitudes and other data were recorded for each event. The reader is referred to the research paper by Durrheim and Labrie (2004) where the acoustic system is explained in detail.

4.4 Brazilian Tensile Strength Tests

Test specimens were circular disks with a thickness-to-diameter ratio of 0.5 to 0.75. The tests were performed using a servo-hydraulic rock mechanics test system. The specimens were loaded in stress control to imminent failure. The specimens were photographed after testing. The test procedure conformed to SOP-T2104 and the ASTM Standard D3967 (ASTM D3967, 2005).

4.5 Direct Shear Strength Tests

The procedure for the direct shear test conformed to the Standard Operating Test Procedure SOP-T 2121(draft), and ASTM Standard D5607 (ASTM D5607, 2006). The direct shear test machine comprised a shear box, base plate, steel table with two columns and an adjustable crossbar above the table, hydraulic control system, hydraulic ram, spherical seat, electric motor, two load cells, three linear variable differential transformers (LVDTs) and a personal computer. The shear box consisted of two halves of a split box made of cast steel. The lower box was free to move on a roller system along four steel rails that are bolted to the base plate. The lower box was pushed forward and pulled backward by means of a screw jack, equipped with a load cell and driven by a variable speed electric motor. The upper box was stationary in the lateral direction, but was allowed to move in the vertical direction. The reader is referred to the research paper by Lau (2002) where the shear test apparatus is explained in detail.

The specimen was encapsulated in the upper box first. The specimen was then locked in a vise when positioned in the box to ensure that the interface lay in a horizontal position and was 3 to 5 mm above the mold surface. Hydrostone was used as the encapsulating material. The upper box with the specimen set in the hydrostone was then weighed. The upper box was then placed on top of the lower box and the specimen was encapsulated in the lower box. The normal load cell and spherical seat were placed between the upper shear box and the hydraulic ram under the adjustable crossbar. One LVDT was mounted in a horizontal position at the end of the lower shear box and two LVDTs were mounted in a vertical position on top of the upper box for the measurement of shear and normal displacements.

The direct shear test was controlled by computer software. A predetermined normal load was first applied on the sample by means of the hydraulic ram and the hydraulic control system. The weight of the normal load system (load cell, spherical seat and the upper box with specimen set in hydrostone) was used in determining the normal load. The shear test was performed by sliding the lower box under the stationary upper box at a shear displacement rate of approximately 0.38 mm/min to a maximum stroke of 10 mm. The normal and shear loads were measured with load cells, and the normal and shear displacements were measured with LVDTs. During testing, analog signals from the load cells and LVDTs were scanned every two seconds. The signals were converted to engineering units and stored in the computer. The computer also provided real time stress-displacement plots throughout the test for monitoring purposes. Photographs of the sheared surfaces were

taken. The test was repeated for the same specimen three additional times at increasing increments of normal load.

5 Analysis of Data

5.1 Zero Pressure Velocity Tests

The P-wave (compressive) and S-wave (shear) velocities were determined by dividing the specimen length by the wave travel time through the specimen. The dynamic properties were then calculated using the following equations:

Dynamic Young's Modulus

$$E_d = \frac{\rho V_s^2 (3V_p^2 - 4V_s^2)}{V_p^2 - V_s^2} \quad (1)$$

where: E_d = dynamic Young's modulus
 V_s = shear wave velocity
 V_p = compressive wave velocity
 ρ = density

Dynamic Shear Modulus

$$G_d = \rho V_s^2 \quad (2)$$

where: G_d = dynamic shear modulus
 V_s = shear wave velocity
 ρ = density

Poisson's Ratio (based on velocity data)

$$\nu_d = \frac{V_p^2 - 2V_s^2}{2(V_p^2 - V_s^2)} \quad (3)$$

where: ν_d = Poisson's Ratio
 V_s = shear wave velocity
 V_p = compressive wave velocity

The velocity measurements and calculated dynamic properties are contained in Tables A-3 and A-4.

5.2 Uniaxial Compression Strength Tests

Data obtained from the uniaxial compression tests included the axial stress (σ), the axial strain (ϵ_a) and the circumferential strain (ϵ_c). Strains are calculated using both bonded gauges and extensometers. Stress and strain were calculated as follows:

Axial Stress

$$\sigma = \frac{P}{A_0} \quad (4)$$

where: σ = uniaxial stress
 P = applied axial load
 A_0 = initial specimen cross-sectional area

Axial Strain

$$\varepsilon_a = \frac{\Delta l}{l_0} \quad (5)$$

where: ε_a = axial strain
 Δl = change in length of specimen
 l_0 = initial length of specimen

Circumferential Strain

$$\varepsilon_c = \frac{\Delta d}{d_0} \quad (6)$$

where: ε_c = circumferential strain
 Δd = change in circumference of specimen
 d_0 = initial circumference of specimen

Volumetric Strain

$$\varepsilon_v = \varepsilon_a + 2\varepsilon_c \quad (7)$$

where: ε_v = volumetric strain
 ε_a = axial strain
 ε_c = circumferential strain

Ultimate uniaxial compressive strength σ_c , tangent Young's modulus of elasticity E , (calculated at 0.4 σ_c) and the Poisson's Ratio ν , were established in each uniaxial compressive test case (ASTM D7012, 2007) using load cell, extensometer, LVDT and strain gauge data. These values were calculated as follows:

Ultimate Uniaxial Compressive Strength

$$\sigma_c = \frac{P_c}{A_0} \quad (8)$$

where: σ_c = ultimate uniaxial compressive strength
 P = axial load at failure
 A_0 = initial specimen cross-sectional area

Young's Modulus of Elasticity

$$E = \frac{\sigma_{40}}{\epsilon_{40}} \quad (9)$$

where: E = tangent Young's Modulus at 40% of peak strength
 σ_{40} = tangent stress at 40% of peak strength
 ϵ_{40} = tangent strain at 40% of peak strength

Poisson's Ratio

$$\nu = \frac{E_{axial}}{E_{lateral}} \quad (10)$$

where: ν = Poisson's Ratio
 E_{axial} = slope of axial stress-strain curve at 40% of peak strength
 $E_{lateral}$ = slope of lateral stress-strain curve at 40% of peak strength

The ultimate uniaxial compressive strength, peak strain, Young's Modulus and Poisson's Ratio values are contained in Tables A-5 and A-6. Specimen stress-strain curves are contained in Appendix B. Two graphs are shown for each specimen except trial run specimens from 27.30 m and 29.38 m in DGR-1. The upper graph displays curves determined from bonded strain gauge data. The bottom graph displays stress-strain data calculated using extensometers.

Crack damage stress σ_{cd} , is the stress level where the ϵ_v - ϵ_a curve reaches a maximum and starts to reverse in direction, indicating dilation due to the formation and growth of unstable cracks. Progressive fracturing failure process starts above σ_{cd} leading to the failure of the rock. Crack damage stress and crack initiation stress levels are contained in Tables A-5 and A-6. Volumetric strain and crack volumetric strain curves are displayed in Appendix B. Appendix C contains photographs of the failed specimens.

Crack initiation stress σ_{ci} , is the stress level where the σ - ϵ_a and ϵ_{dv} - ϵ_a curves start to deviate from linear elastic behaviour, indicating the development and growth of stable cracks. The crack volumetric strain ϵ_{dv} is the difference between the volumetric strain ϵ_v observed in the test and the elastic volumetric strain ϵ_{ev} calculated by assuming ideal linear elastic behaviour throughout the test. The value of σ_{ci} , was derived from the plot of the ϵ_{dv} - ϵ_a curve.

Crack Volumetric Strain

$$\epsilon_{dv} = \epsilon_v - \epsilon_{ev} \quad (11)$$

where: ϵ_{dv} = crack volumetric strain
 ϵ_v = volumetric strain
 ϵ_{ev} = elastic volumetric strain

5.3 Acoustic Emission (AE) Tests

Acoustic Emission (AE) tests provided a non-destructive analysis of micro-crack formation, orientations and mechanisms and their effect on the mechanics of a test specimen. Coalescence of micro-cracks into macro-cracks cause major damage to a specimen and eventually leads to failure. AE are sound waves emitted by micro-cracks as they are created or move. Sound waves propagated through the specimen and were recorded continuously during the uniaxial compressive test.

Cumulative counts were recorded from the 6 AE channels during uniaxial testing. AE counts showed the amount of fracturing that occurred in the specimen. The cumulative hits for the six channels were summed and are plotted as hits versus stress on the figures contained in Appendix B. The source locations of AE events are shown displayed three-dimensionally (3D), adjacent to the photograph of the actual failed specimen in Appendix C. The 3D graph and the photograph are displayed vertically as per the test configuration. AE transducer locations are shown in green and the source locations are shown in red. AE source locations delineated regions of damage. Micro-crack distributions, mapped in 3D through time, describe damage accumulation, crack coalescence and macro-fracture propagation.

5.4 Brazilian Tensile Strength Tests

The tensile strengths of the specimens were calculated as follows:

Brazilian Tensile Strength

$$\sigma_t = \frac{2P}{\pi Dt} \quad (12)$$

where: σ_t = Brazilian Tensile Strength
 P = load at failure
 D = diameter of the specimen
 t = thickness of the specimen

The specimen, diameter, thickness, density, Brazilian tensile strength, and the orientation of the axis of loading with respect to the failure mode are contained in Table A-7. A photograph of the failed specimens is contained in Appendix E.

5.5 Direct Shear Strength Tests

Direct shear tests were conducted on eleven specimens comprising intact and non-intact shear surfaces. Each specimen was tested at four increasing increments of normal stresses between 0.6 and 2.4 MPa. Test results in the form of plots of shear stress versus shear displacement and shear stress versus normal stress are presented in Appendix D.

The direct shear test was performed by applying a shear load on the specimen under a constant normal load and measuring the normal and shear displacements. The stress values were calculated by dividing the loads by the nominal areas (initial cross-sectional areas) of the interfaces (Equations 13 and 14). The test procedure made no provision for the measurement of pore pressures. The stress values determined before shearing were expressed in terms of total stress. After shearing, the shear plane provided a drainage path for dissipation of pore pressures, and the stress values were expressed in terms of effective stress.

$$\sigma_n = \frac{P_n}{A} \tag{13}$$

$$\tau = \frac{P_s}{A} \tag{14}$$

where: σ_n = normal stress
 τ = shear stress
 P_n = normal load
 P_s = shear load
 A = nominal area

Strength values measured in the direct shear test included peak shear strength and residual strength. The strength values were measured from the stress-displacement plots obtained from the shear tests (see Appendix D). Due to the scattering of data in those plots, polynomial curve fitting was performed on stress and displacement data, employing a linear, quadratic or cubic equation.

Table A-8 presents the strength values obtained from the shear tests. Graphs of peak shear strength and residual strength versus normal stress were plotted from the results for all test samples (Figures D-1 to D-8). The residual strength can be seen to increase steadily with normal stress in most of the tests.

6 Results and Conclusions

This report has described the apparatus and procedures used to conduct various mechanical and dynamic property tests on rock units originating from sedimentary bedrock underlying the Bruce site. Information on specimen geological description and formation was provided by Intera Engineering Limited and is contained in Appendix F. The laboratory testing program was conducted during the interim of February to August of 2007. Forty-seven uniaxials, twenty Brazilians and eight shear tests were completed. The following conclusions can be made.

The Uniaxial Compressive strengths separate the rock units into different strength categories according to ASTM guide D5878 (ASTM D5878, 2005), from weakest to strongest as follows:

brecciated dolostone	weak	(5-25 MPa)
dolomitic shale	medium strong	(25-50 MPa)
shale	medium strong	(25-50 MPa)
shale with limestone layers	medium strong	(25-50 MPa)
limestone with shale layers	medium strong	(25-50 MPa)
dolostone	strong	(50-100 MPa)
argillaceous limestone	very strong	(100-250 MPa)
crystalline dolostone	very strong	(100-250 MPa)

Young's modulus and Poisson's ratio values were consistent with the strength determinations. Inspection of stress-strain curves contained in Appendix B confirms that many specimens failed due to the existence of planes of weakness as evidenced by abrupt shifts in the curves. AE curves of cumulative hits increase and coincide with the stress-strain curve shifts. The extent of weakness planes is seen first-hand by inspection of photographs of the failed specimen contained in Appendix C.

Failure modes of the Brazilian specimens were greatly influenced by the presence of shale layers and anisotropy with bedding planes perpendicular to the axis of the core. The failures modes logged in Table A-7 confirm that

not many of the specimens failed by classical diametral planes, but by the combination of diametral planes and slabbing. The photograph in Appendix E provides a pictorial presentation of the failure modes of the tested specimens.

The majority of shear tests were conducted as residual strength shear tests on open joints or planes of weakness. Test values of direct shear and residual shear strengths with the applied normal stresses are shown in Table A-8. In the majority of tests, residual shear strength increased with increasing application of normal stress. Appendix D contains graphs of shear and residual shear stress versus displacement for each of the eight specimens for each increment of applied normal stress. Appendix D also contains graphs of residual shear stress versus normal stress for each tested specimen. Linear fitting of the residual versus normal stress data was employed and is displayed in the graphs.

7 Data Quality and Use

Data on geomechanical strength properties of DGR-1 and DGR-2 core described in this Technical Report are based on testing conducted in accordance with established and well defined ASTM testing procedures.

The results presented in this Technical Report are suitable for assessing the geomechanical strength properties of bedrock formations intersected by DGR-1 and DGR-2, and the development of descriptive geomechanical models of the Bruce DGR site.

8 Disclaimer

Any determination and/or reference made in this report with respect to any specific commercial product, process or service by trade name, trademark, manufacturer or otherwise shall be considered to be opinion; CANMET-MMSL makes no, and does not intend to make any, representations or implied warranties of merchantability or fitness for a particular purpose nor is it intended to endorse, recommend or favour any specific commercial product, process or service. The views and opinions of authors expressed herein do not necessarily state or reflect those of CANMET-MMSL and may not be used for advertising or product endorsement purposes.

9 References

Durrheim, R.J., and Labrie, D., 2004. "Data-Driven Simulation of the Rock Mass response to Mining (Part 1): Laboratory Experimentation using Nepean Sandstone Models"; South African Inst. of Min. and Met; 2nd Int. Seminar on Deep and High Stress Mining Johannesburg, South Africa: pp. 365-394.

Intera Engineering Ltd., 2007a. Test Plan for Geomechanical Lab Testing of DGR-1 & DGR-2 Core, Revision 2, June 22, Ottawa.

Intera Engineering Ltd., 2007b. Project Quality Plan, DGR Site Characterization, Revision 3, January 17, Ottawa.

Lau, J.S.O., 2002. "A laboratory Testing Program to Investigate the Mechanisms Leading to Debonding at Concrete-Rock Interfaces"; JSO Lau Consulting Services Inc.; Ottawa, Canada: 51p..

ASTM D2845, 2005. "Standard Test Method for Laboratory Determination of Pulse Velocities and Ultrasonic Constants of Rock"; Annual Book of ASTM Standards, Vol. 04.08.

ASTM D3967, 2005. "Standard Test Method for the Splitting Tensile Strength of Intact Rock Core Specimens"; Annual Book of ASTM Standards, Vol. 04.08.

ASTM D4543, 2007. "Standard Practice for Preparing Rock Core as Cylindrical Test Specimens and Verifying

Conformance to Dimensional and Shape Tolerances”; Annual Book of ASTM Standards, Vol. 04.08.

ASTM D5607, 2006. “Standard Test Method for Performing Laboratory Direct Shear Strength Tests of Rock Specimens under Constant Normal Force”; Annual Book of ASTM Standards, Vol. 04.08.

ASTM D5878, 2005. “Standard Guides for Using Rock-Mass Classification Systems for Engineering Purposes”; Annual Book of ASTM Standards, Vol. 04.08.

ASTM D7012, 2007. “Standard Test Method for Compressive Strength and Elastic Moduli of Intact Rock Core Specimens under Varying States of Stress and Temperatures”; Annual Book of ASTM Standards, Vol. 04.08.

ASTM E1237, 2003. “Standard Guide for Installing Bonded Resistance Strain”; Annual Book of ASTM Standards, Vol. 03.01.

APPENDIX A

Data and Calculation Tables

Table A-1. Dimensions and densities of DGR-1 uniaxial specimens

Test	Depth	Length	Diameter	Mass	Density
(No)	(m)	(mm)	(mm)	(g)	(Mg/m³)
1	27.30	170.67	68.38	1669.50	2.66
2	29.38	175.36	68.18	1717.00	2.68
3	70.84	166.00	65.57	1463.00	2.61
4	108.62	178.83	74.63	2066.50	2.64
5	160.93	163.96	66.75	1544.50	2.69
6	171.14	161.13	67.20	1429.50	2.50
7	183.60	184.21	70.96	1917.50	2.63
8	206.55	188.86	75.25	2117.00	2.52
9	266.20	173.06	75.55	1870.50	2.41
10	286.69	178.15	75.39	1990.00	2.50
11	314.88	169.5	75.68	1983.50	2.60
12	367.06	173.17	75.98	2283.00	2.91
13	386.55	172.01	75.82	2081.50	2.68
14	415.16	168.7	75.92	1998.50	2.62
15	438.10	174.05	75.39	2079.00	2.68
16	455.22	170.49	76.08	2058.50	2.66
17	460.41	154.95	76.06	1845.50	2.62

Table A-2. Dimensions and densities of DGR-2 uniaxial specimens

Test	Depth	Length	Diameter	Mass	Density
(No)	(m)	(mm)	(mm)	(g)	(Mg/m³)
18	457.21	175.45	75.82	2147.00	2.71
19	474.71	180.85	76.08	2230.00	2.71
20	491.32	179.61	75.76	2167.00	2.68
21	502.78	178.58	75.91	2176.00	2.69
22	519.61	173.95	75.94	2110.50	2.68
23	533.94	183.32	74.92	2163.00	2.68
24	580.99	151.73	74.89	1769.50	2.65
25	586.35	177.45	75.96	2131.00	2.65
26	587.51	183.20	75.65	2179.00	2.65
27	606.50	176.93	76.05	2154.00	2.68
28	646.42	140.32	76.08	1646.00	2.58
29	654.97	175.92	75.60	2102.00	2.66
30	655.32	187.43	75.60	2222.50	2.64
31	660.68	175.24	76.05	2107.00	2.65
32	661.61	174.44	75.58	2111.50	2.70
33	666.79	182.43	75.69	2209.00	2.58
34	668.46	175.38	75.61	2119.50	2.66
35	673.26	174.15	75.47	2096.00	2.72
36	674.11	175.28	75.79	2118.00	2.66
37	676.45	173.70	75.50	2100.00	2.70
38	679.83	173.45	75.81	2098.00	2.68
39	683.02	182.56	75.47	2197.50	2.69
40	688.22	189.34	75.36	2263.00	2.68
41	694.11	187.29	75.40	2276.50	2.72
42	695.15	183.18	75.31	2219.50	2.72
43	702.69	190.67	75.42	2304.50	2.71
44	704.47	180.04	75.78	2161.50	2.66
45	710.29	187.65	75.39	2252.00	2.69
46	719.38	184.53	75.41	2206.00	2.68
47	737.16	196.62	75.14	2353.50	2.70

Table A-3. Dynamic elastic constants of DGR-1 specimens

Test	Depth	Length	P-Wave Time	P-Wave Velocity	S-Wave Time	S-Wave Velocity	E	Shear Modulus	Poisson's Ratio
(No)	(m)	(mm)	(μs)	(km/s)	(μs)	(km/s)	(GPa)	(GPa)	(ν)
1	27.30	170.67	28.60	5.97	58.60	2.91	60.72	22.60	0.34
2	29.38	175.36	33.20	5.28	63.00	2.78	54.35	20.78	0.31
3	70.84	166.00	29.00	5.72	56.00	2.96	60.40	22.94	0.32
4	108.62	178.83	46.30	3.86	72.80	2.46	36.99	15.94	0.16
5	160.93	163.96	46.00	3.56	82.00	2.00	27.34	10.76	0.27
6	171.14	161.13	37.60	4.29	72.80	2.21	32.30	12.25	0.32
7	183.60	184.21	43.60	4.23	76.80	2.40	38.23	15.14	0.26
8	206.55	188.86	46.80	4.04	95.20	1.98	26.60	9.92	0.34
9	266.20	173.06	55.20	3.14	88.00	1.97	21.93	9.33	0.18
10	286.69	178.15	42.40	4.20	89.60	1.99	26.82	9.89	0.36
11	314.88	169.50	34.40	4.93	68.00	2.49	42.93	16.16	0.33
12	367.06	173.17	31.20	5.55	64.00	2.71	57.23	21.29	0.34
13	386.55	172.01	31.20	5.51	60.60	2.84	56.99	21.59	0.32
14	415.16	168.70	66.40	2.54	160.00	1.05	8.12	2.91	0.40
15	438.10	174.05	36.00	4.83	65.60	2.65	48.39	18.84	0.28
16	455.22	170.49	44.00	3.87	84.00	2.03	28.69	10.94	0.31
17	460.41	154.95	80.00	1.94	168.00	0.92	6.04	2.23	0.35

Table A-4. Dynamic elastic constants of DGR-2 specimens

Test	Depth	Length	P-Wave Time	P-Wave Velocity	S-Wave Time	S-Wave Velocity	E	Shear Modulus	Poisson's Ratio
(No)	(m)	(mm)	(μ s)	(km/s)	(μ s)	(km/s)	(GPa)	(GPa)	(ν)
18	457.21	175.45	42.20	4.16	75.40	2.33	37.34	14.68	0.27
19	474.71	180.85	42.60	4.25	77.40	2.34	37.99	14.81	0.28
20	491.32	179.61	45.60	3.94	78.40	2.29	34.96	14.05	0.24
21	502.78	178.58	36.80	4.85	55.60	3.21	61.68	27.76	0.11
22	519.61	173.95	38.80	4.48	72.80	2.39	39.81	15.29	0.30
23	533.94	183.32	32.40	5.66	55.60	3.30	72.32	29.09	0.24
24	580.99	151.73	38.00	3.99	78.00	1.95	26.93	10.02	0.34
25	586.35	177.45	54.00	3.29	92.00	1.93	24.40	9.86	0.24
26	587.51	183.20	54.80	3.34	99.20	1.85	23.11	9.03	0.28
27	606.50	176.93	55.60	3.18	104.00	1.70	20.17	7.76	0.30
28	646.42	140.32	72.00	1.95	208.00	0.67	3.36	1.17	0.43
29	654.97	175.92	38.80	4.53	66.40	2.65	46.37	18.68	0.24
30	655.32	187.43	52.20	3.59	121.00	1.55	17.57	6.34	0.39
31	660.68	175.24	29.50	5.94	55.60	3.15	68.57	26.30	0.30
32	661.61	174.44	30.60	5.70	55.80	3.13	67.76	26.37	0.28
33	666.79	182.43	33.60	5.43	65.00	2.81	53.60	20.34	0.32
34	668.46	175.38	32.80	5.35	63.80	2.75	53.11	20.11	0.32
35	673.26	174.15	35.20	4.95	65.80	2.65	49.50	19.04	0.30
36	674.11	175.28	32.40	5.41	58.60	2.99	60.82	23.76	0.28
37	676.45	173.70	31.80	5.46	58.80	2.95	60.96	23.57	0.29
38	679.83	173.45	36.20	4.79	65.60	2.64	48.00	18.74	0.28
39	683.02	182.56	39.80	4.59	69.60	2.62	46.55	18.51	0.26
40	688.22	189.34	44.60	4.25	79.60	2.38	38.54	15.16	0.27
41	694.11	187.29	34.00	5.51	69.40	2.70	53.22	19.83	0.34
42	695.15	183.18	30.80	5.95	63.00	2.91	61.76	22.99	0.34
43	702.69	190.67	36.00	5.30	66.80	2.85	57.10	22.04	0.30
44	704.47	180.04	51.60	3.49	100.00	1.80	22.75	8.63	0.32
45	710.29	187.65	42.80	4.38	90.80	2.07	31.17	11.48	0.36
46	719.38	184.53	67.60	2.73	116.00	1.59	16.84	6.77	0.24
47	737.16	196.62	44.40	4.43	72.40	2.72	47.72	19.91	0.20

Table A-5. Static elastic constants of DGR-1 specimens

Specimen		Ultimate Uniaxial Strength	Transducers					Bonded Gauges				
Test	Depth		Peak Strain	E	Poisson's Ratio	Crack Damage Stress	Crack Initiation Stress	Peak Strain	E	Poisson's Ratio	Crack Damage Stress	Crack Initiation Stress
(No)	(m)	(MPa)	(%)	(GPa)	(v)	(σ_s =MPa)	(σ_d =MPa)	(%)	(GPa)	(v)	(σ_s =MPa)	(σ_d =MPa)
1	27.30	70.64	0.25	50.68	0.21	69.11	25.61	n/a	n/a	n/a	n/a	n/a
2	29.38	126.10	0.35	49.08	0.29	67.62	55.62	n/a	n/a	n/a	n/a	n/a
3	70.84	96.89	0.57	28.27	0.12	n/a	n/a	n/a	62.26	0.19	n/a	n/a
4	108.62	90.10	0.35	35.77	0.19	76.60	39.10	0.11	46.17	0.23	76.60	36.10
5	160.93	38.32	0.48	10.66	0.61	12.88	15.12	0.31	13.29	0.67	11.37	15.87
6	171.14	34.33	0.35	15.80	0.23	17.38	13.64	0.10	43.90	0.68	n/a	n/a
7	183.60	34.29	0.40	10.12	n/a	n/a	n/a	0.10	34.86	0.39	18.13	13.63
8	206.55	14.98	0.15	8.47	0.24	n/a	n/a	0.20	5.75	0.05	11.33	9.81
9	266.20	2.83	0.68	0.47	0.11	n/a	1.03	0.42	0.69	0.18	n/a	n/a
10	286.69	7.32	0.23	5.83	0.43	2.88	1.25	0.17	n/a	n/a	3.62	2.83
11	314.88	85.55	0.38	31.20	0.35	66.85	44.34	0.25	37.18	0.41	49.59	33.84
12	367.06	195.79	0.58	42.05	0.36	142.43	72.00	0.48	45.85	0.40	157.08	40.44
13	386.55	158.31	0.47	41.21	0.31	154.57	60.08	0.39	39.70	0.43	147.81	73.57
14	415.16	12.64	0.34	4.45	0.38	7.53	5.28	0.14	11.67	0.14	n/a	n/a
15	438.10	80.33	0.34	29.97	0.26	56.34	24.09	0.32	28.61	0.30	70.59	31.60
16	455.22	51.82	0.56	9.91	0.36	49.59	17.32	0.47	11.15	0.46	49.59	36.08
17	460.41	18.77	0.56	4.98	0.10	15.07	7.56	0.30	4.21	0.09	13.56	6.81

Table A-6. Static elastic constants of DGR-2 specimens

Specimen		Ultimate Uniaxial Strength	Transducers					Bonded Gauges				
Test	Depth		Peak Strain	E	Poisson's Ratio	Crack Damage Stress	Crack Initiation Stress	Peak Strain	E	Poisson's Ratio	Crack Damage Stress	Crack Initiation Stress
(No)	(m)	(MPa)	(%)	(GPa)	(ν)	(σ_s =MPa)	(σ_d =MPa)	(%)	(GPa)	(ν)	(σ_s =MPa)	(σ_d =MPa)
18	457.21	31.40	0.52	11.93	0.25	19.58	12.83	0.10	16.28	0.48	15.09	12.83
19	474.71	57.84	0.47	15.53	0.38	33.10	24.84	0.35	14.94	0.36	30.84	21.09
20	491.32	50.66	0.64	11.91	0.30	48.44	18.68	0.42	12.95	0.47	30.58	19.43
21	502.78	44.09	0.50	16.35	0.20	30.84	19.60	0.18	21.91	0.12	n/a	n/a
22	519.61	62.94	0.48	17.80	0.53	27.05	27.05	0.29	19.11	0.37	n/a	n/a
23	533.94	135.11	0.40	43.06	0.15	n/a	69.85	0.24	57.80	0.27	n/a	65.36
24	580.99	18.73	0.46	3.63	0.02	n/a	n/a	0.26	13.37	0.08	n/a	n/a
25	586.35	53.31	0.55	13.44	0.10	45.82	20.34	0.46	14.01	0.18	50.34	21.08
26	587.51	41.31	0.58	9.57	0.17	39.08	16.56	0.46	11.02	0.33	34.58	15.82
27	606.50	21.73	0.66	4.09	0.09	17.30	9.06	0.55	6.54	0.32	11.31	9.06
28	646.42	20.78	0.53	5.76	0.09	15.81	6.79	0.18	10.71	0.08	14.31	9.05
29	654.97	144.83	0.49	36.18	0.21	109.60	45.09	0.43	36.13	0.33	95.35	69.09
30	655.32	58.32	0.42	22.64	0.05	48.60	27.37	0.17	39.26	0.30	48.60	48.60
31	660.68	128.99	0.32	47.46	0.20	125.26	75.00	0.30	46.31	0.32	122.26	122.26
32	661.61	165.59	0.42	42.47	0.24	161.78	74.44	0.40	42.47	0.37	117.16	75.98
33	666.79	110.60	0.31	39.99	0.20	n/a	53.08	0.34	36.00	0.31	n/a	n/a
34	668.46	84.23	0.36	34.22	0.26	44.88	34.99	0.20	45.55	0.59	n/a	n/a
35	673.26	78.40	0.37	27.79	0.12	55.63	28.23	0.23	17.38	0.22	n/a	n/a
36	674.11	111.86	0.39	38.49	0.13	n/a	46.18	0.29	40.57	0.32	n/a	n/a
37	676.45	121.06	0.32	43.34	0.15	116.51	49.53	0.25	44.66	0.42	94.46	39.65
38	679.83	108.74	0.41	33.45	0.25	105.02	55.95	0.32	37.42	0.54	n/a	n/a
39	683.02	94.49	0.38	30.37	0.24	84.63	43.49	0.44	26.19	0.43	68.65	36.66
40	688.22	31.98	0.61	4.79	0.03	30.63	13.80	0.19	18.20	0.22	29.87	12.28
41	694.11	39.54	0.40	16.70	0.13	13.79	2.25	0.16	n/a	n/a	n/a	n/a
42	695.15	67.32	0.28	36.76	0.47	49.04	16.92	0.16	41.47	0.22	n/a	n/a
43	702.69	58.21	0.40	20.63	n/a	n/a	n/a	0.09	n/a	n/a	n/a	n/a
44	704.47	50.19	0.61	15.53	0.38	34.02	24.20	0.15	26.41	0.16	33.24	31.73
45	710.29	38.86	0.31	30.55	0.11	n/a	n/a	0.10	30.24	0.13	22.97	14.54
46	719.38	31.66	0.58	9.43	0.08	21.45	10.74	0.35	11.48	0.14	26.02	8.47
47	737.16	113.04	0.31	45.82	0.13	113.04	41.59	0.31	44.18	0.38	113.04	50.80

Table A-7. Brazilian test data for DGR-2 specimens

Test	Depth	Diameter	Thickness	X-area	Volume	Mass	Density	Failure	*Failure Load	Tensile Strength
(No.)	(m)	(mm)	(mm)	(cm ²)	(cm ³)	(g)	(Mg/m ³)	Mode	(N)	(MPa)
1	525.92	75.82	46.58	45.15	210.31	555.63	2.64	3	45225.773	-8.152
2	534.22	75.36	43.60	44.60	194.47	503.70	2.59	2	13831.293	-2.680
3	554.09	75.94	42.51	45.29	192.54	499.66	2.60	3	6834.134	-1.348
4	558.15	75.91	46.45	45.26	210.22	539.84	2.57	3	18265.637	-3.298
5	573.35	75.57	51.84	44.85	232.52	607.35	2.61	1	34148.348	-5.549
6	624.81	75.93	49.16	45.28	222.60	575.17	2.58	2	7778.329	-1.327
7	627.12	76.19	50.91	45.59	232.11	605.72	2.61	3	15989.452	-2.624
8	640.41	76.15	53.23	45.54	242.43	623.96	2.57	2	12920.819	-2.029
9	643.35	76.37	51.20	45.81	234.53	606.28	2.59	2	13949.317	-2.271
10	645.60	76.31	49.86	45.74	228.04	589.90	2.59	2	11706.884	-1.959
11	658.78	75.61	45.49	44.90	204.25	536.41	2.63	1	25802.334	-4.776
12	670.15	75.69	47.92	45.00	215.62	476.30	2.21	1	50772.918	-8.912
13	677.37	76.02	50.37	45.39	228.62	608.07	2.66	1	48295.570	-8.046
14	688.58	75.31	49.34	44.54	219.78	588.08	2.68	3	23930.805	-4.100
15	692.20	75.54	38.52	44.82	172.64	461.89	2.68	3	17001.090	-3.720
16	696.57	75.66	50.22	44.96	225.79	609.16	2.70	1	28769.805	-4.802
17	698.84	75.98	47.11	45.34	213.60	566.63	2.65	3	27673.863	-4.922
18	703.05	75.62	43.67	44.91	196.13	519.78	2.65	1	42106.559	-8.117
19	703.94	75.58	49.31	44.86	221.23	584.73	2.64	3	18619.709	-3.181
20	706.98	75.87	50.56	45.21	228.58	602.10	2.63	1	33811.129	-5.611

* Failure Modes:

1 – Diametral

2 – Slabbing

3 – Combination of 1 and 2

Table A-8. Shear test data for DGR-2 specimens

Test	Depth	Diameter	Length	Mass	Density	Peak Shear Stress	Residual Shear Stress	Normal Stress
(No.)	(m)	(mm)	(mm)	(g)	(Mg/m ³)	(MPa)	(MPa)	(MPa)
1	613.37	75.76	114.57	1209.74	2.34		0.671 0.813 1.023 1.441	0.823 1.194 1.618 2.195
2	616.59	75.88	113.81	1324.00	2.57		0.632 0.920 1.207 1.344	0.813 1.150 1.753 1.994
3	646.72	76.12	112.73	1321.50	2.58	1.379	<-intact-> 0.660 1.160 1.307 1.381	1.050 0.730 1.194 1.543 2.182
4	692.00	75.36	101.12	1194.90	2.65		0.614 0.559 0.772 0.949	0.909 1.128 1.696 2.245
5	697.86	75.63	126.28	1437.40	2.53	5.894	<-intact-> 2.750 2.448 5.105 4.458	1.039 0.771 1.341 1.895 2.330
6	702.23	75.69	109.10	1230.80	2.51		0.741 0.685 1.199 1.281	0.713 1.103 1.643 2.042
7	705.86	75.65	130.63	1435.70	2.45	2.617	<-intact-> 1.643 2.566 2.198 2.616	0.884 0.915 1.254 2.001 2.370
8	708.57	75.43	114.78	1363.40	2.66		0.982 1.126 1.556 1.997	0.729 1.216 1.845 2.204

Table A-8. Shear test data for DGR-2 specimens continued

Test (No.)	Depth (m)	Diameter (mm)	Length (mm)	Mass (g)	Density (Mg/m ³)	Peak Shear Stress (MPa)	Residual Shear Stress (MPa)	Normal Stress (MPa)
9	664.94	75.869				4.008	<-intact-> 0.684 0.824 0.923 1.214	0.624 0.525 1.039 1.429 1.968
10	673.06	75.53				3.033	<-intact-> 0.797 1.139 1.541 1.989	0.640 0.569 0.967 1.483 2.000
11	684.00	75.72				3.649	<-intact-> 0.943 1.084 1.327 1.494	0.617 0.516 0.976 1.578 2.051

APPENDIX B

Stress-Strain Curves of Uniaxial Tests

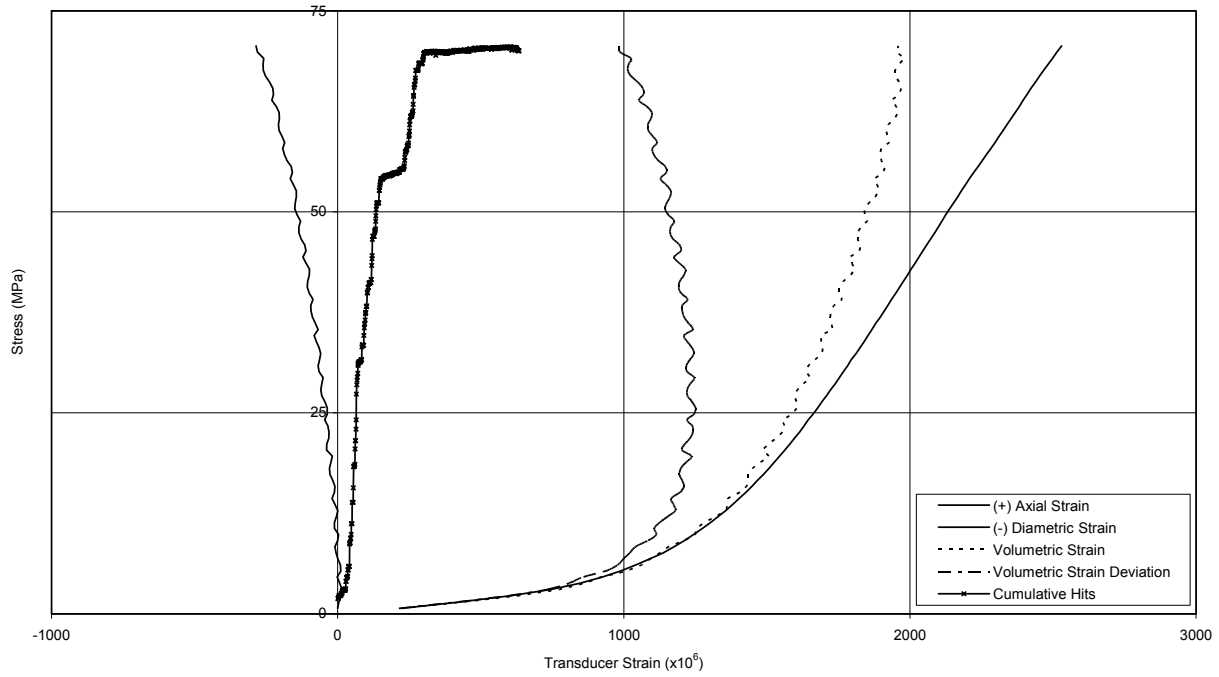


Figure B-1 Specimen DGR-1, 27.30 m

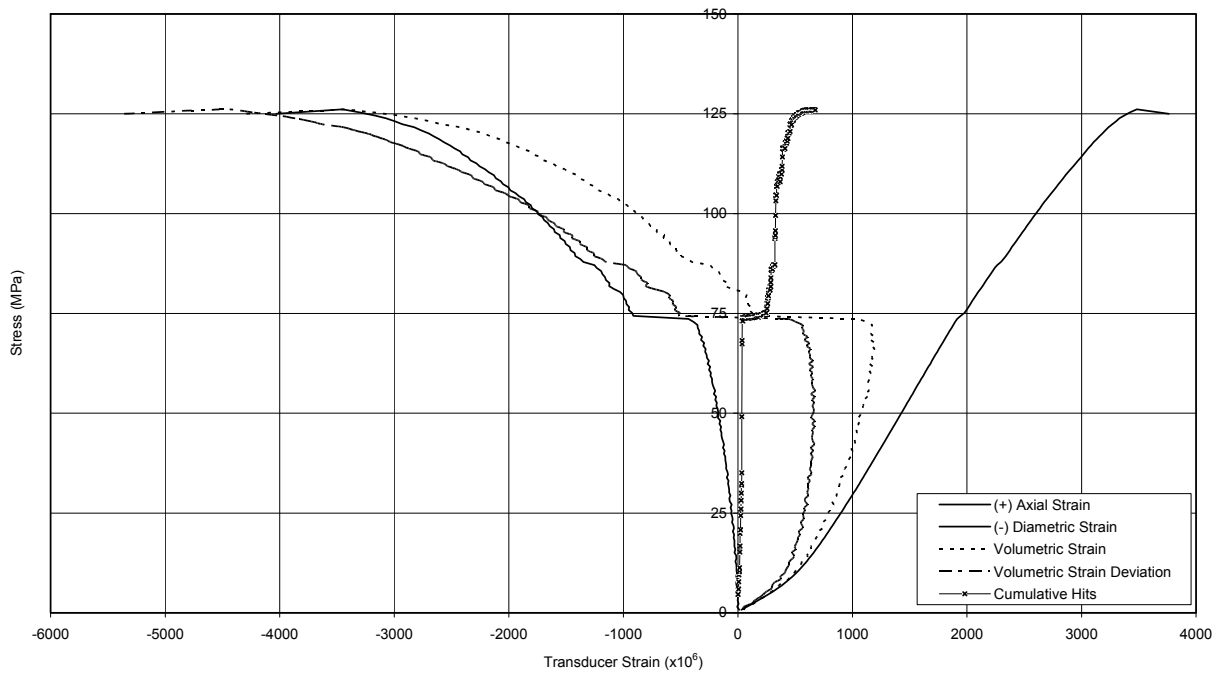


Figure B-2 Specimen DGR-1, 29.38 m

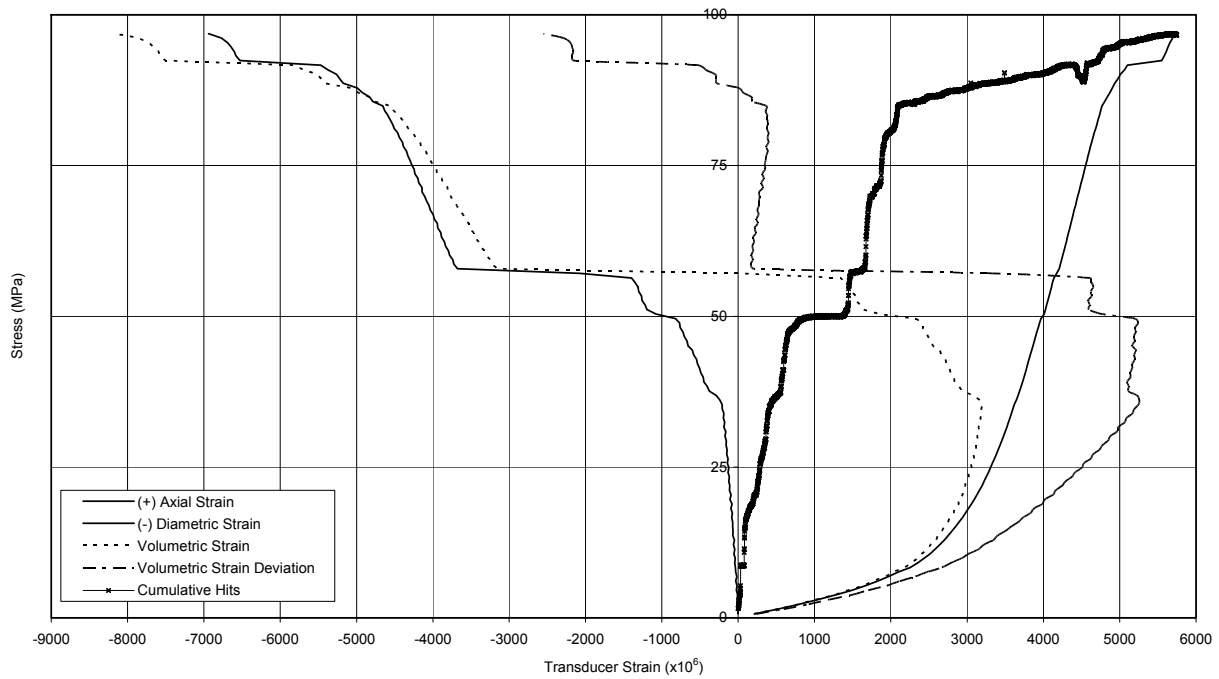
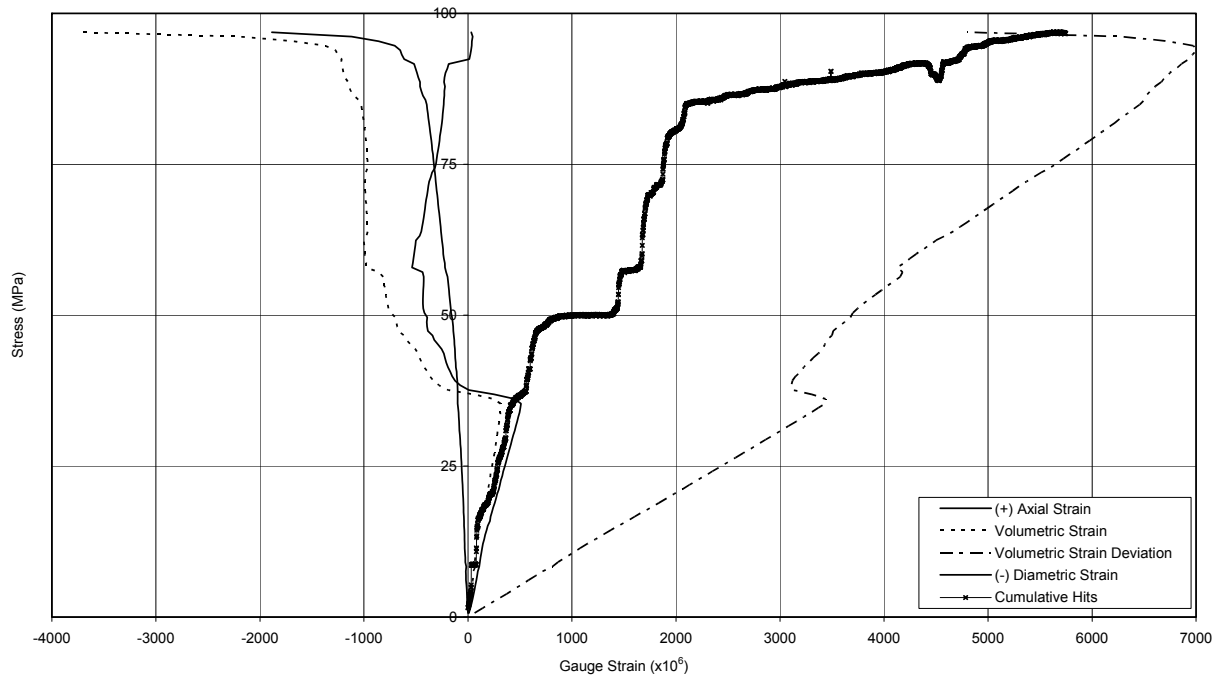


Figure B-3 Specimen DGR-1, 70.84 m

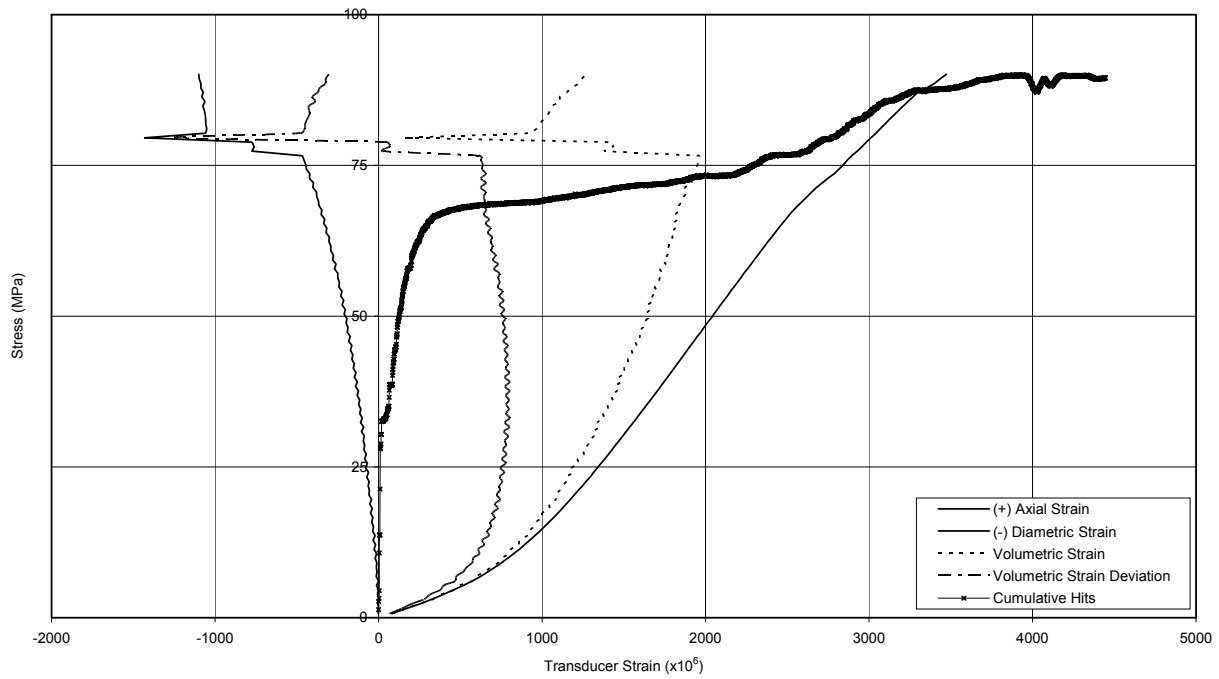
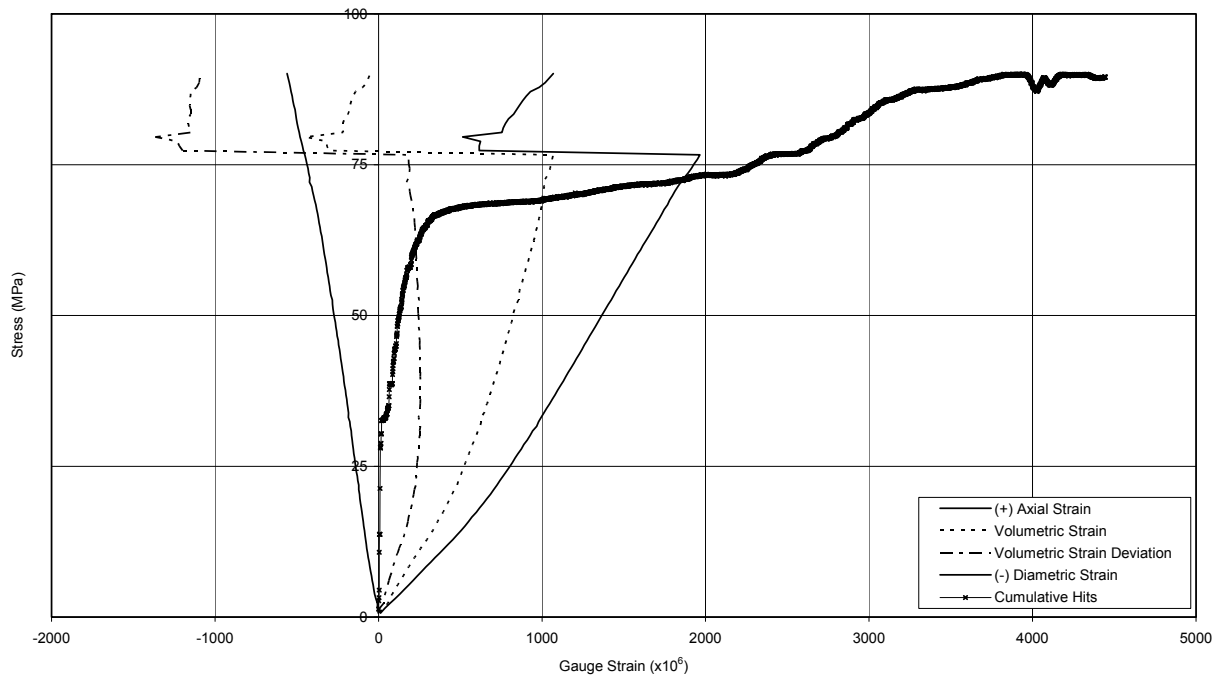


Figure B-4 Specimen DGR-1, 108.62 m

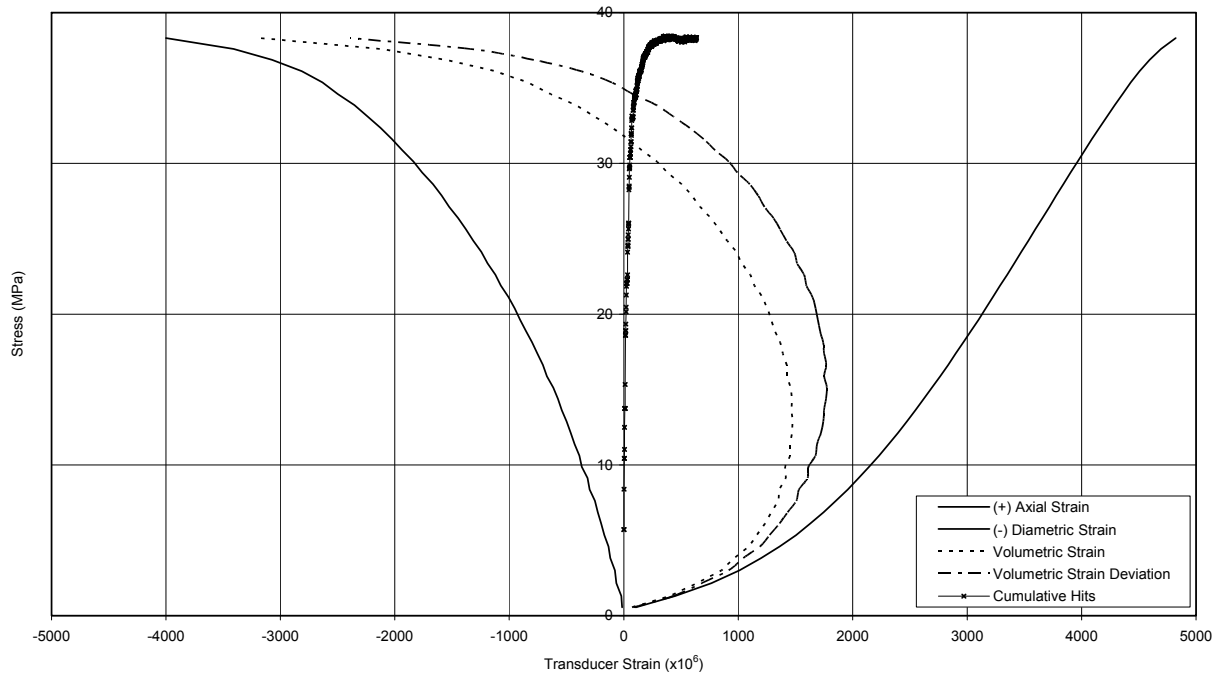
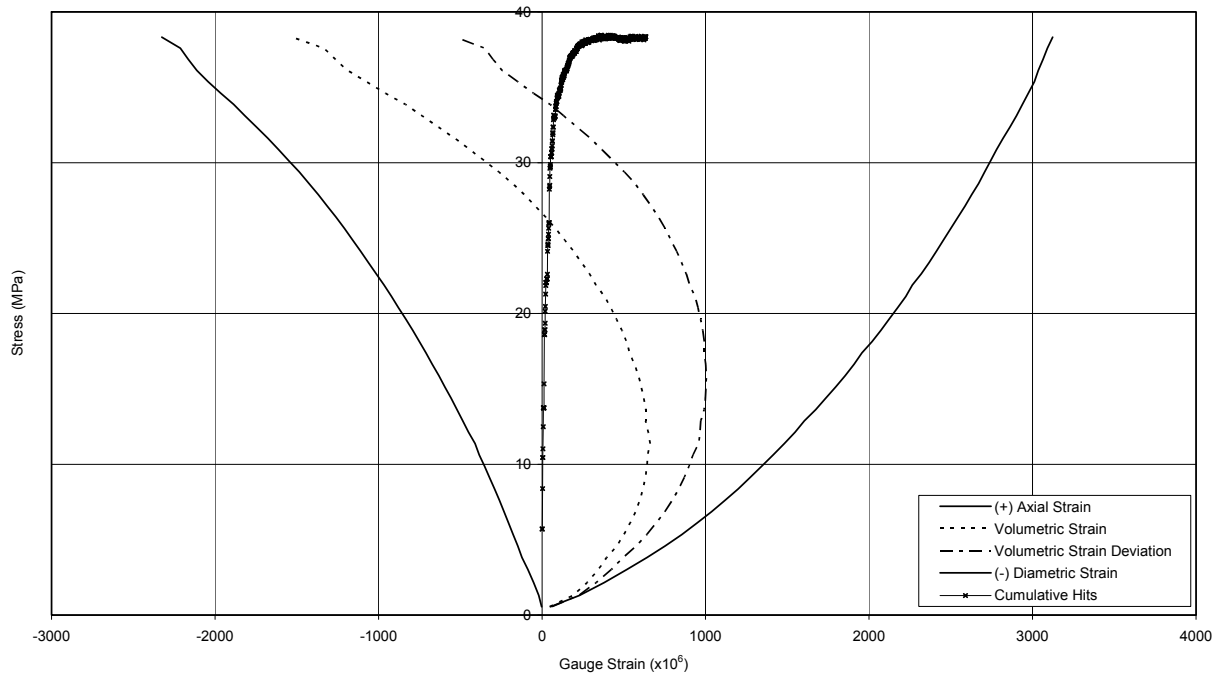


Figure B-5 Specimen DGR-1, 160.93 m

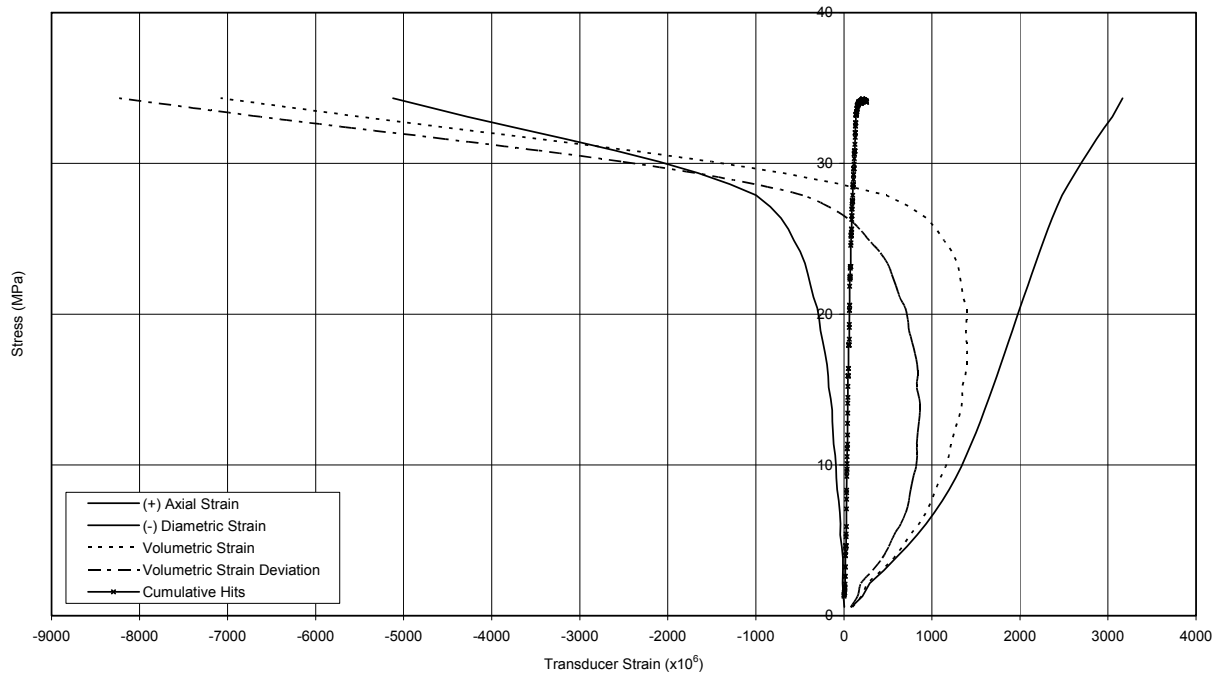
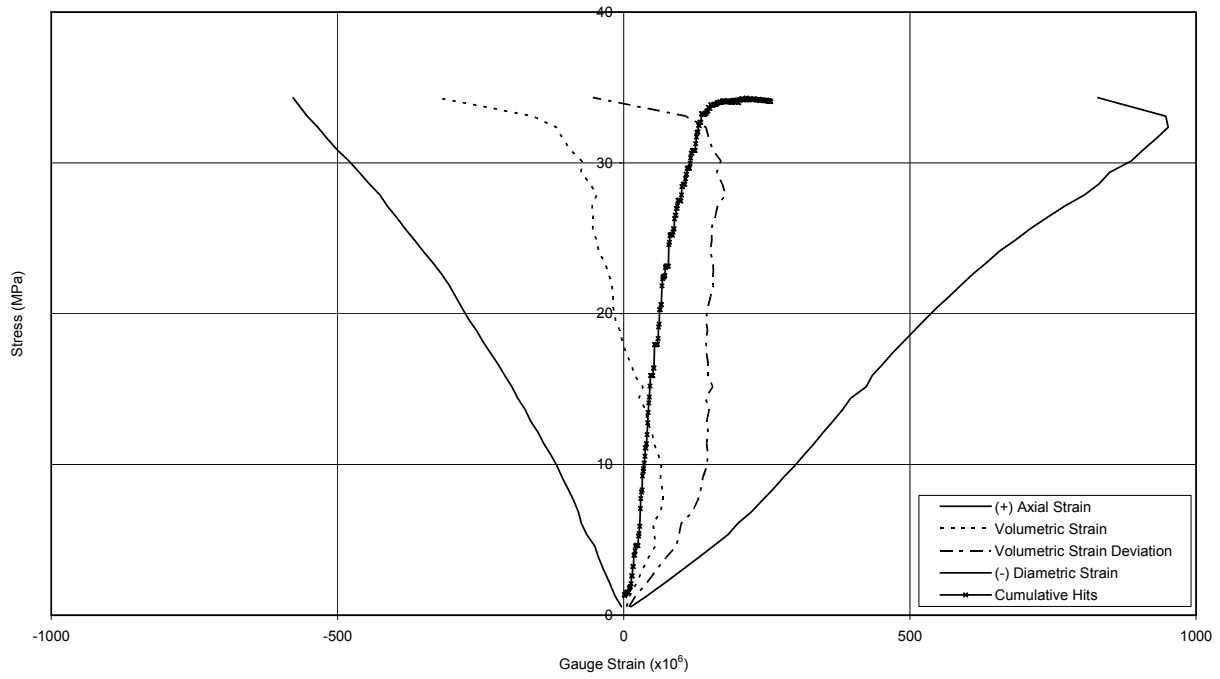


Figure B-6 Specimen DGR-1, 171.14 m

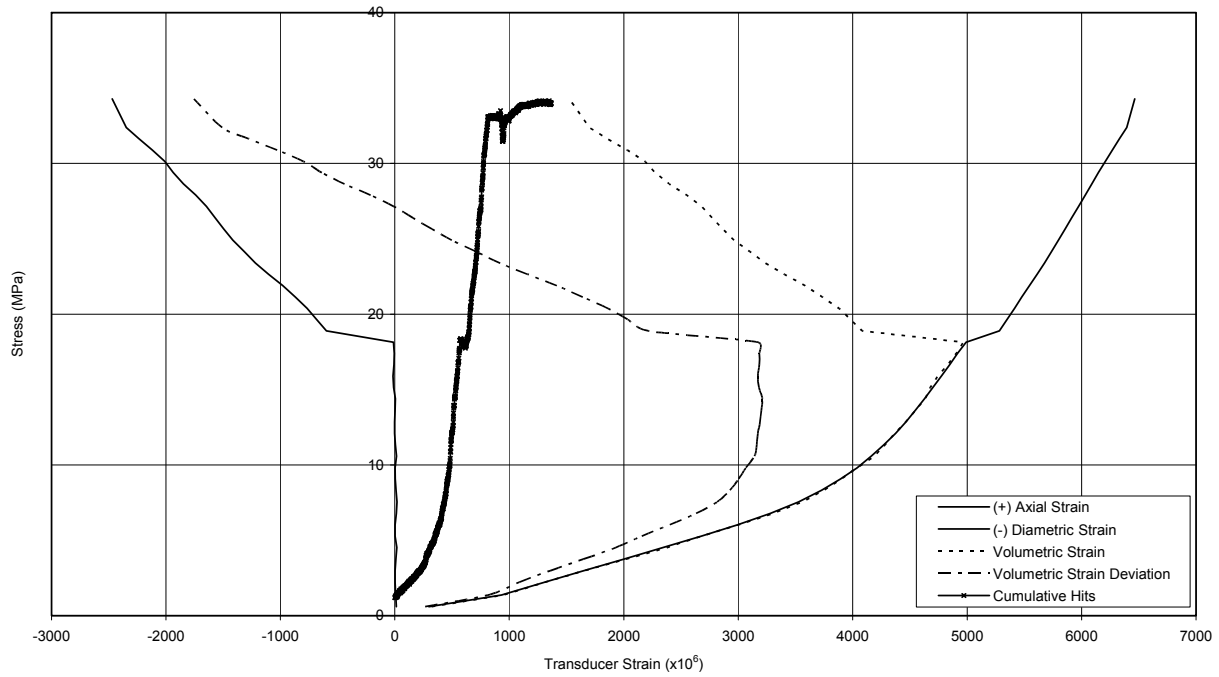
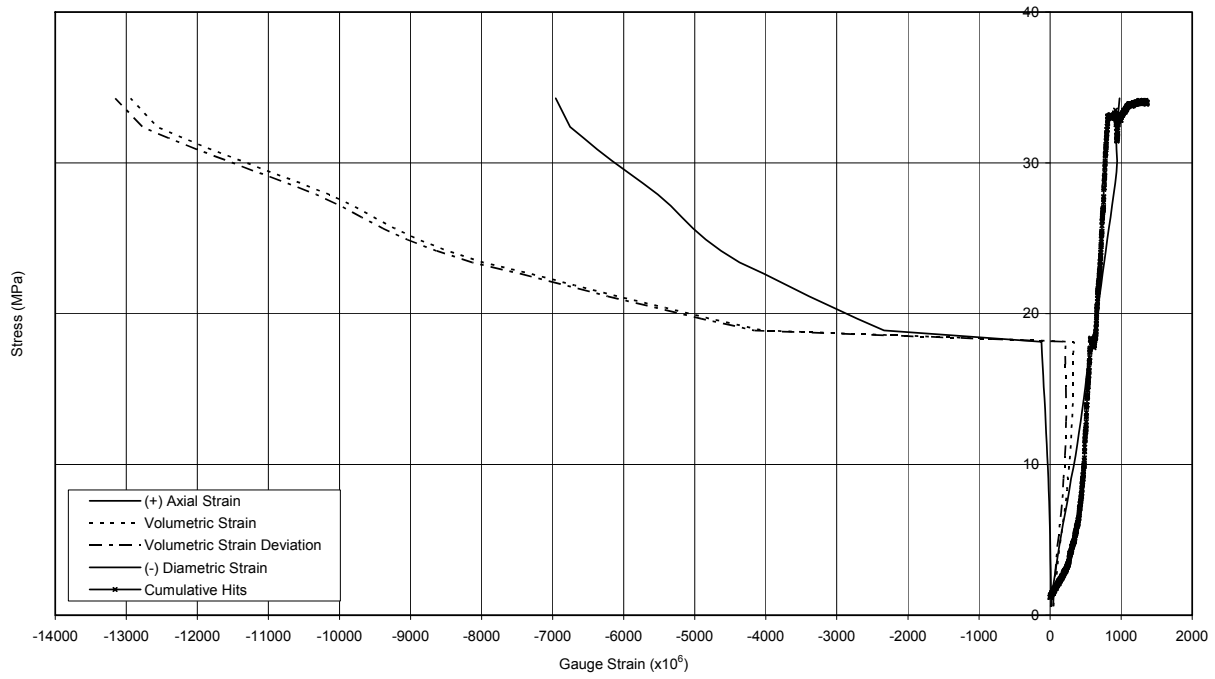


Figure B-7 Specimen DGR-1, 183.60 m

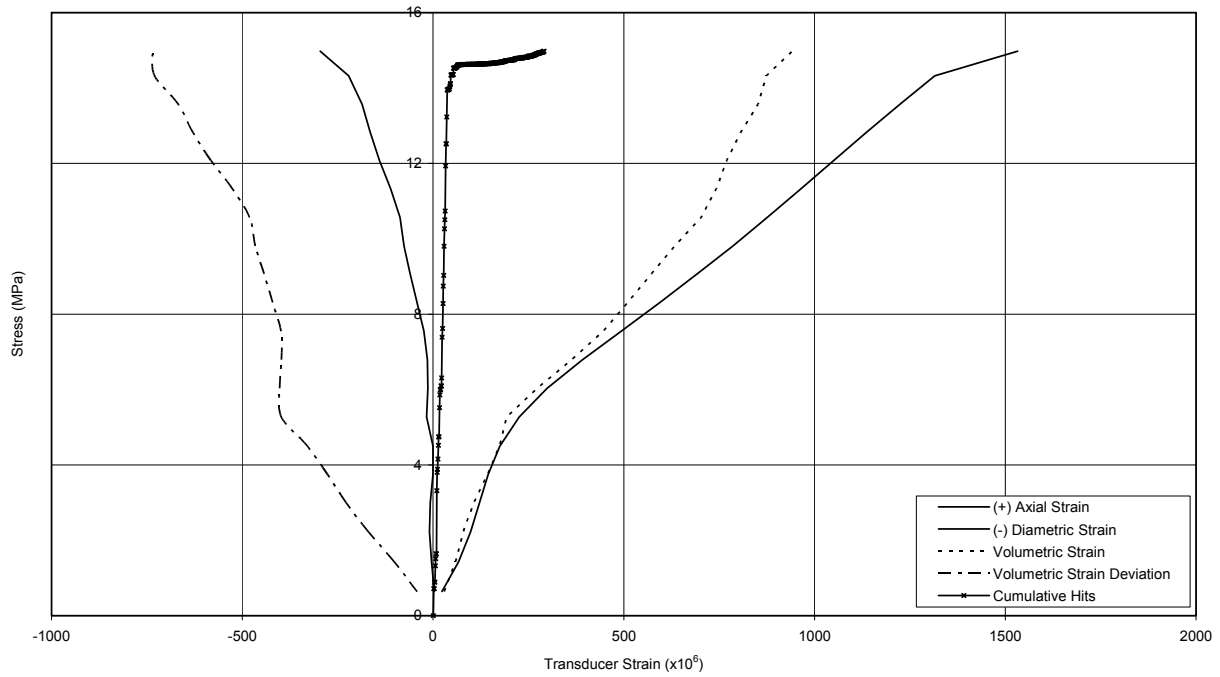
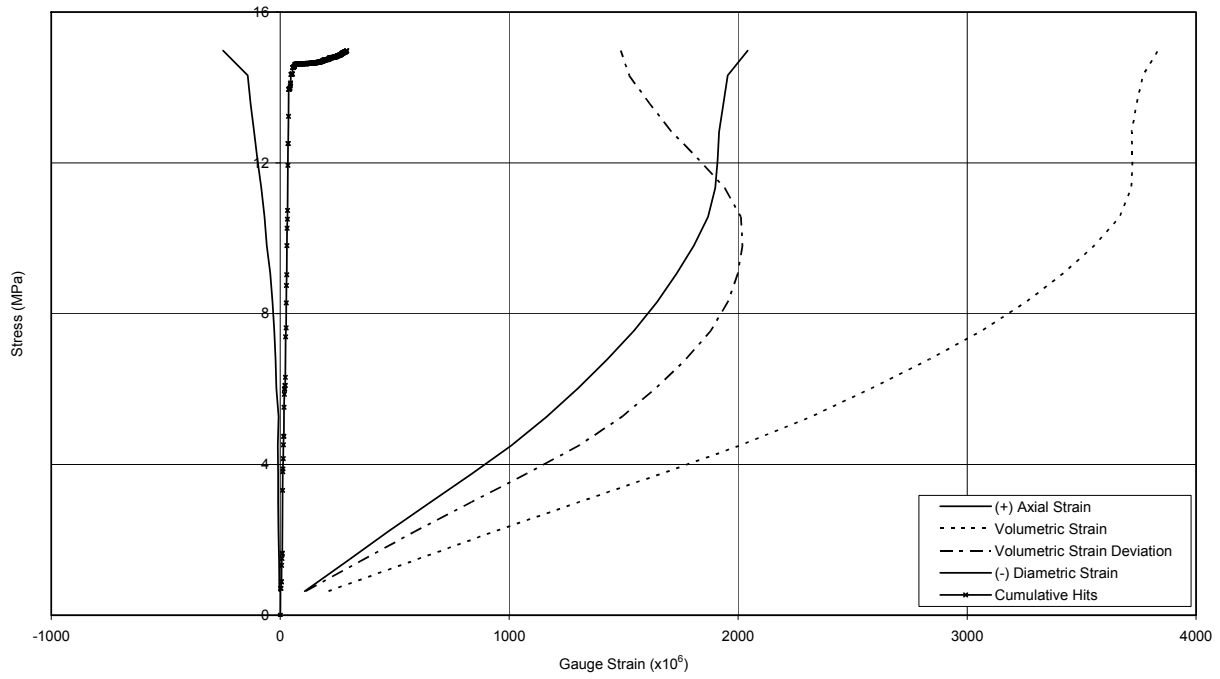


Figure B-8 Specimen DGR-1, 206.55 m

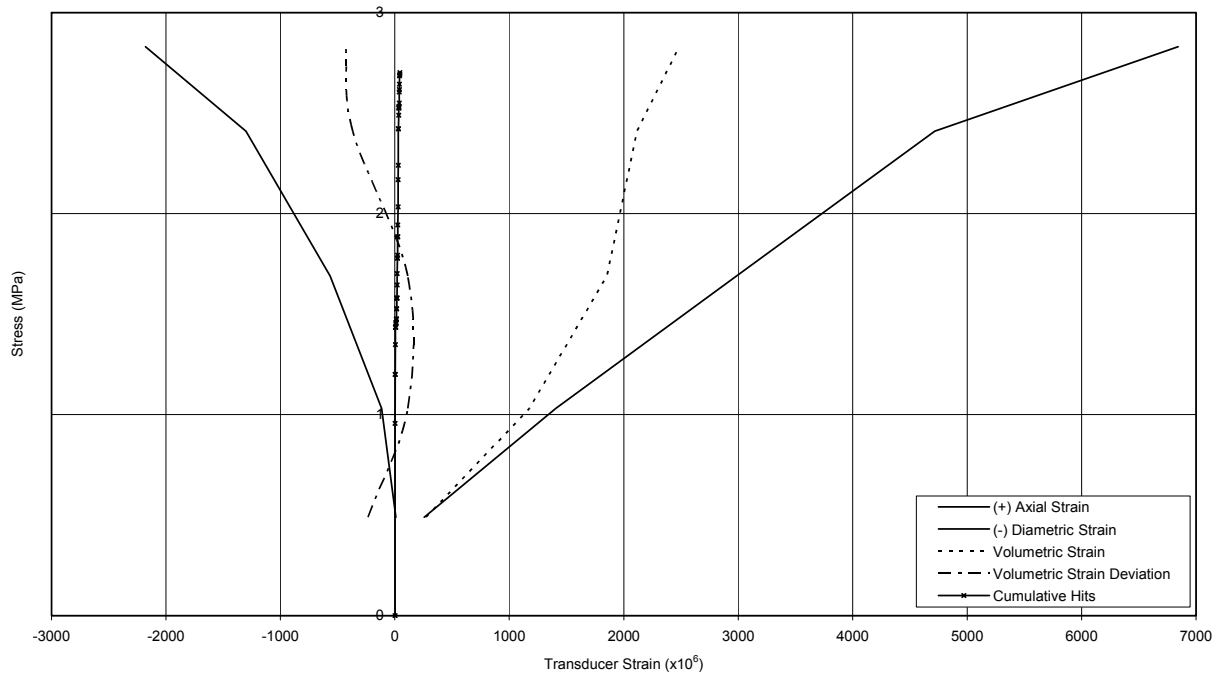
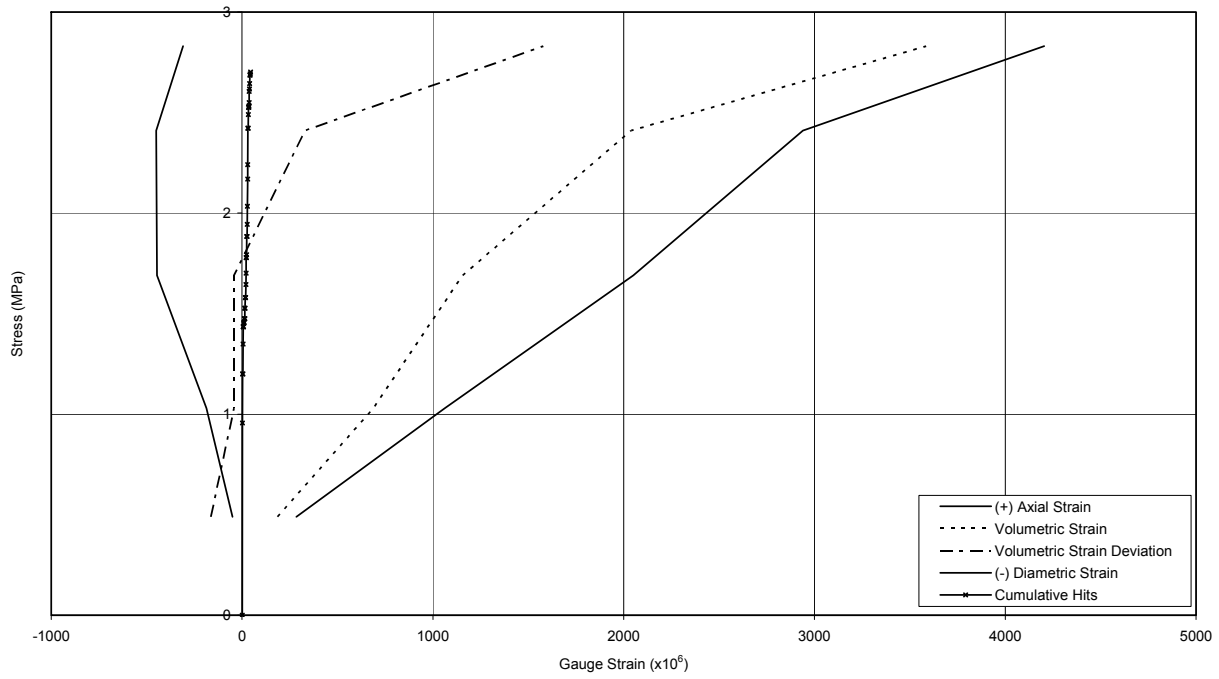


Figure B-9 Specimen DGR-1, 266.20 m

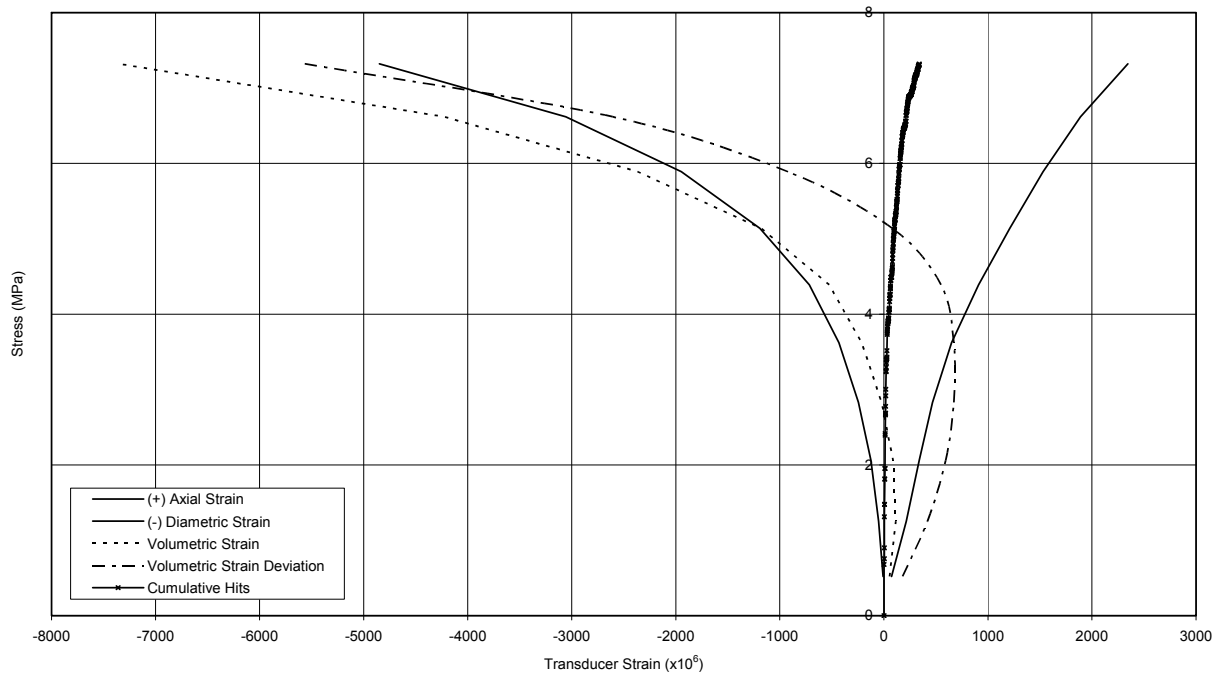
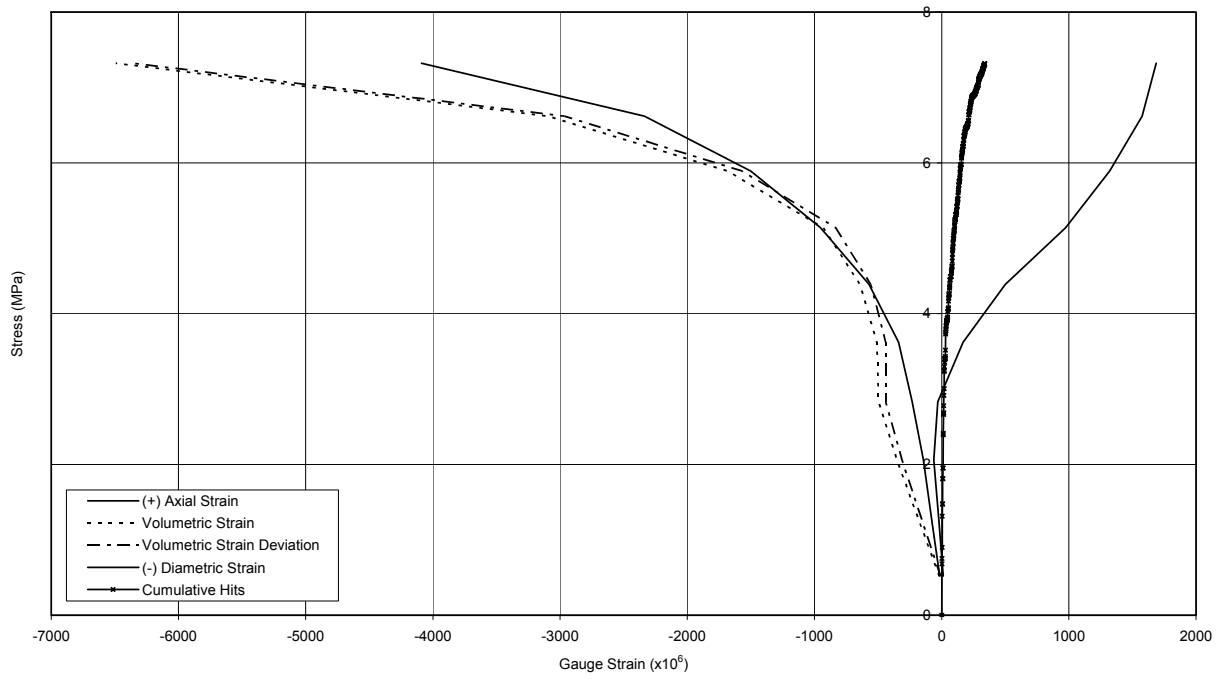


Figure B-10 Specimen DGR-1, 286.69 m

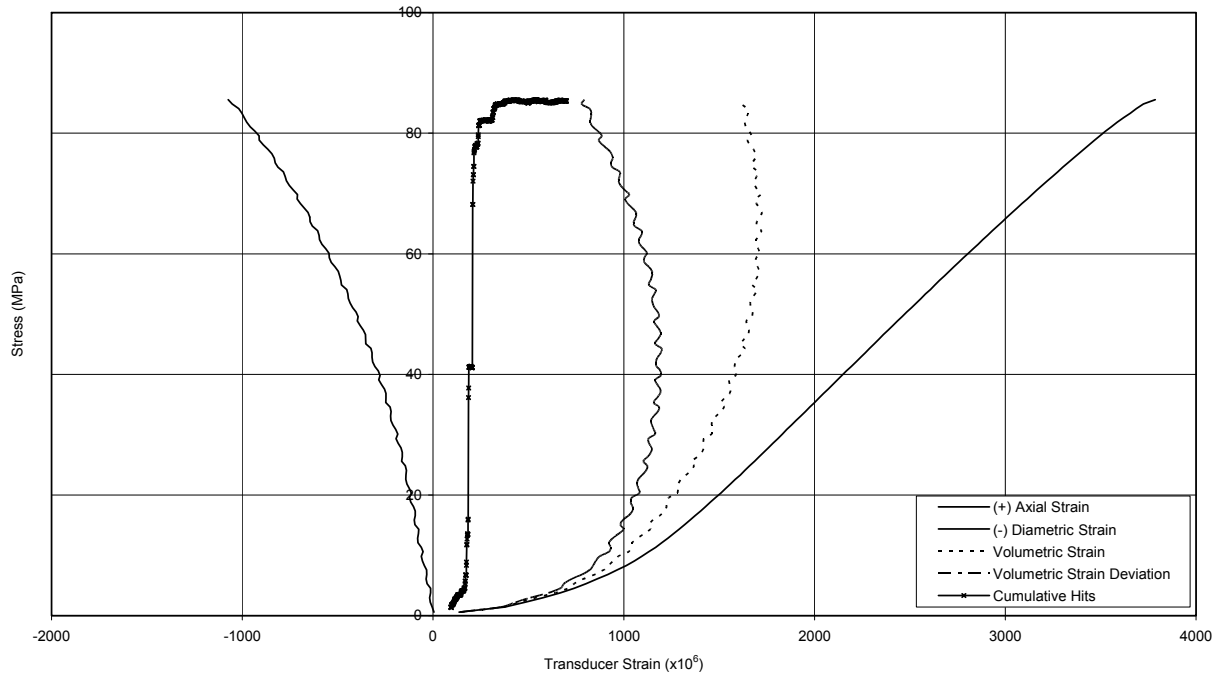
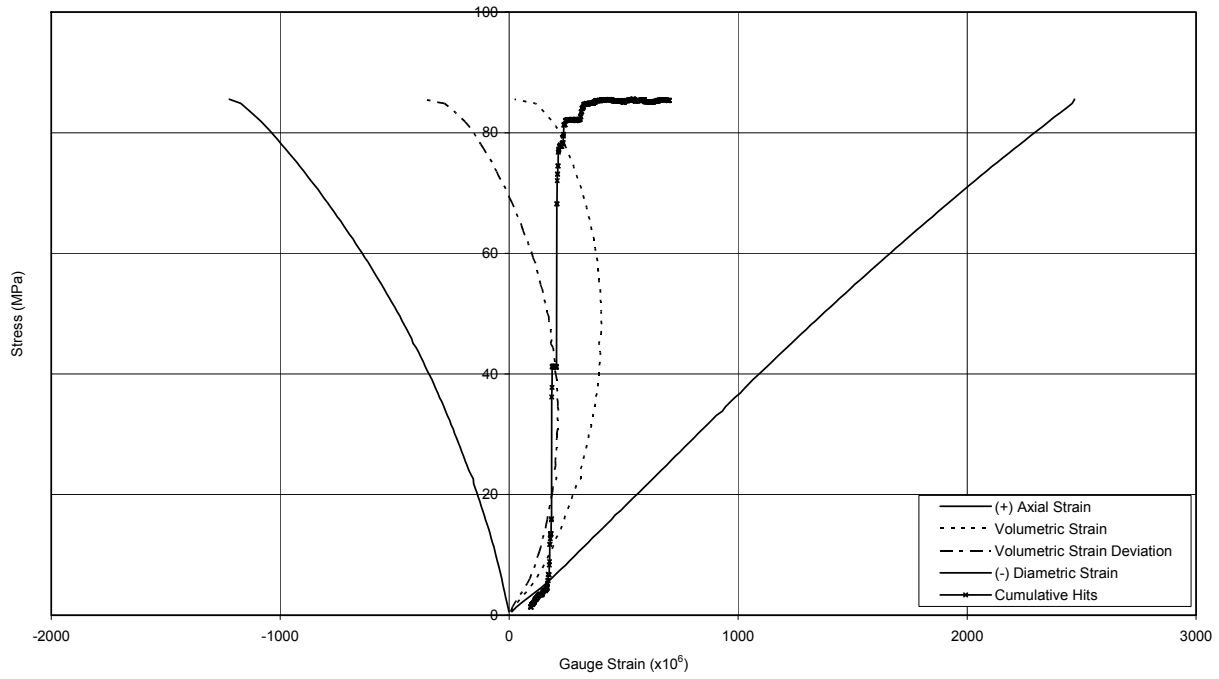


Figure B-11 Specimen DGR-1, 314.88 m

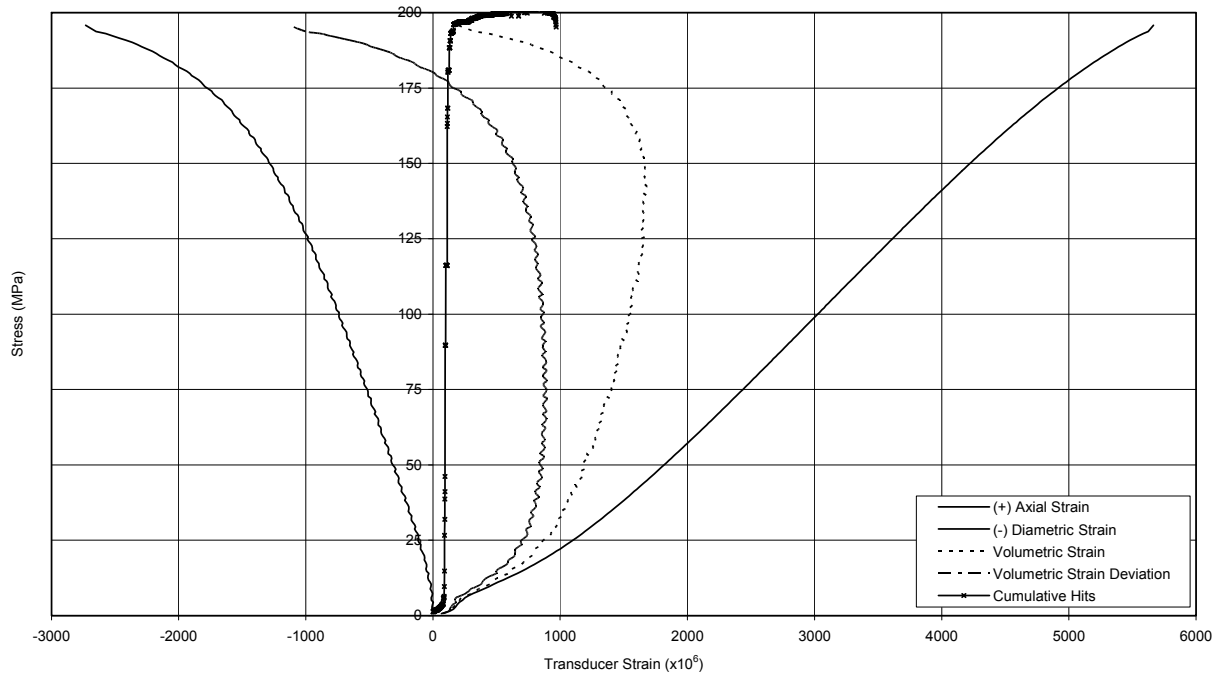
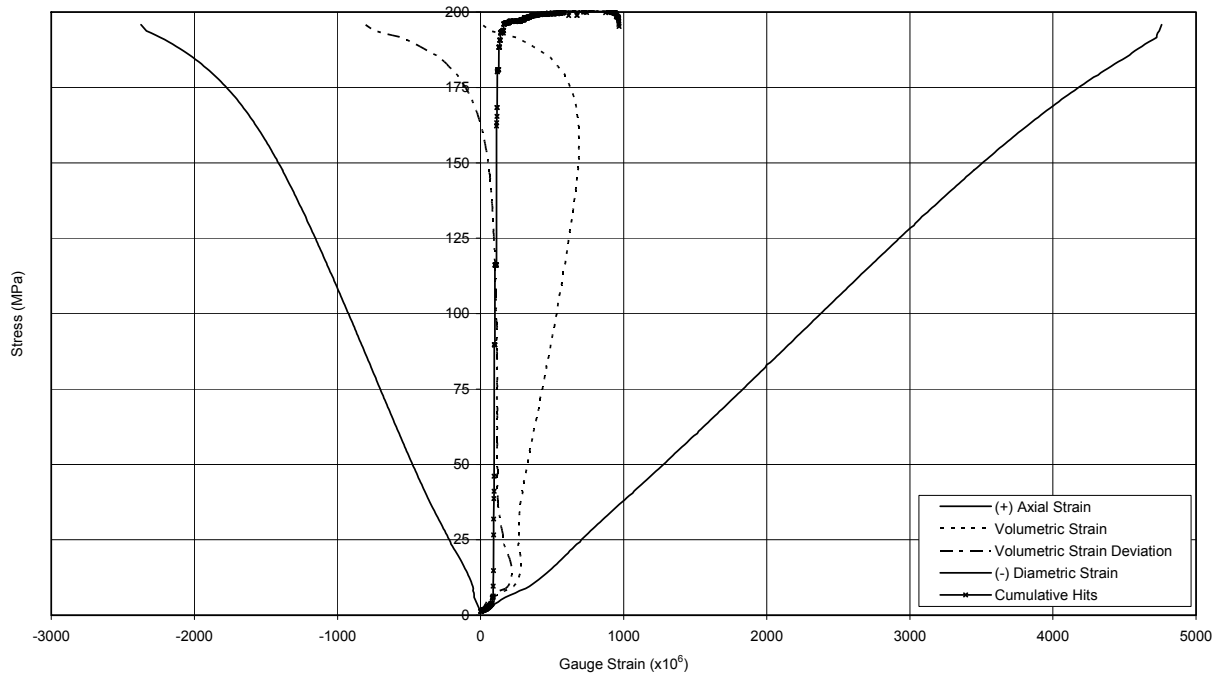


Figure B-12 Specimen DGR-1, 367.06 m

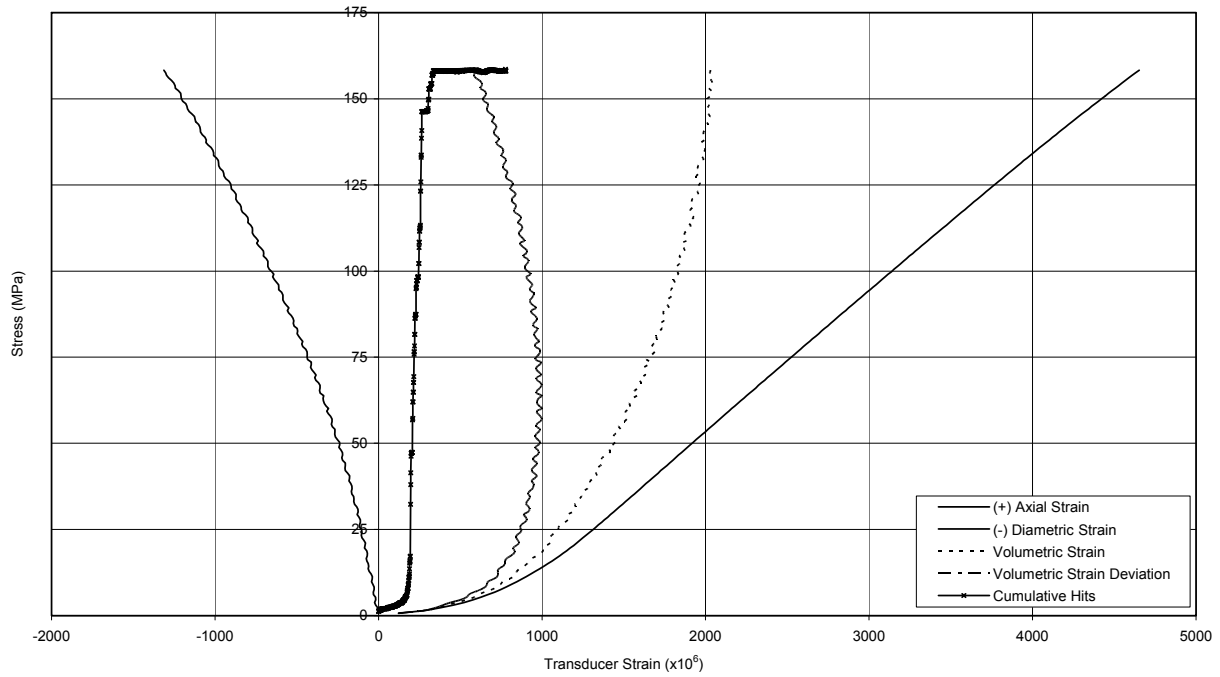
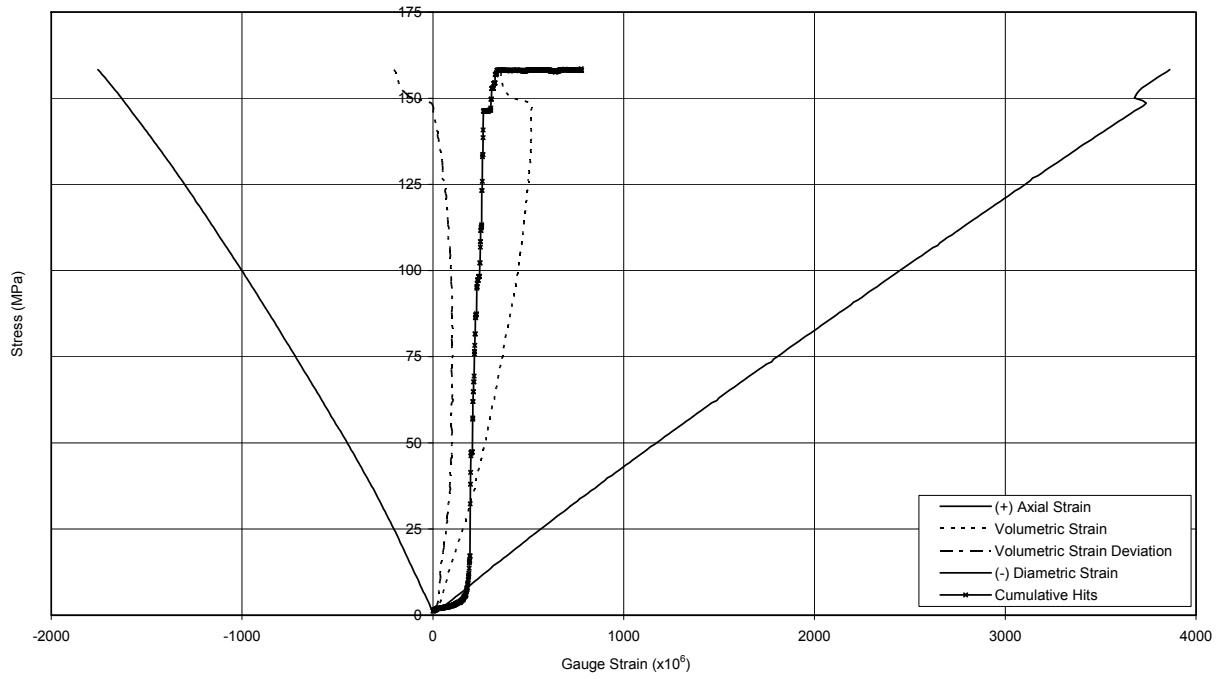


Figure B-13 Specimen DGR-1, 386.55 m

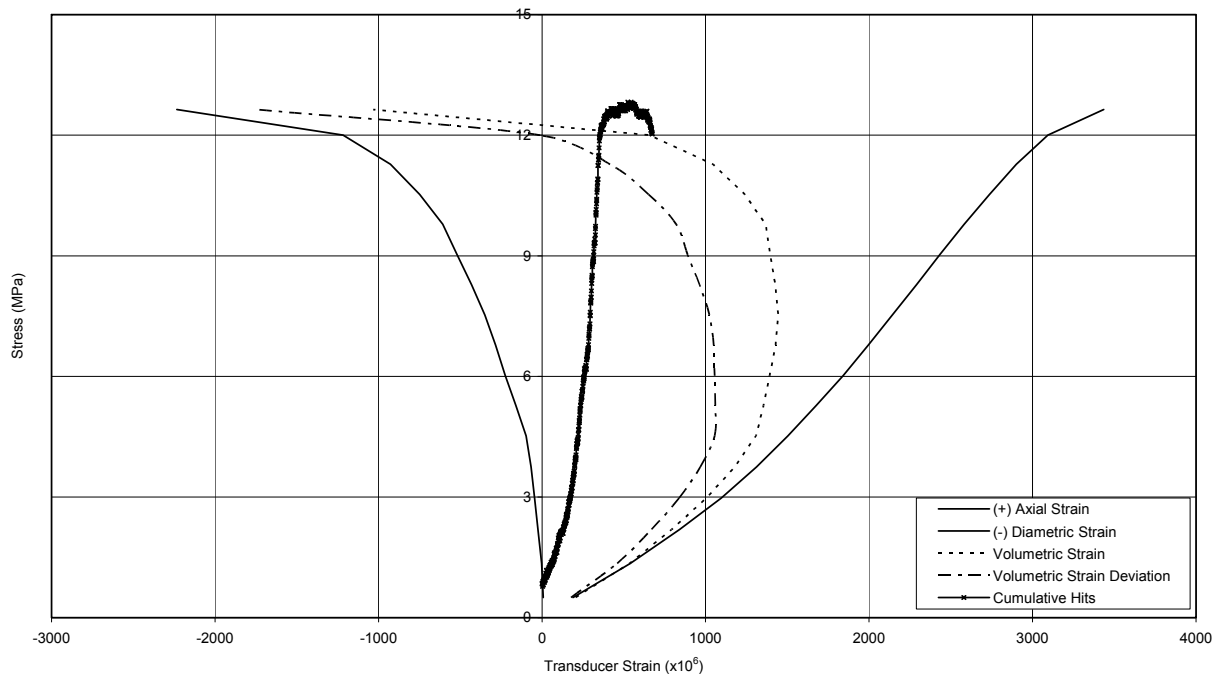
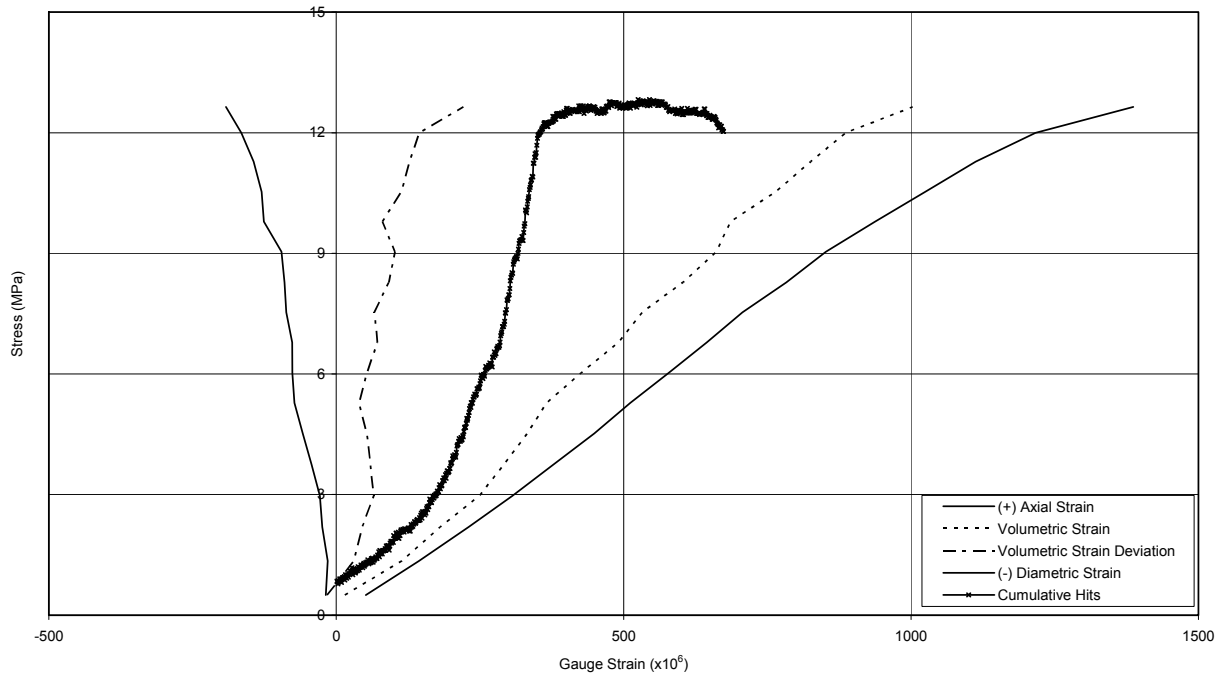


Figure B-14 Specimen DGR-1, 415.16 m

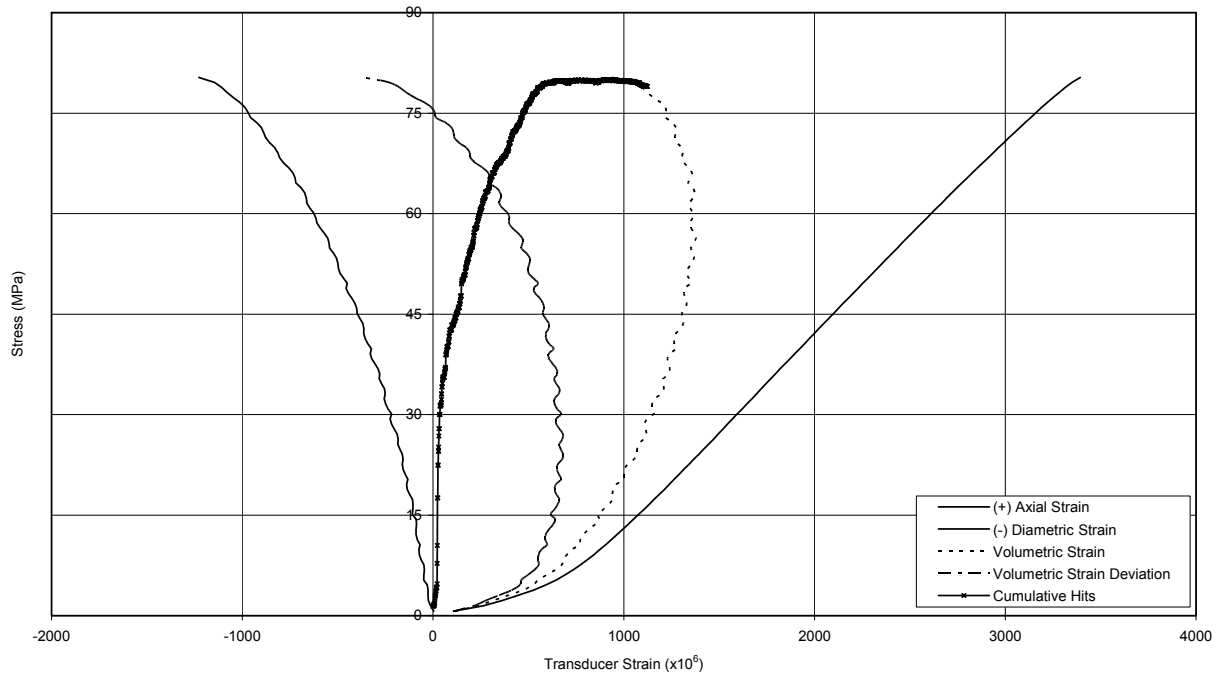
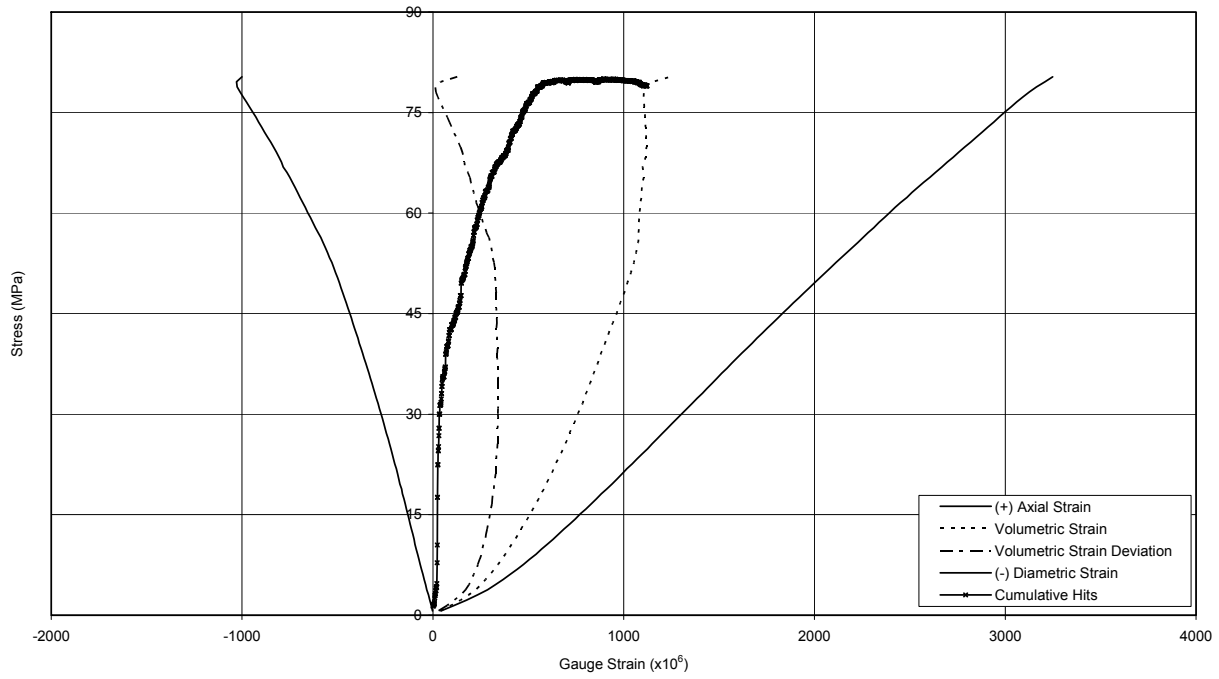


Figure B-15 Specimen DGR-1, 438.10 m

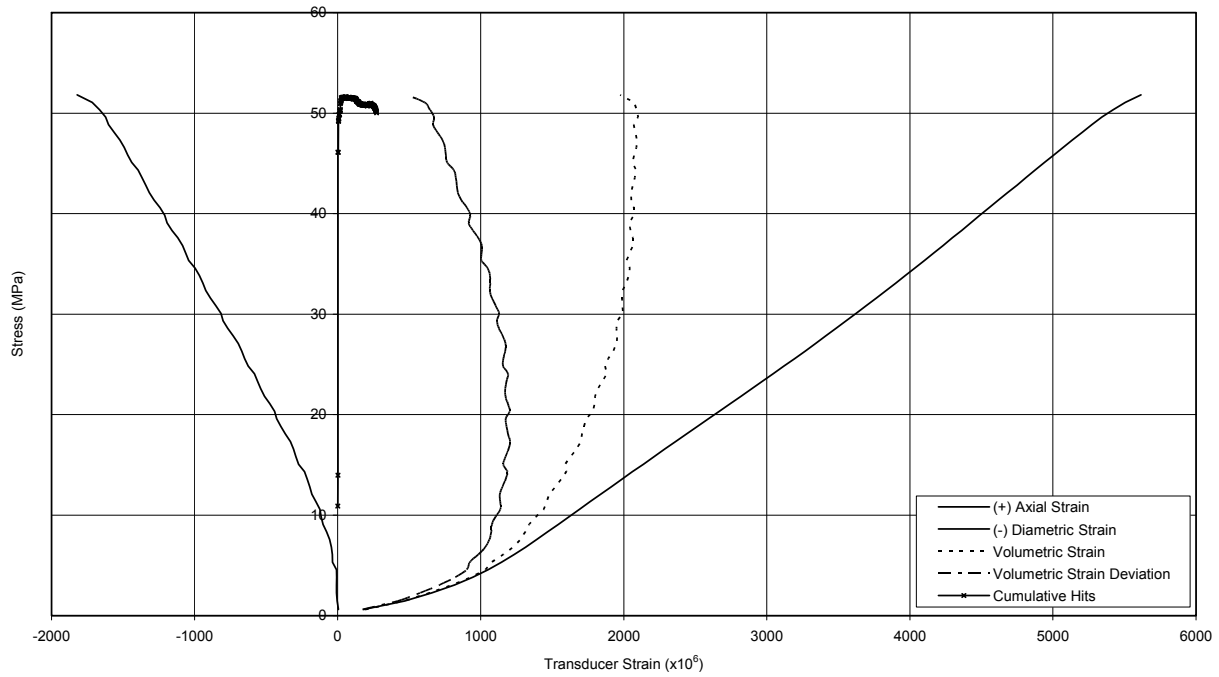
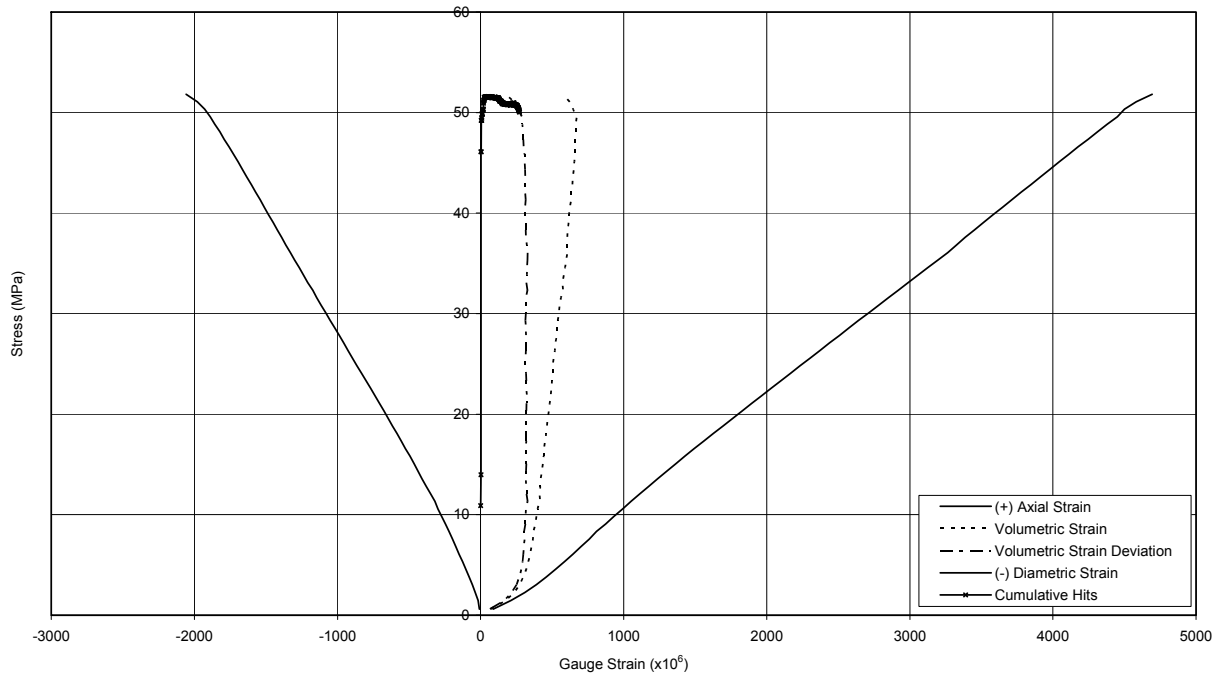


Figure B-16 Specimen DGR-1, 455.22 m

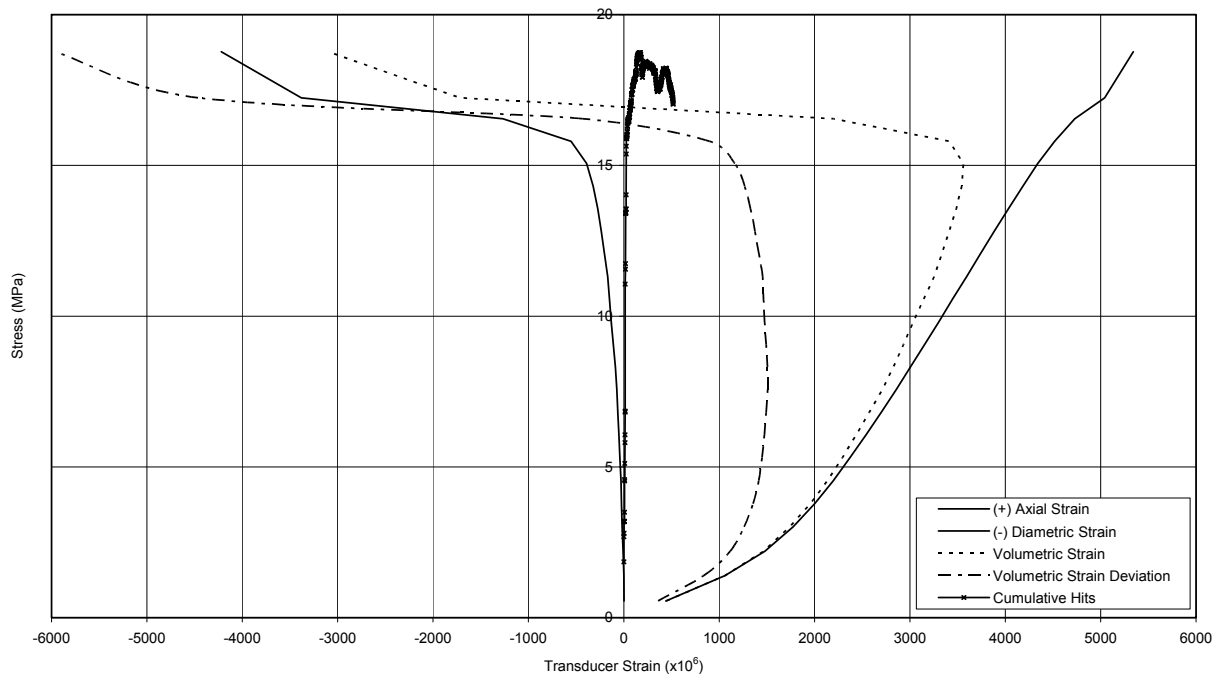
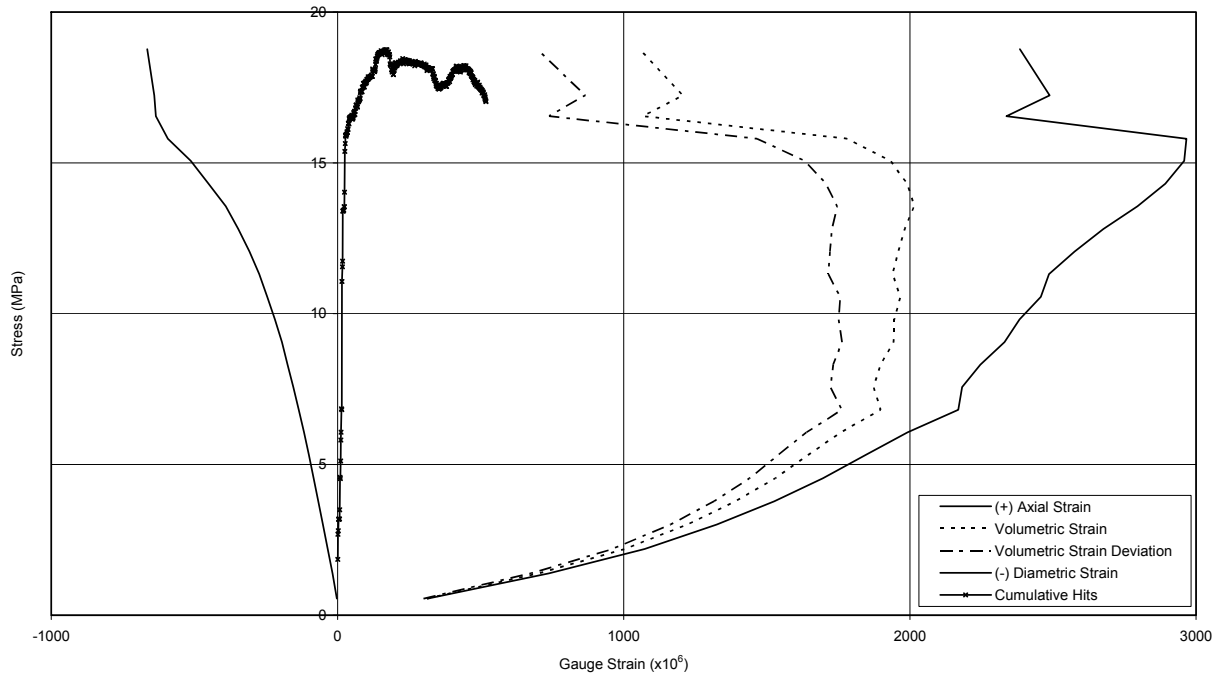


Figure B-17 Specimen DGR-1, 460.41 m

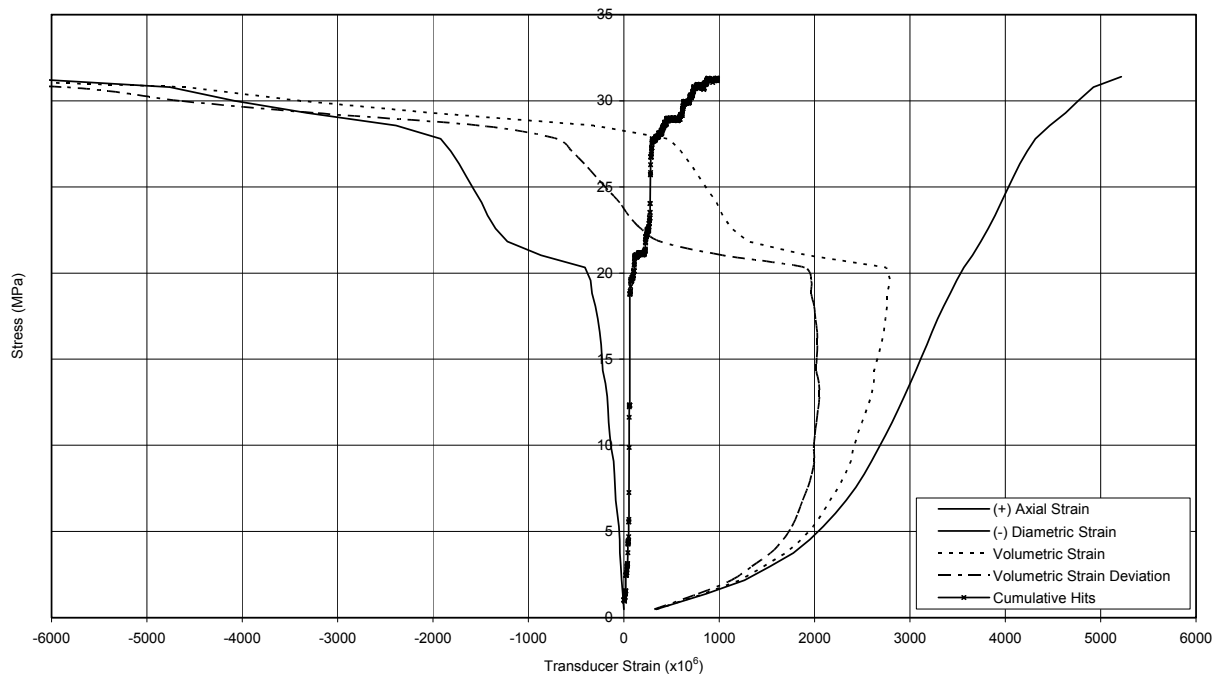
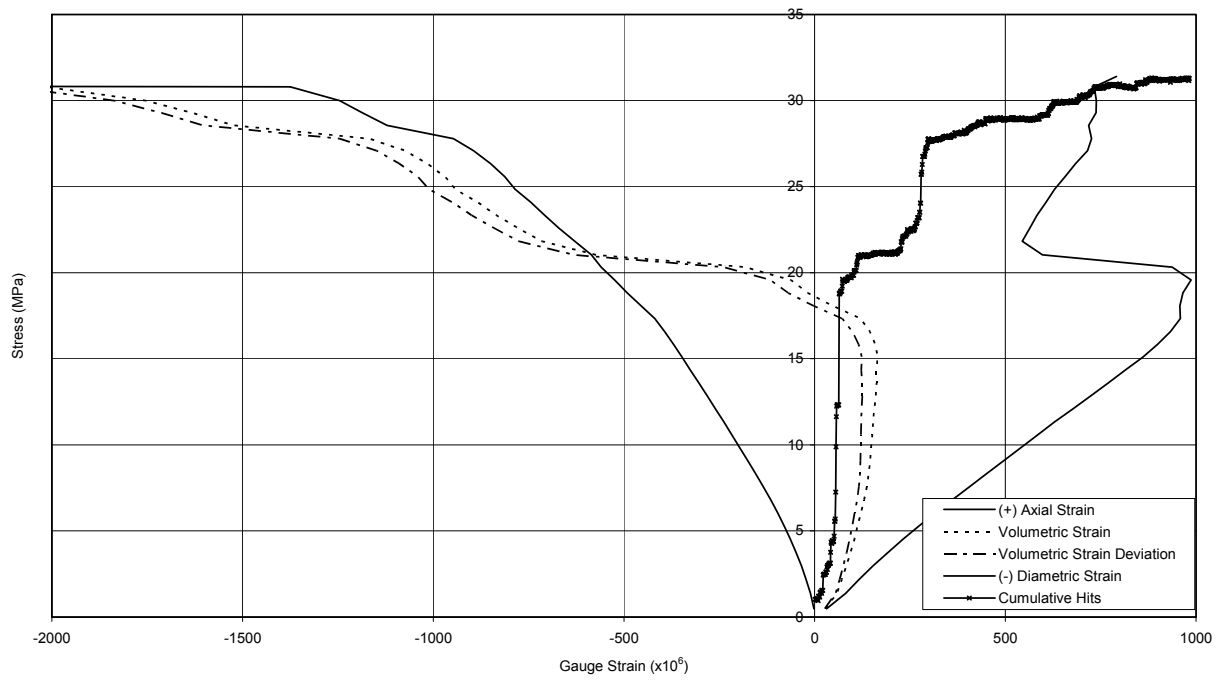


Figure B-18 Specimen DGR-2, 457.21 m

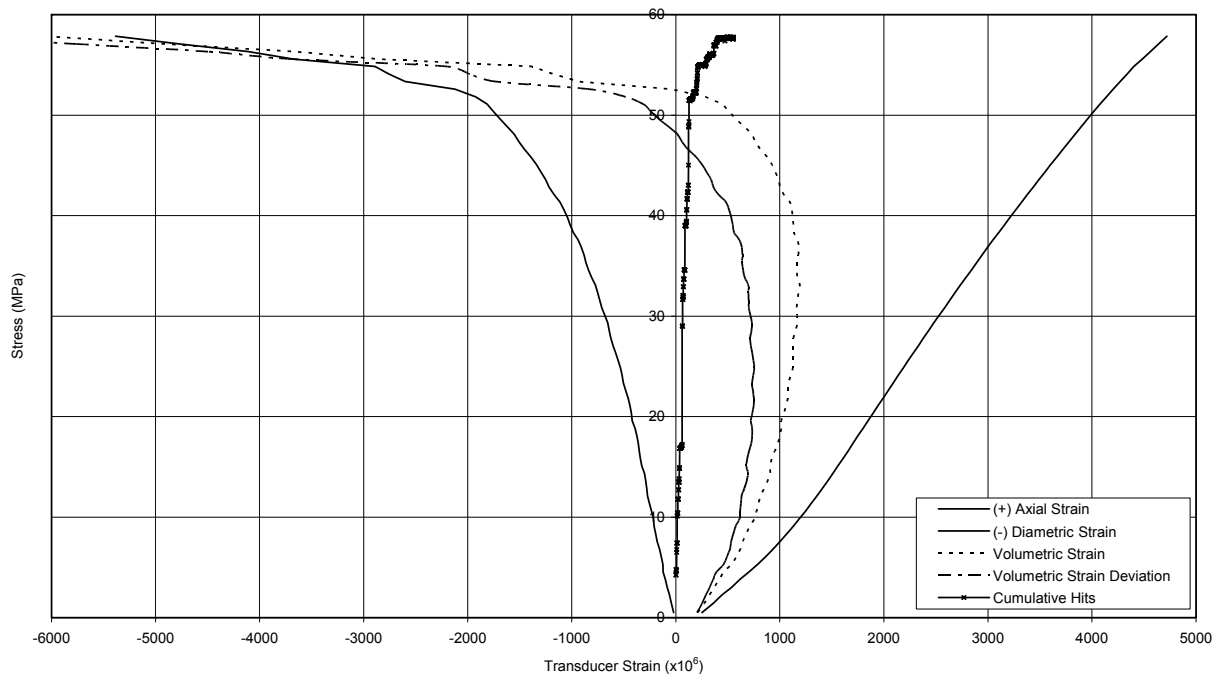
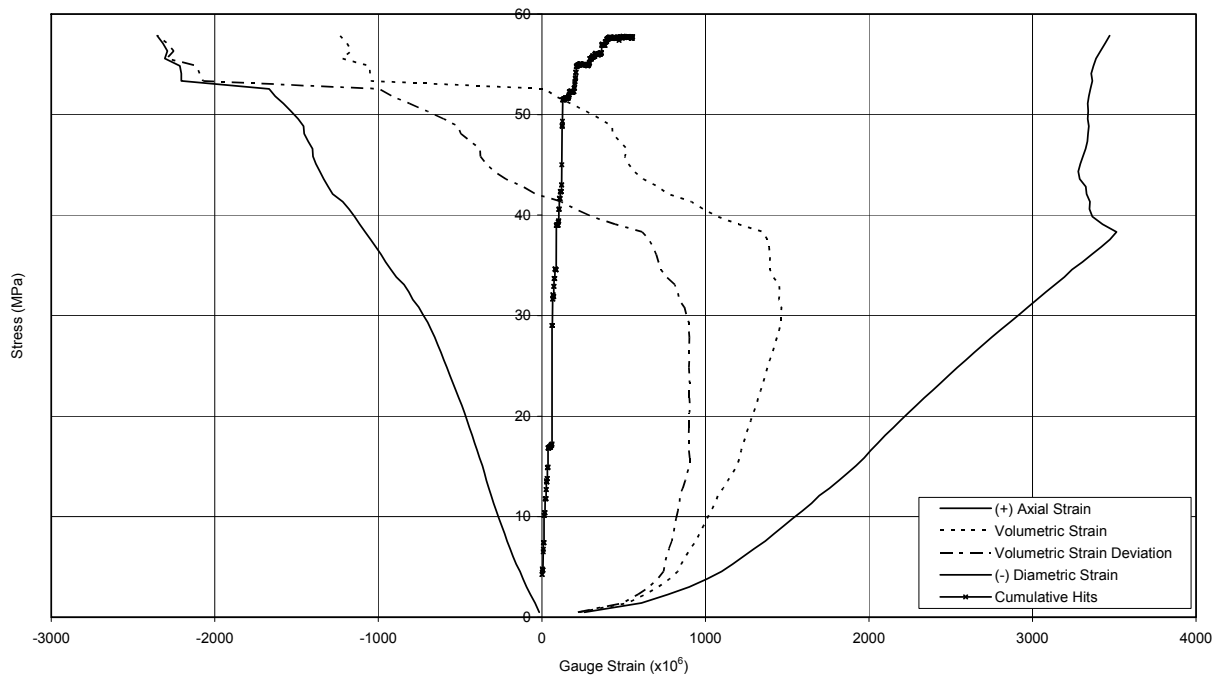


Figure B-19 Specimen DGR-2, 474.71 m

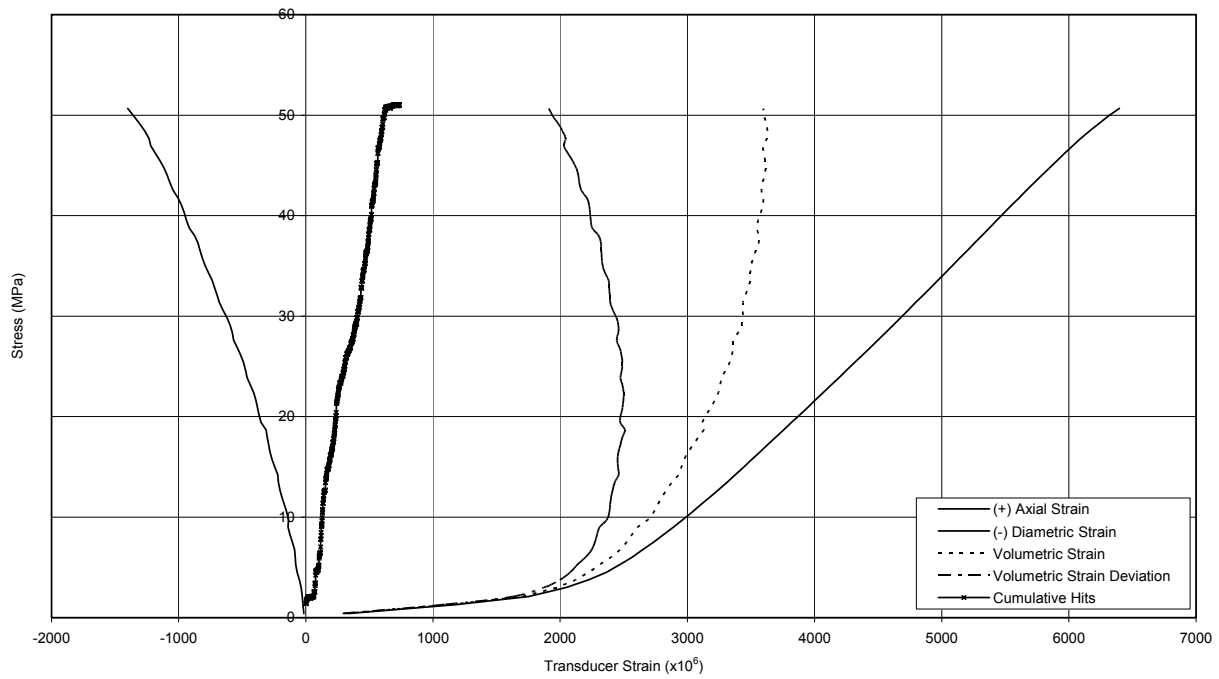
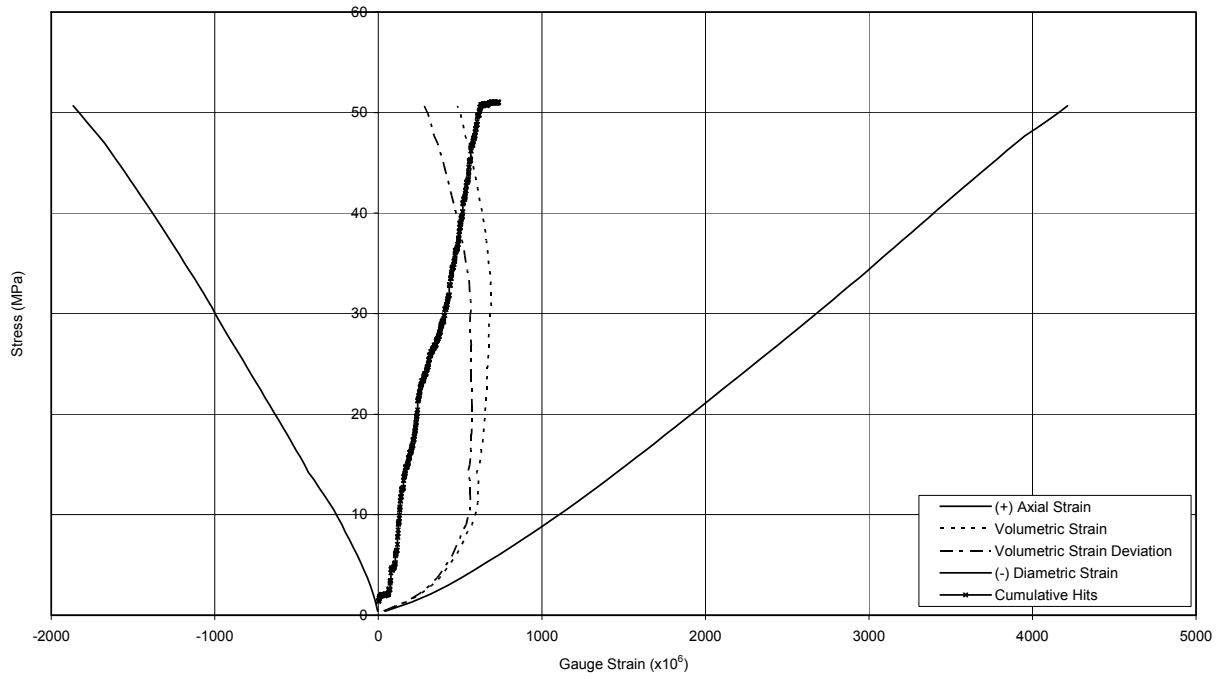


Figure B-20 Specimen DGR-2, 491.32 m

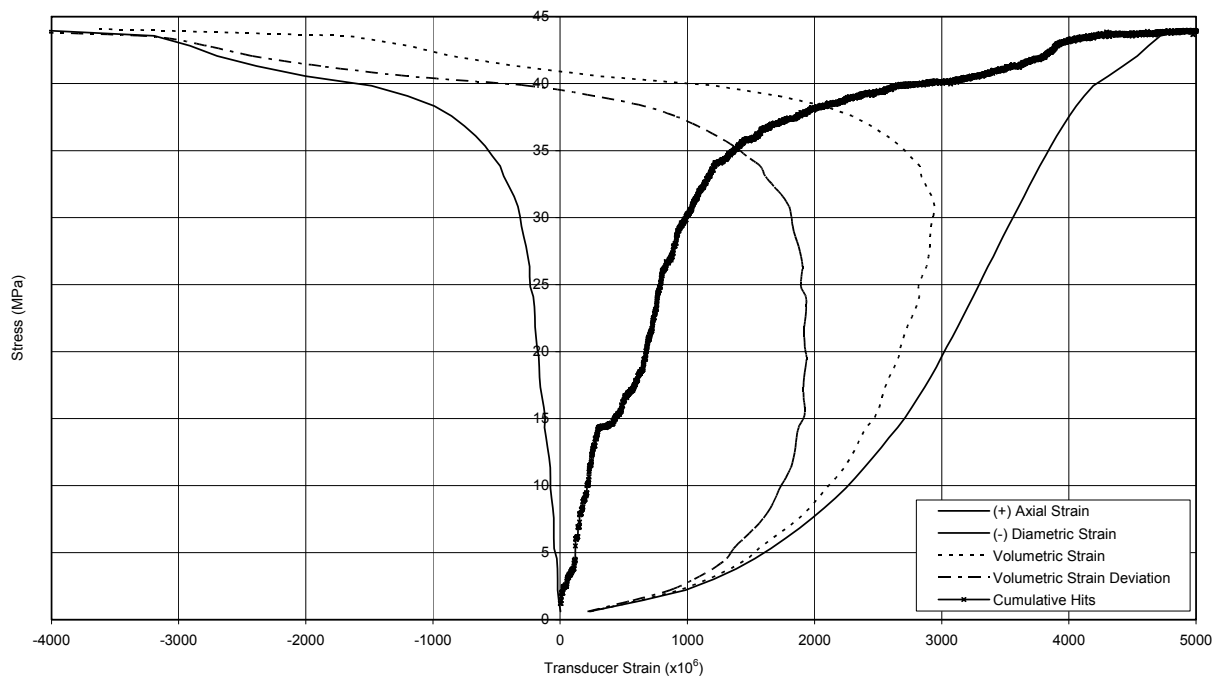
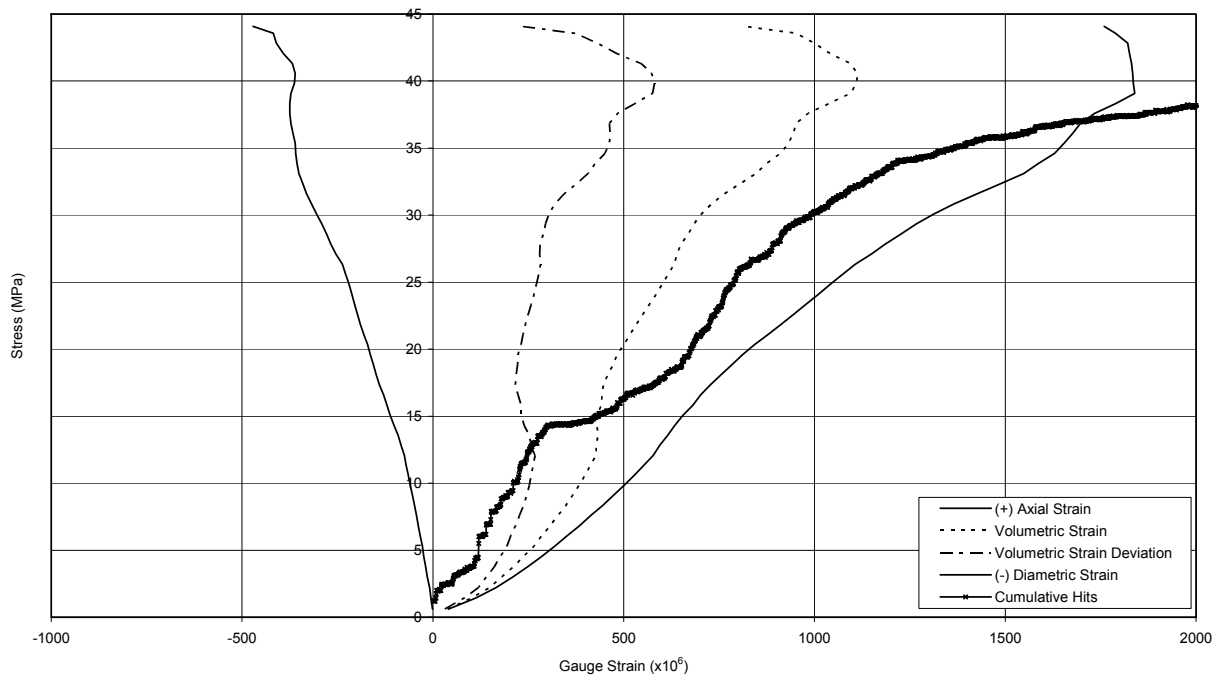


Figure B-21 Specimen DGR-2, 502.78 m

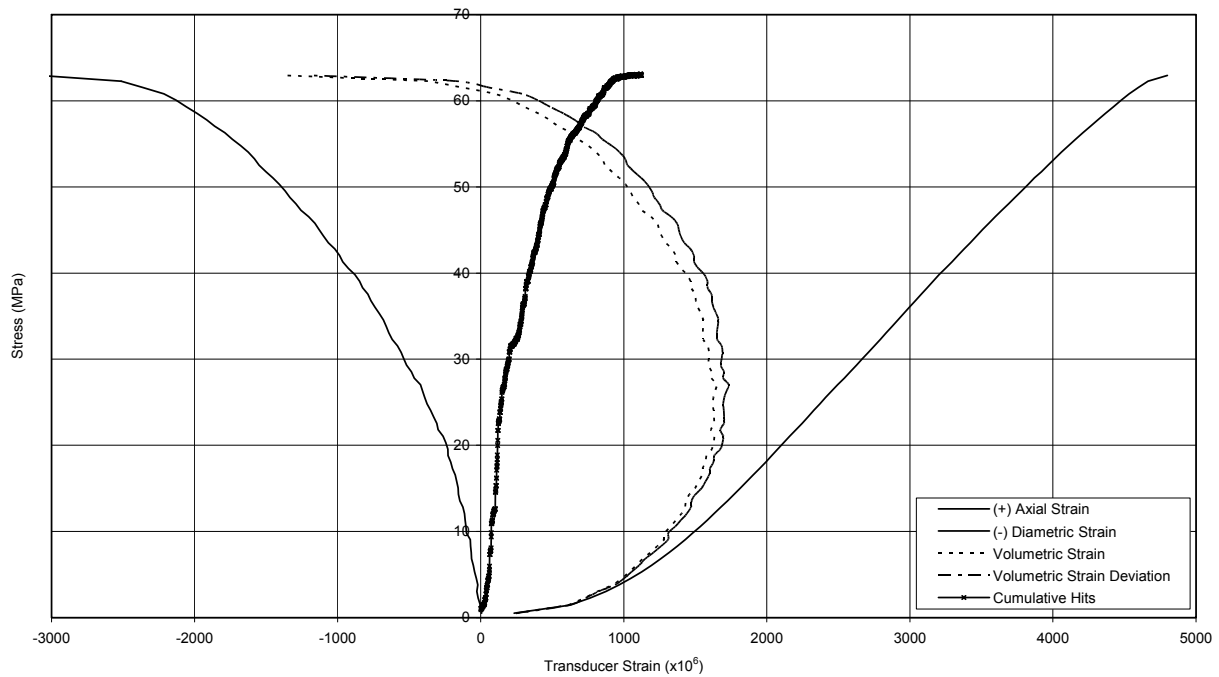
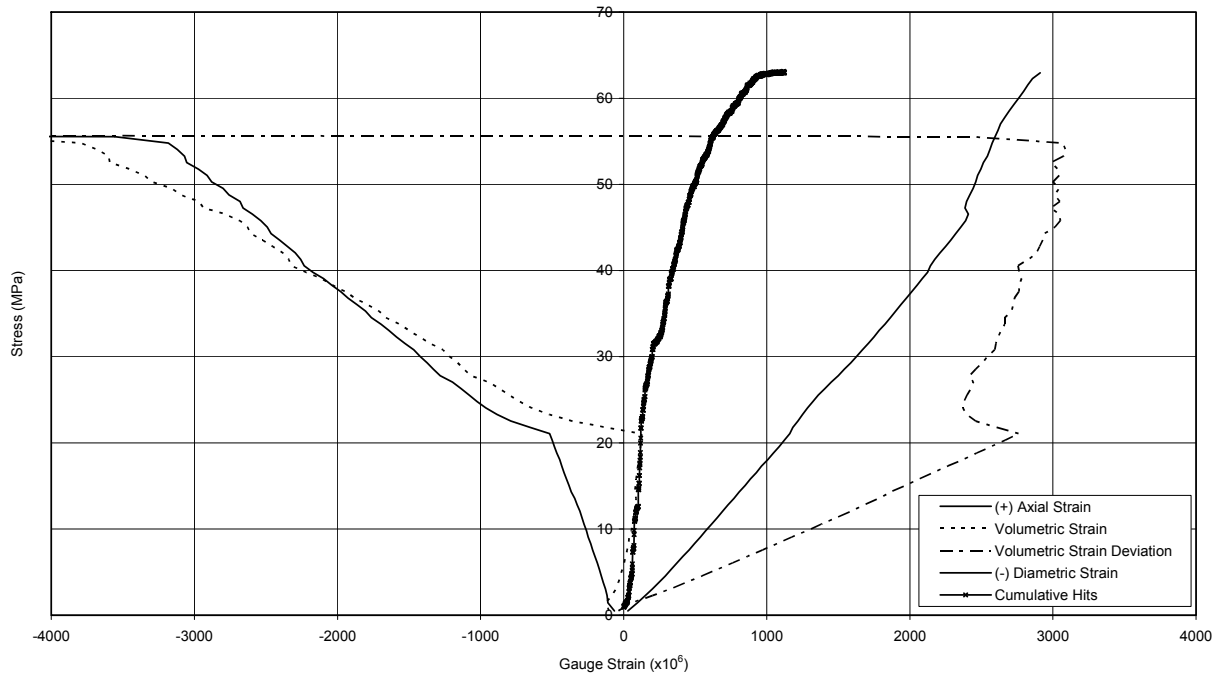


Figure B-22 Specimen DGR-2, 519.61 m

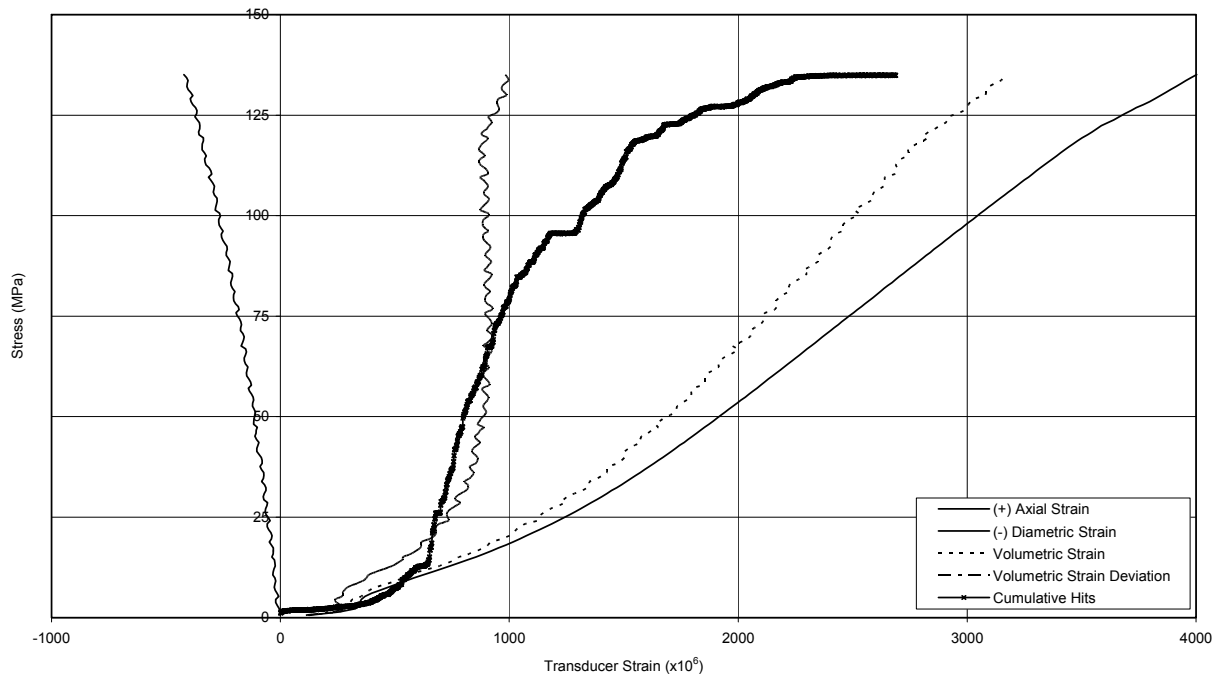
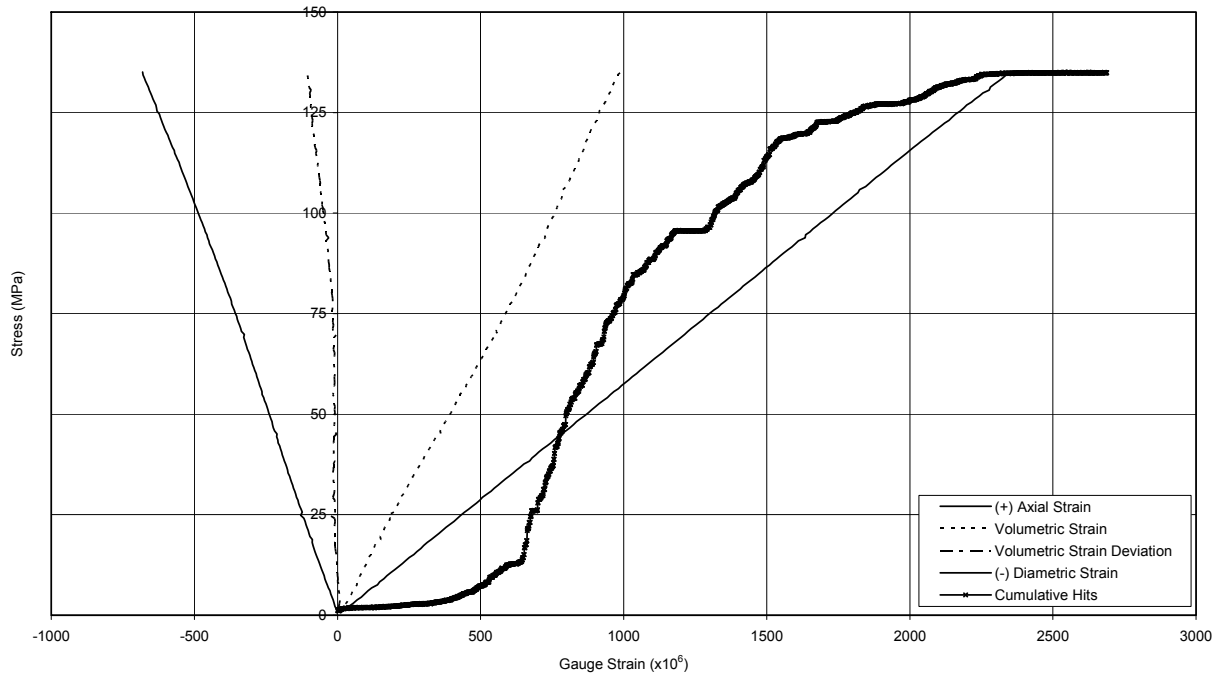


Figure B-23 Specimen DGR-2, 533.94 m

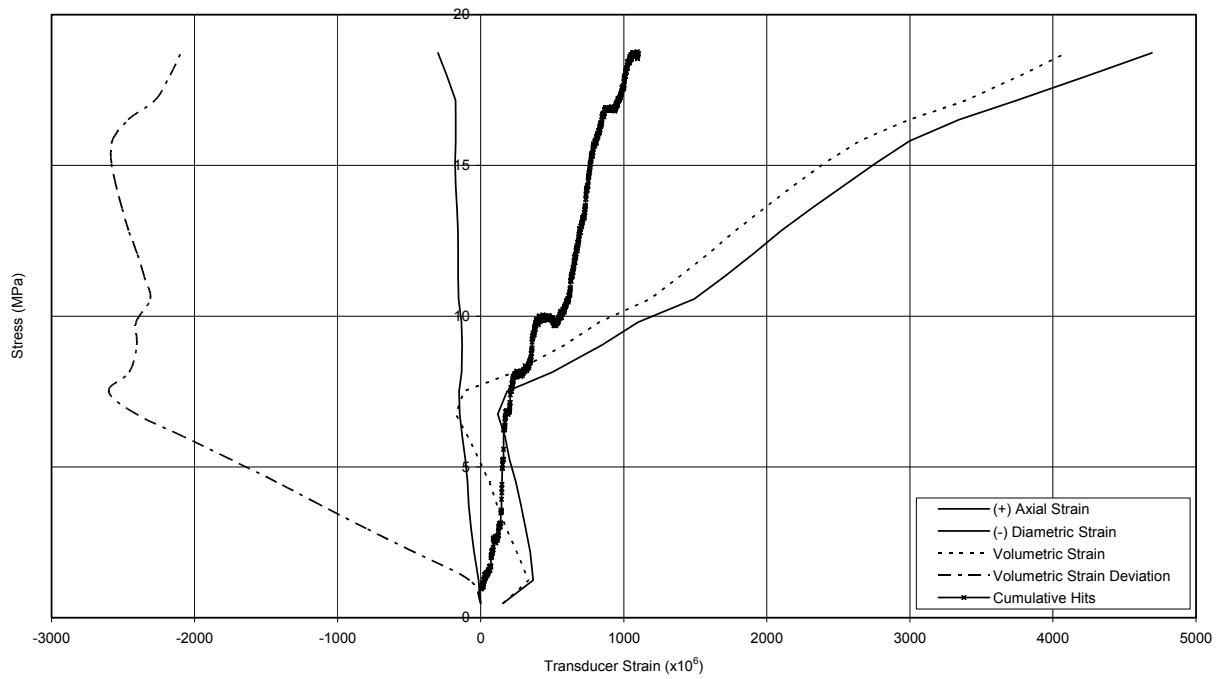
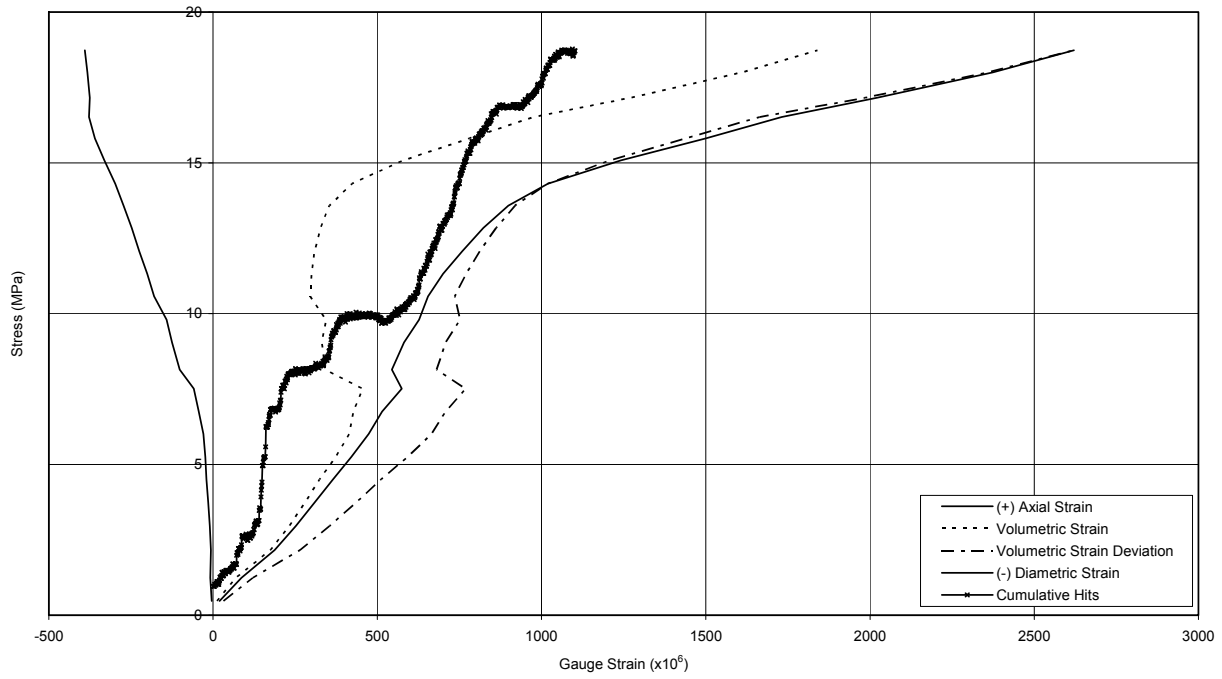


Figure B-24 Specimen DGR-2, 580.99 m

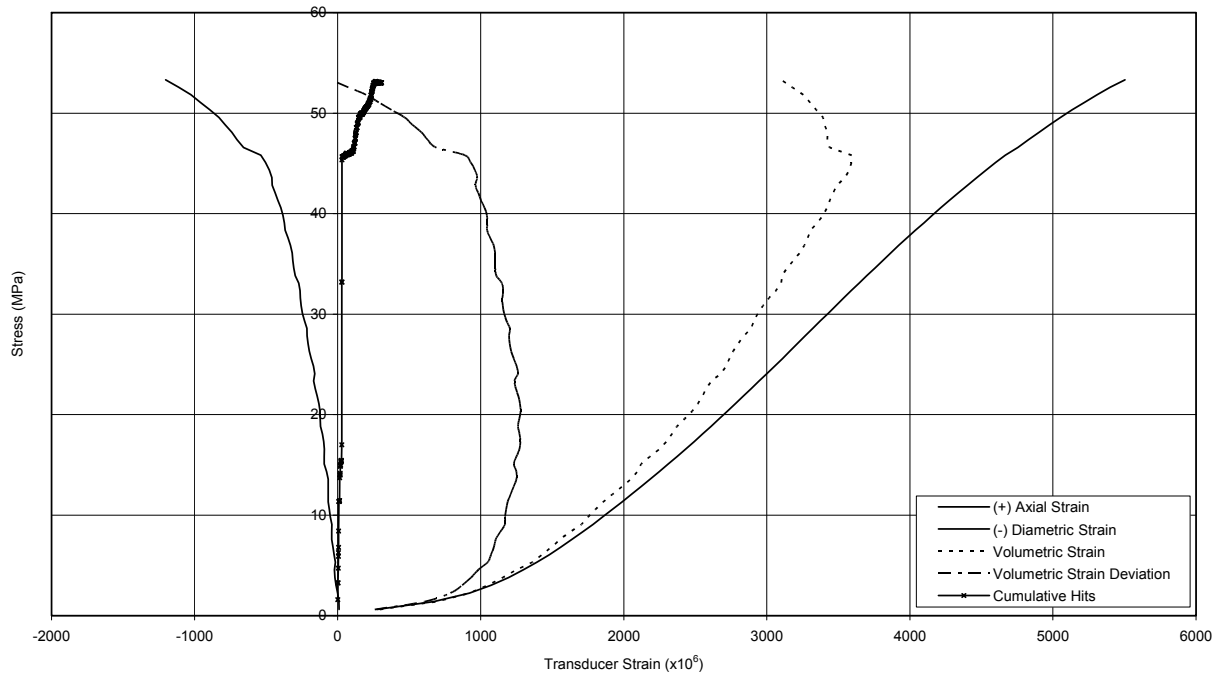
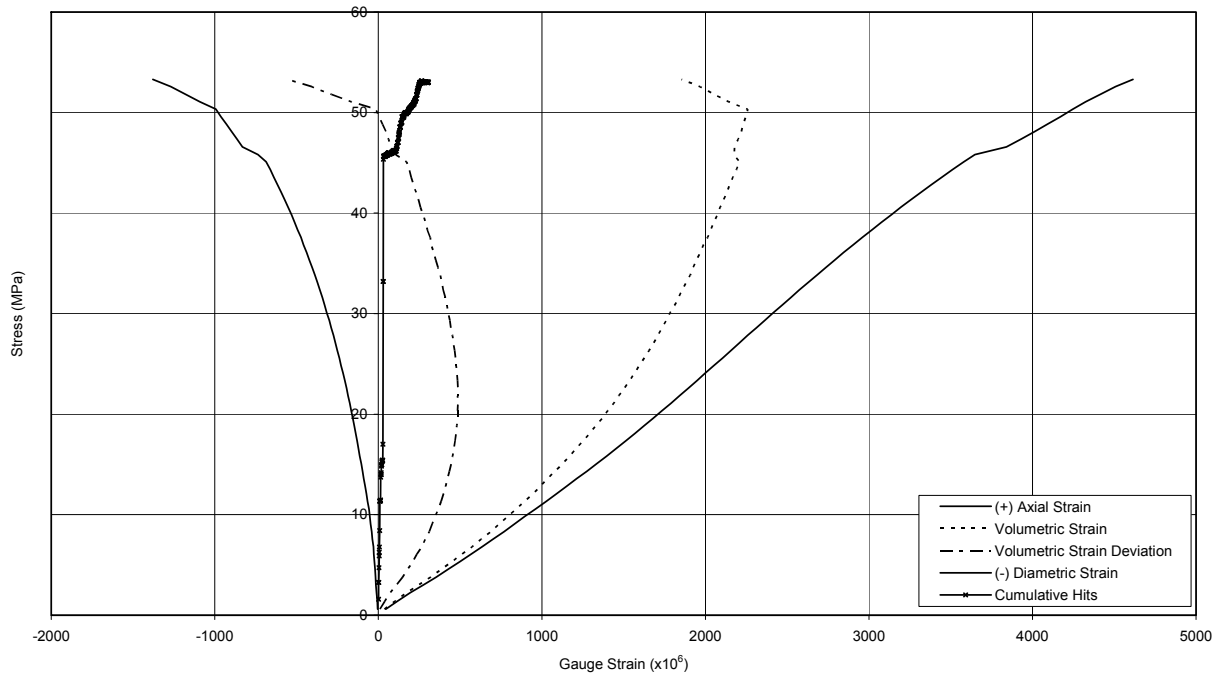


Figure B-25 Specimen DGR-2, 586.35 m

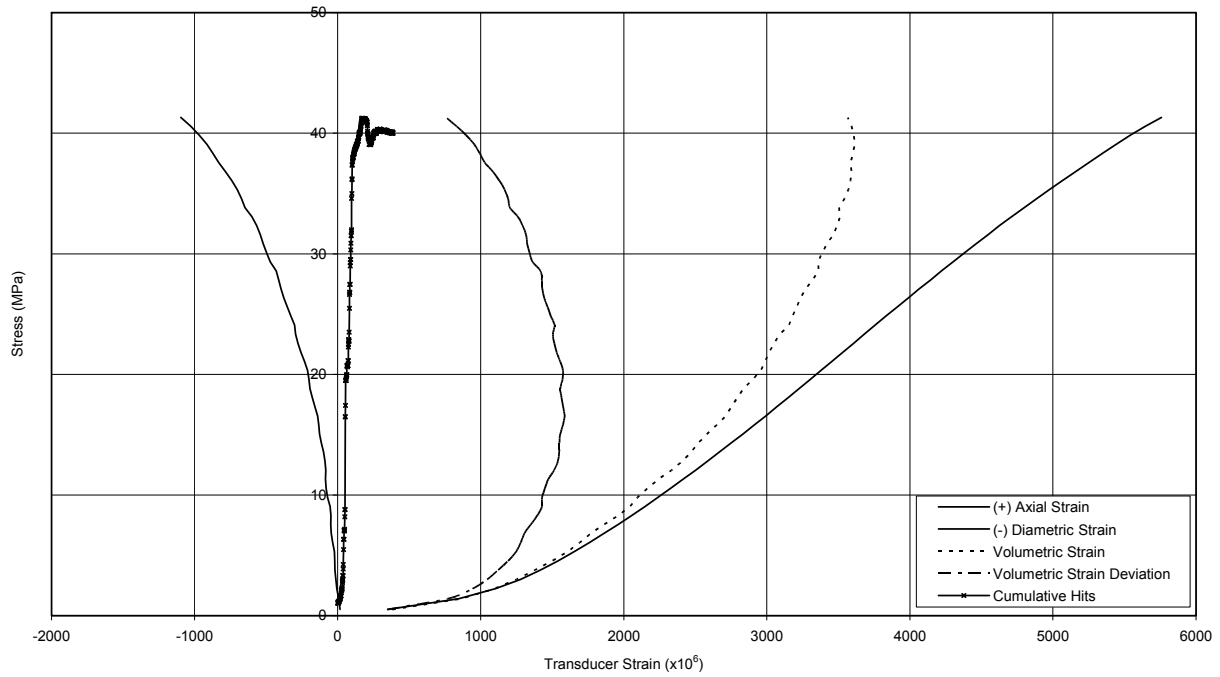
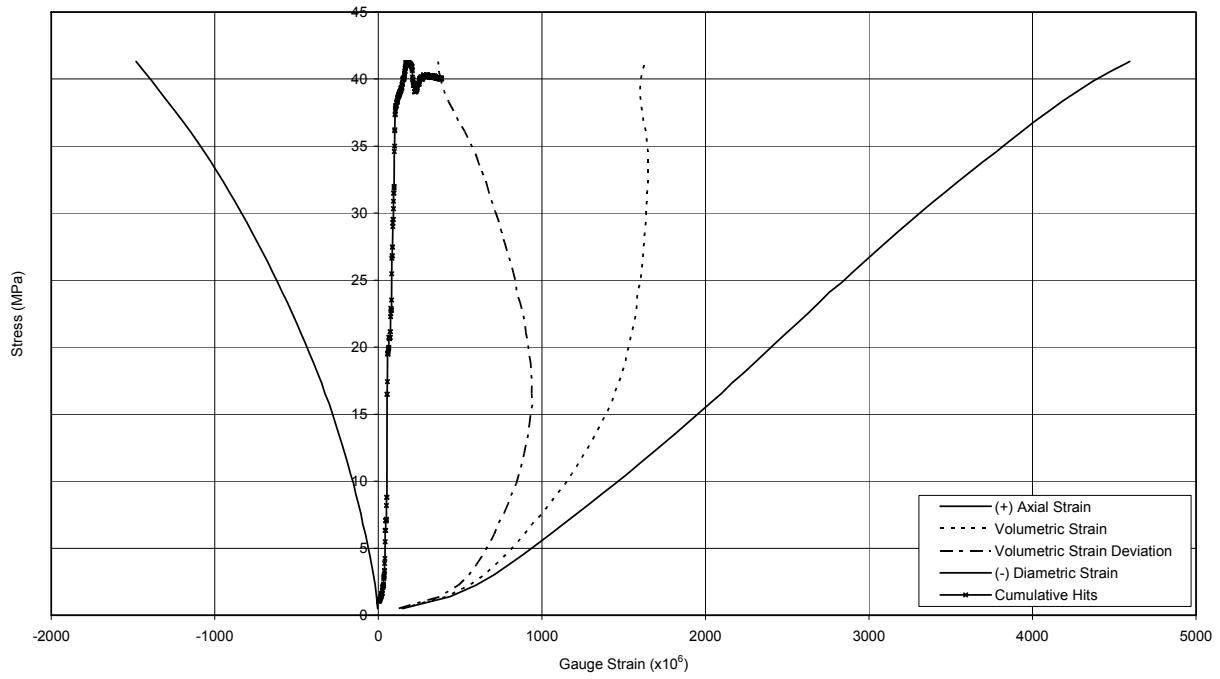


Figure B-26 Specimen DGR-2, 587.51 m

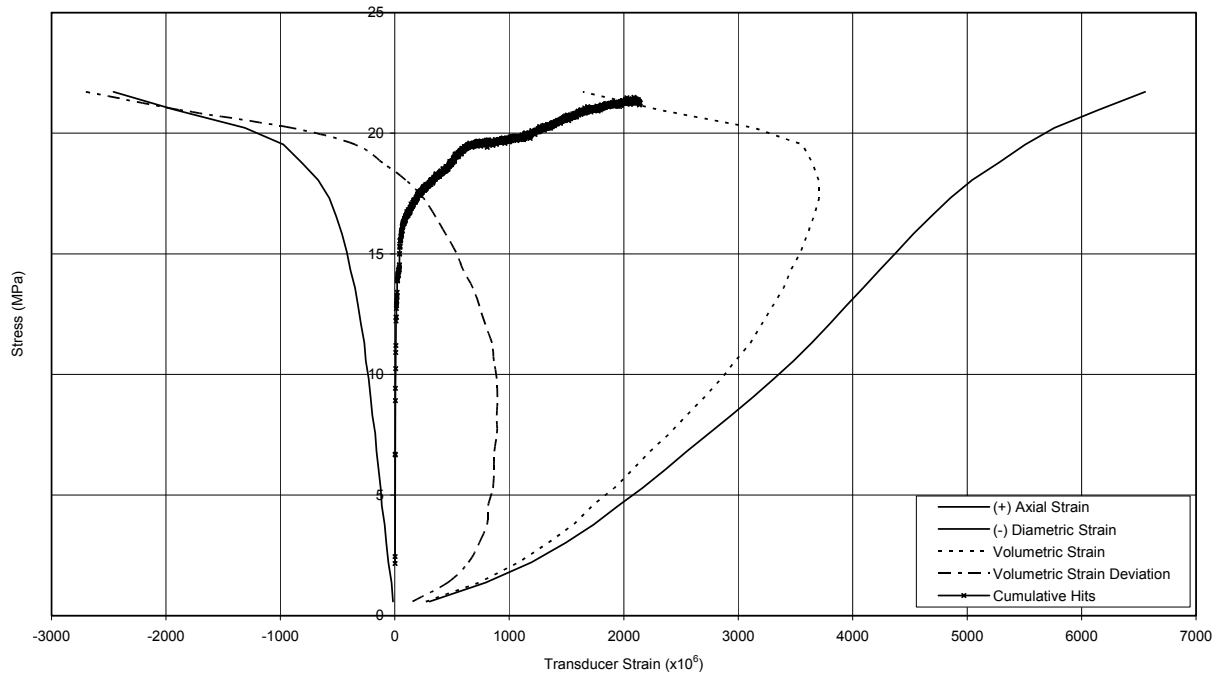
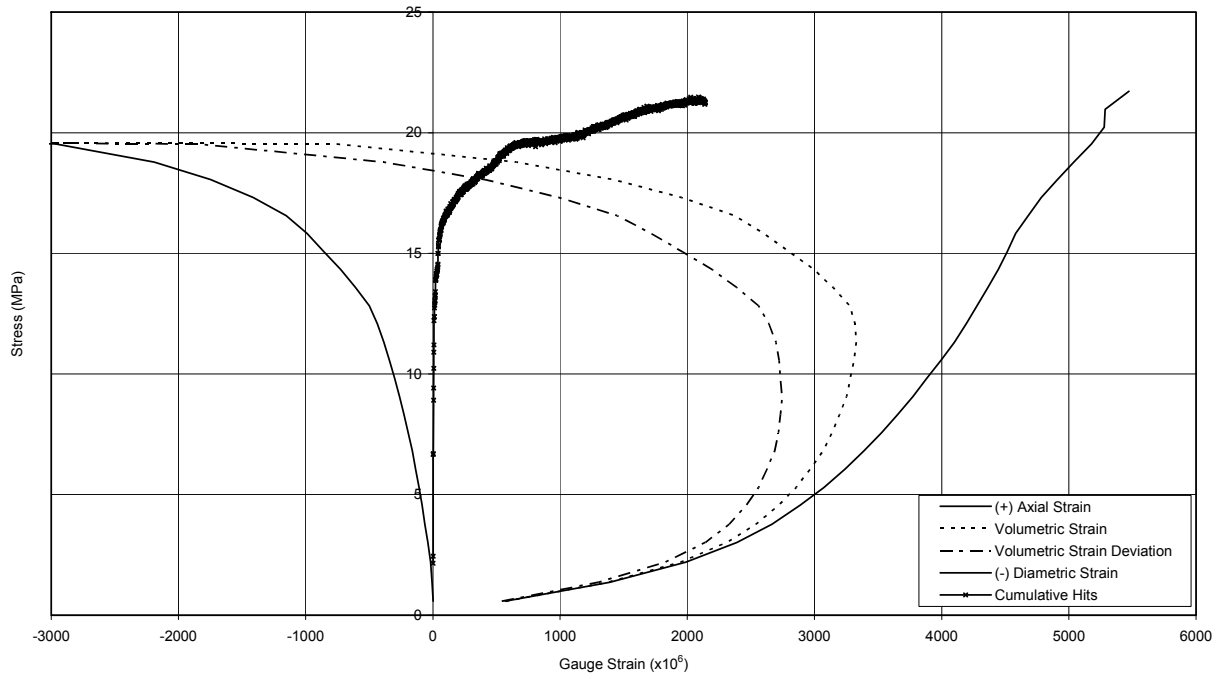


Figure B-27 Specimen DGR-2, 606.50 m

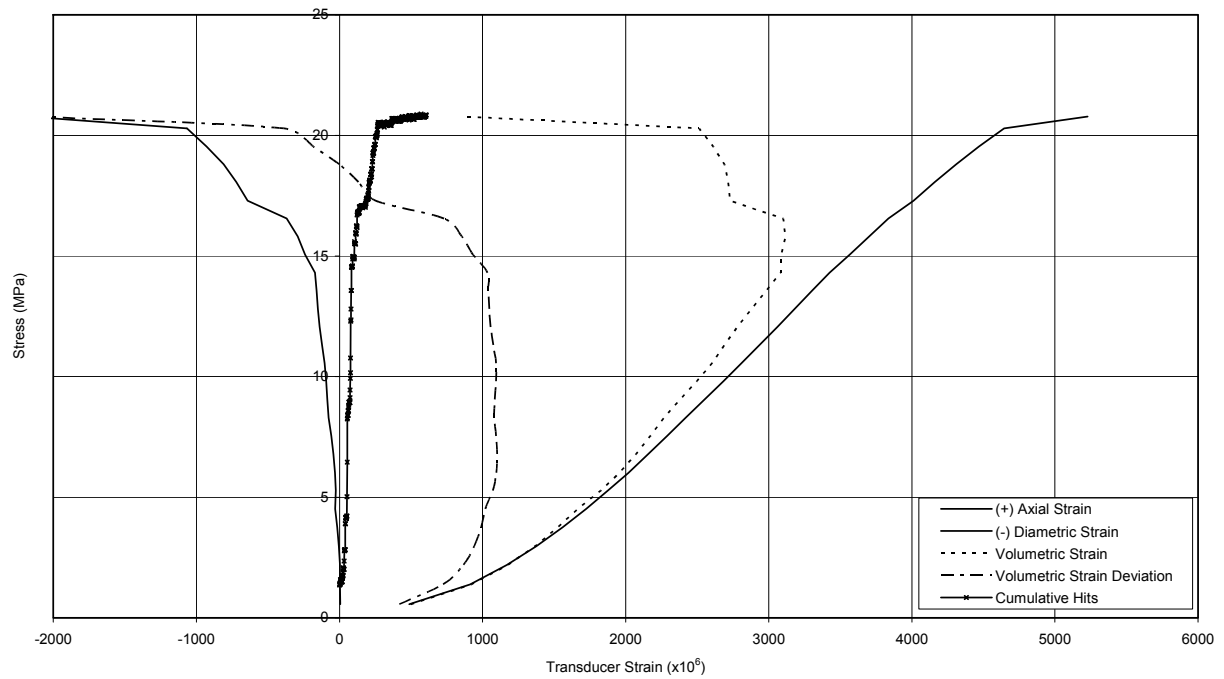
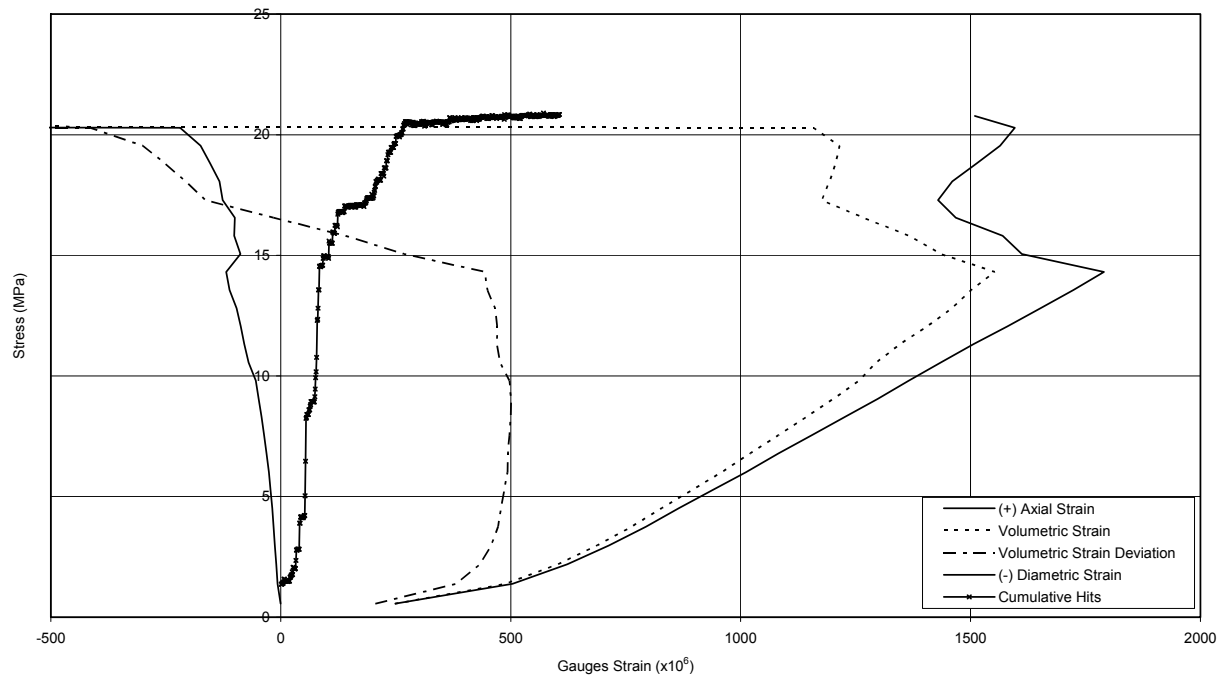


Figure B-28 Specimen DGR-2, 646.42 m

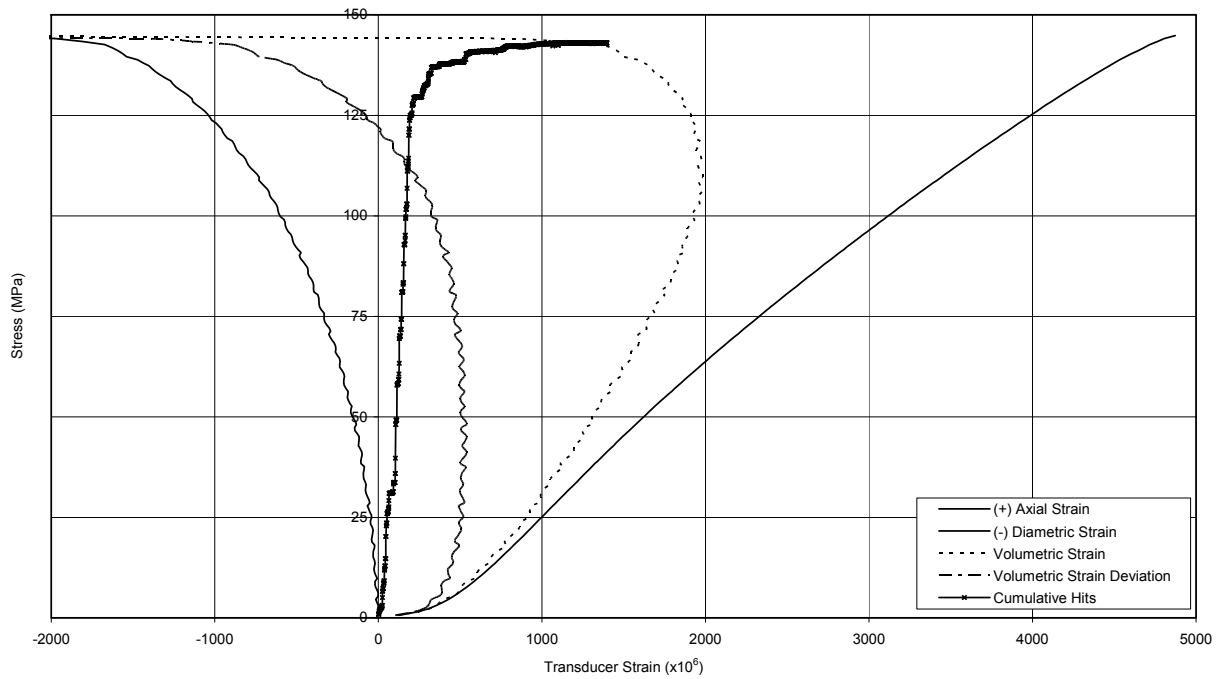
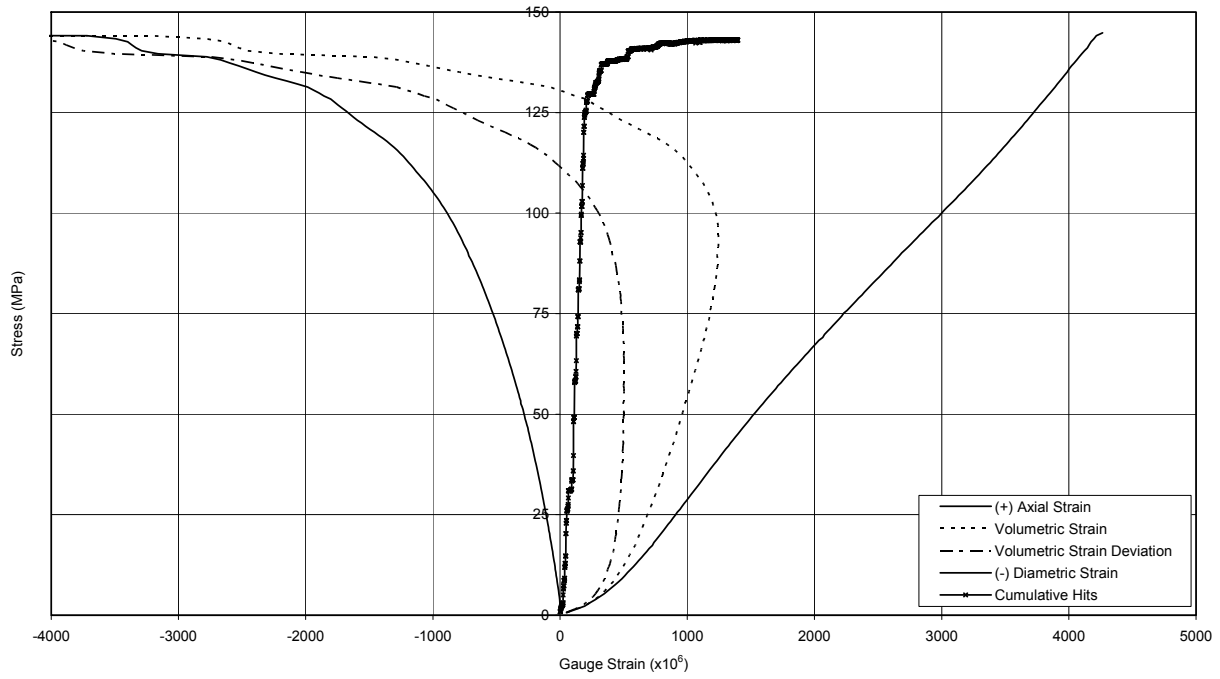


Figure B-29 Specimen DGR-2, 654.97 m

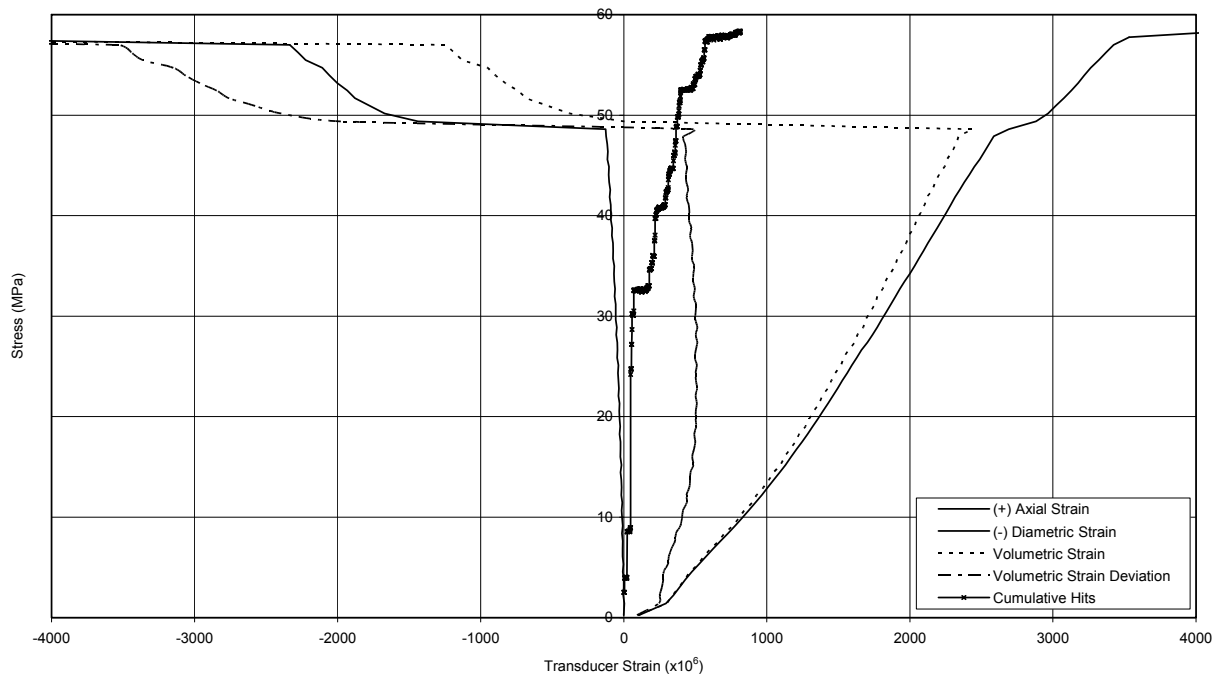
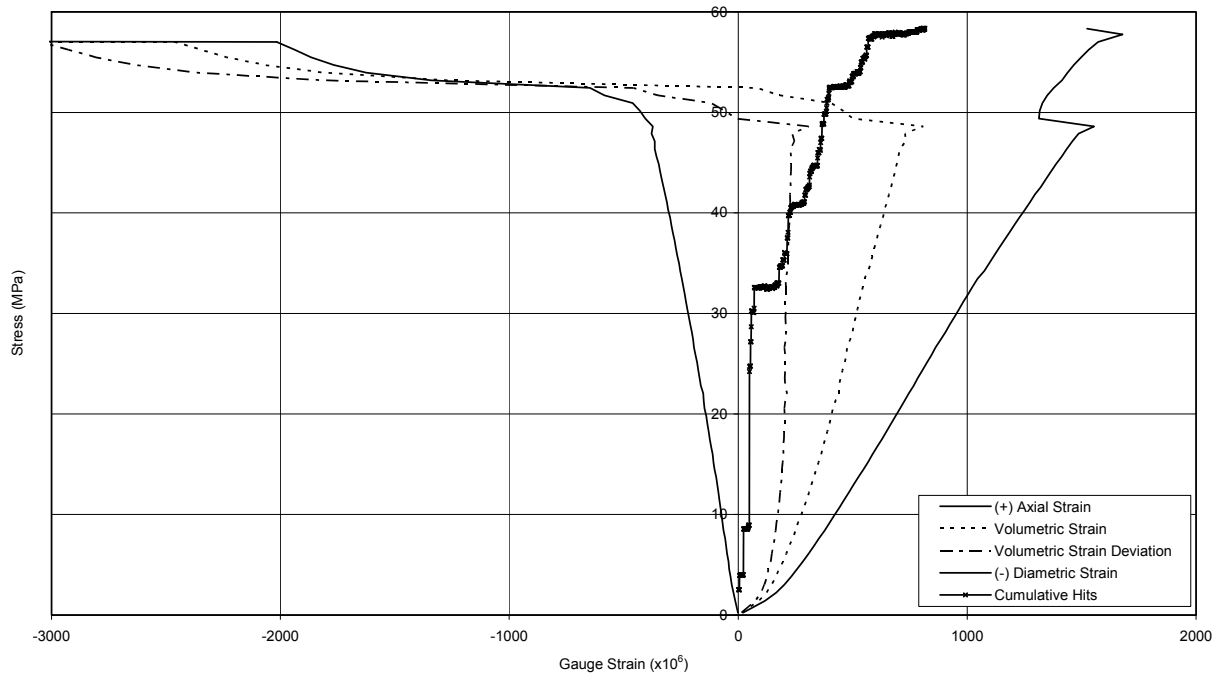


Figure B-30 Specimen DGR-2, 655.32 m

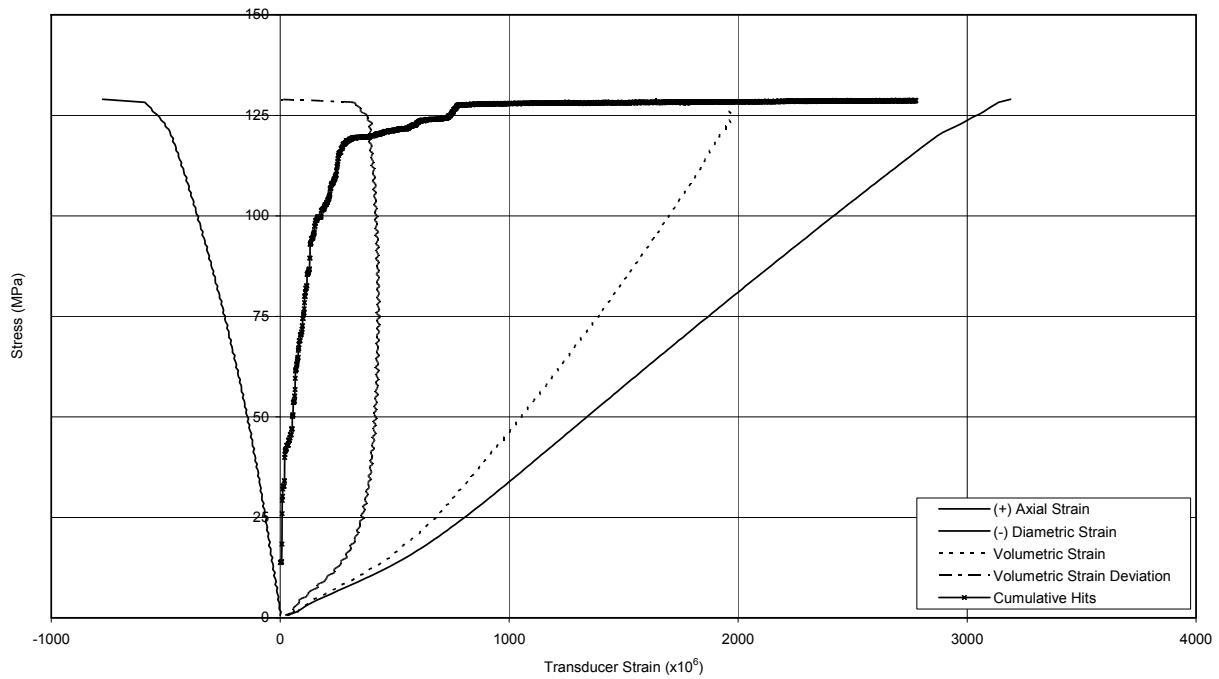
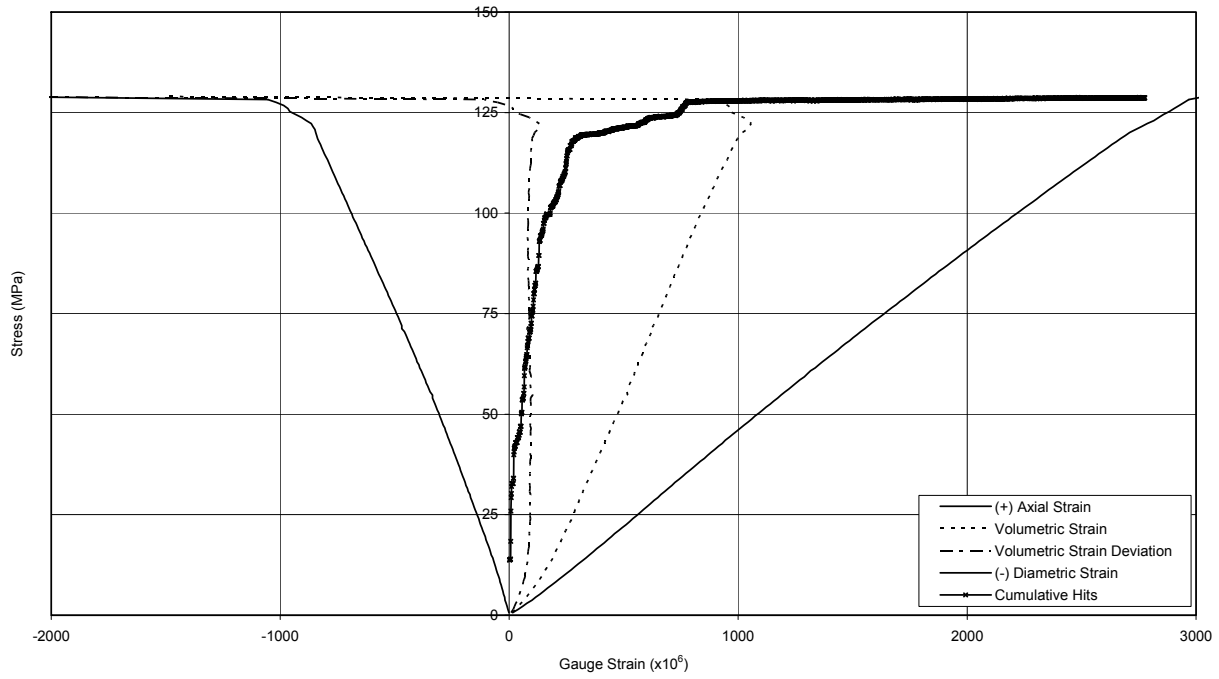


Figure B-31 Specimen DGR-2, 660.68 m

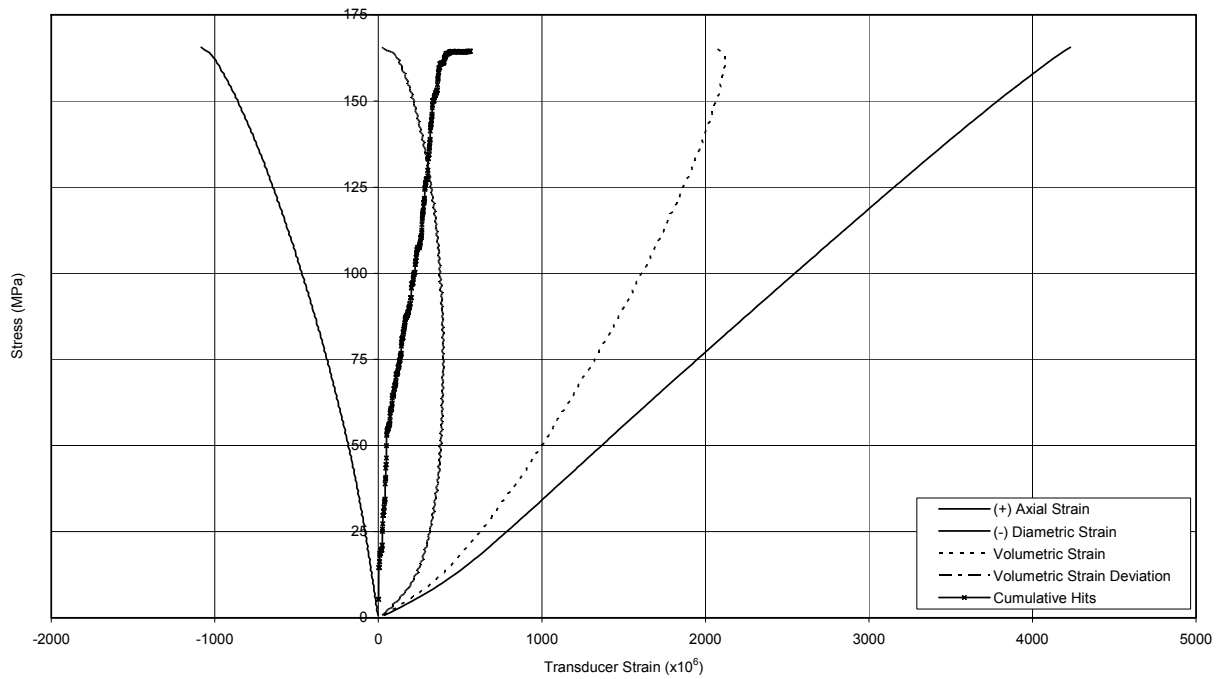
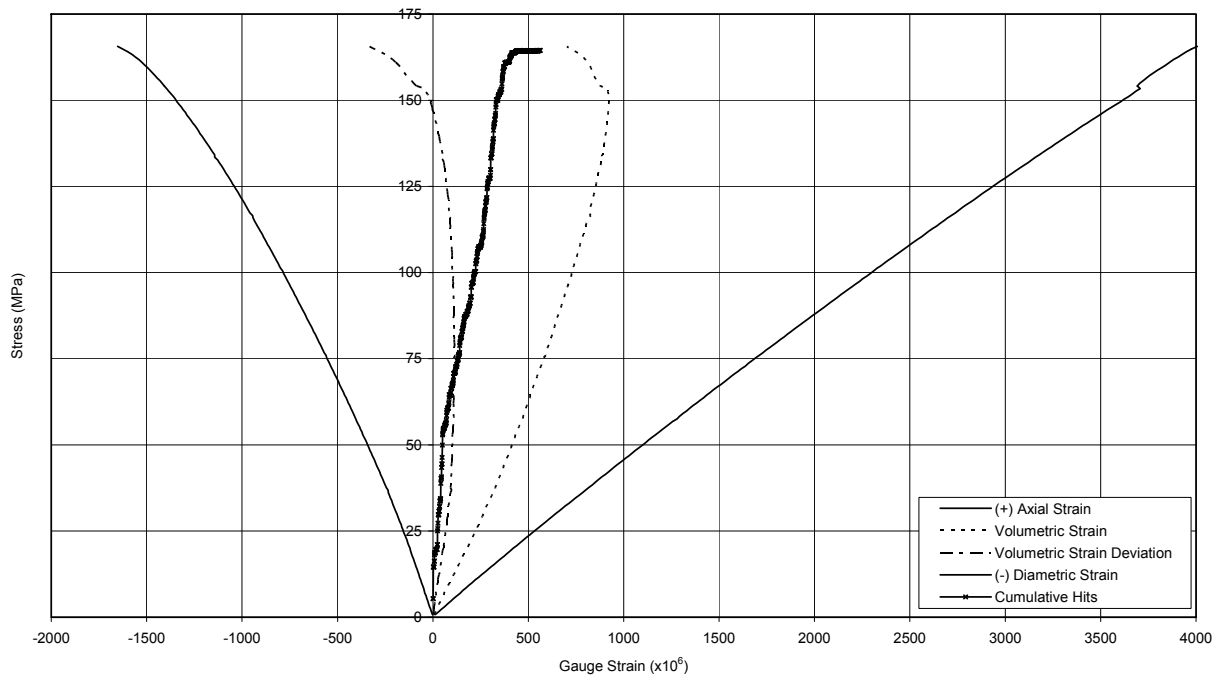


Figure B-32 Specimen DGR-2, 661.61 m

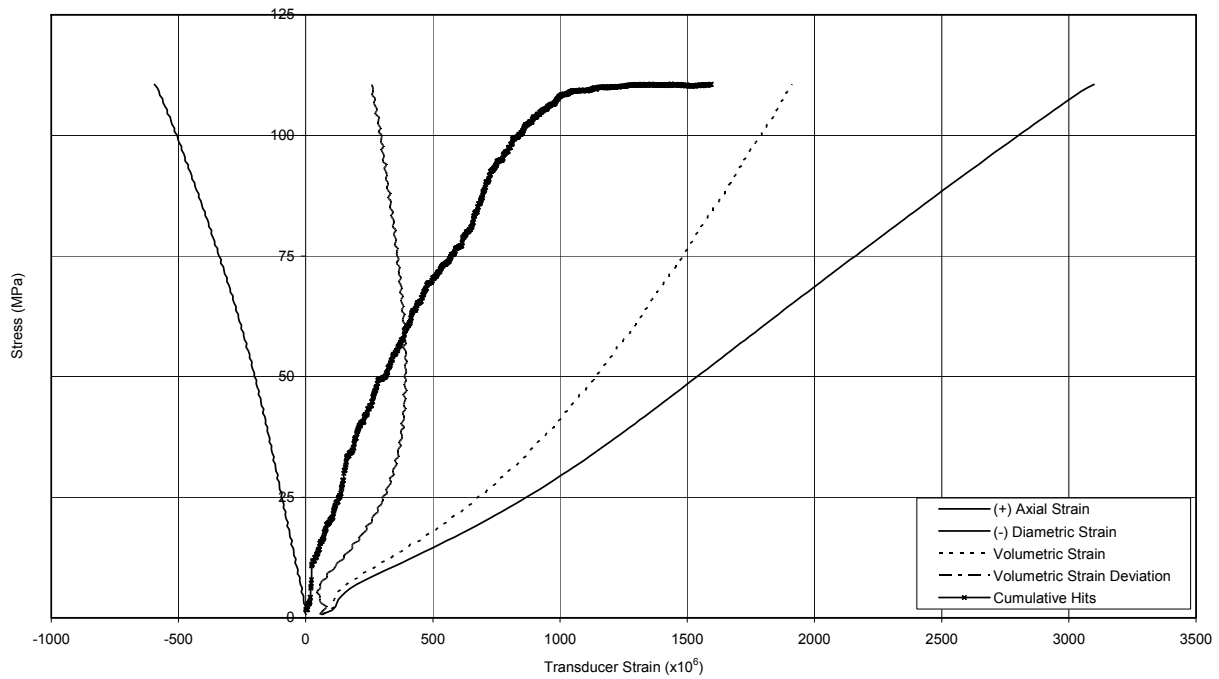
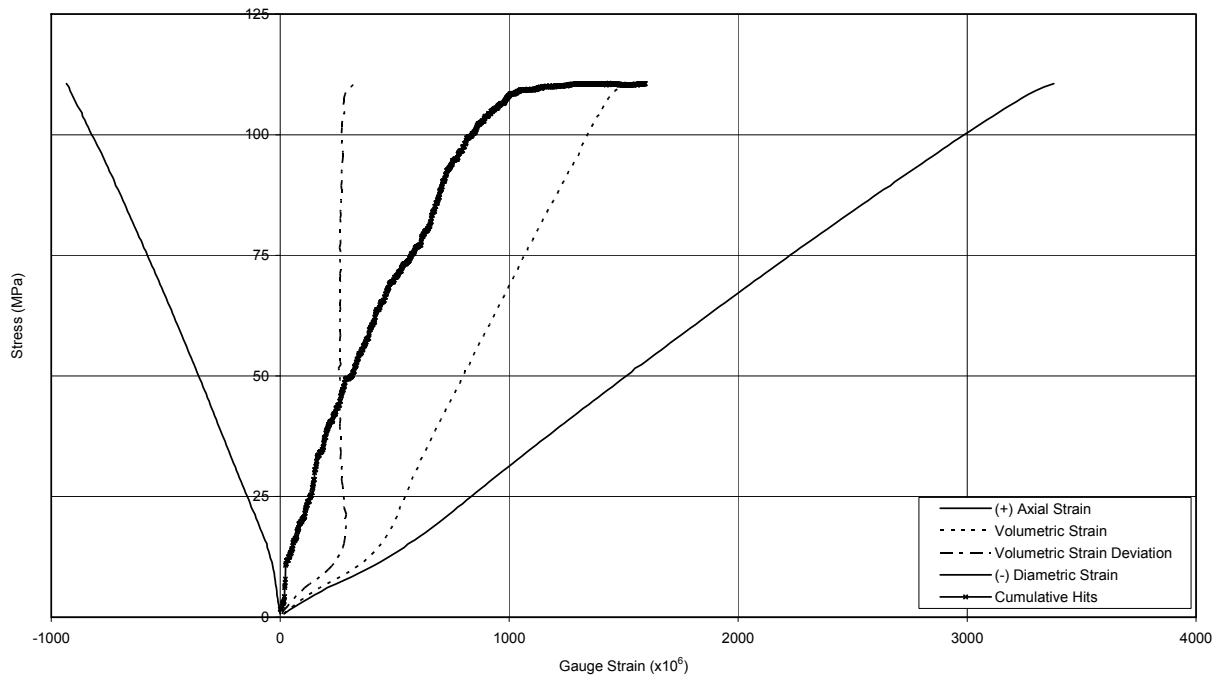


Figure B-33 Specimen DGR-2, 666.79 m

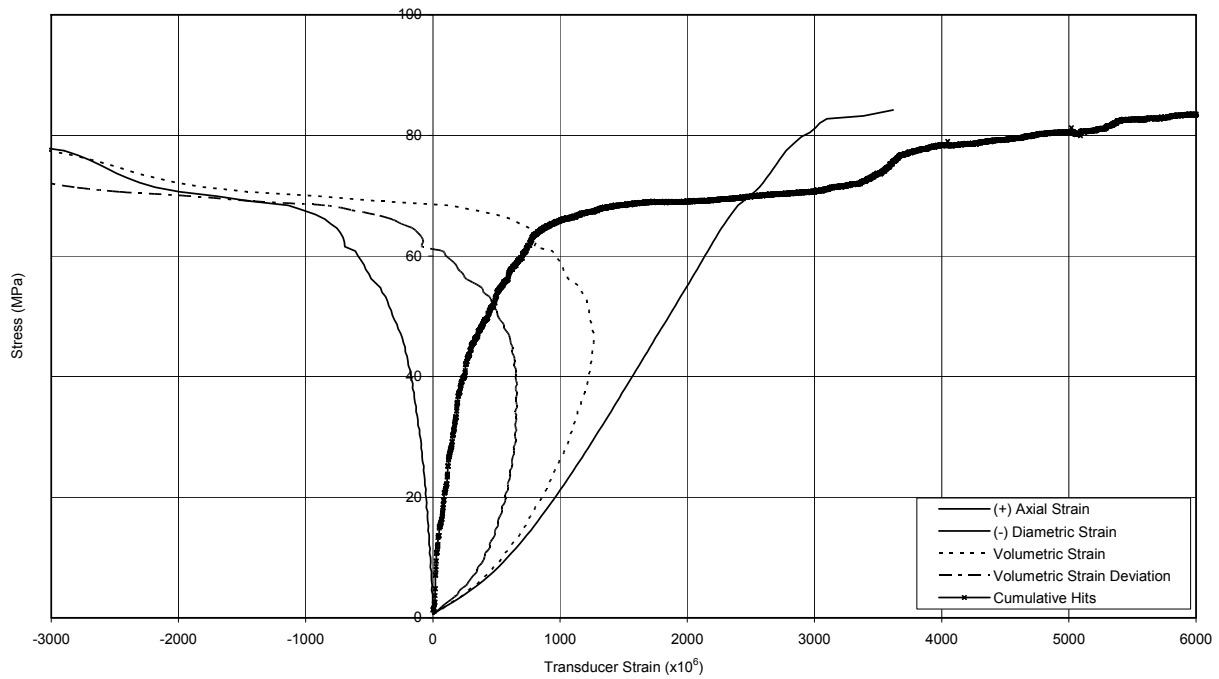
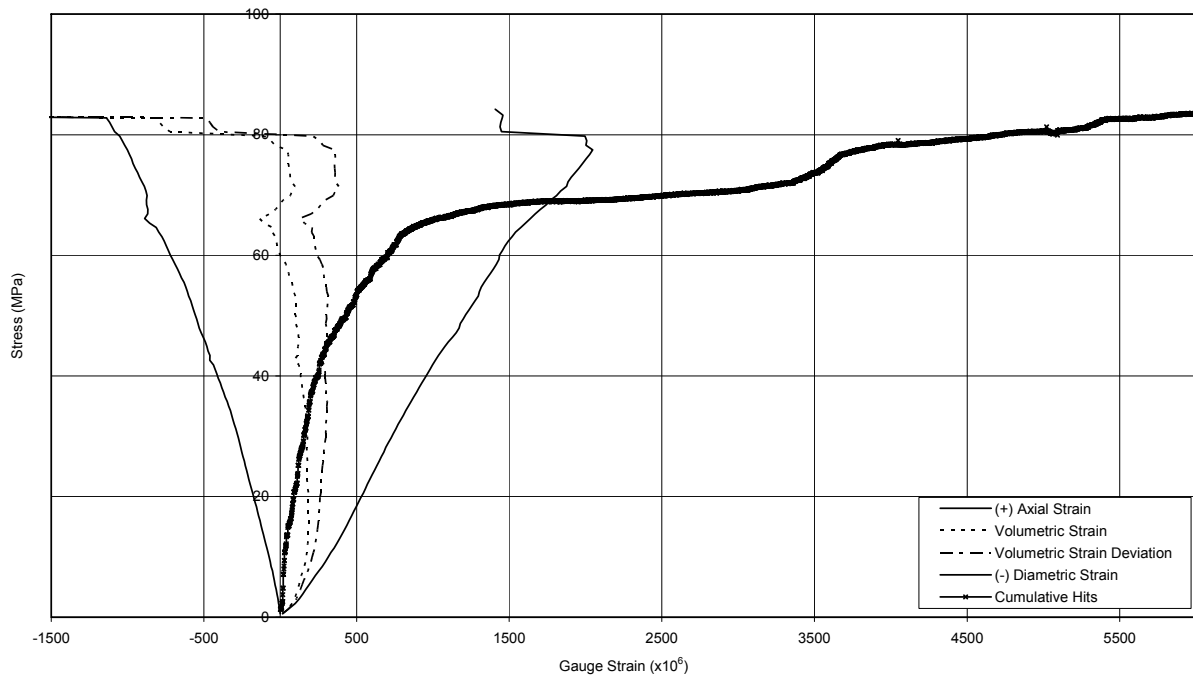


Figure B-34 Specimen DGR-2, 668.46 m

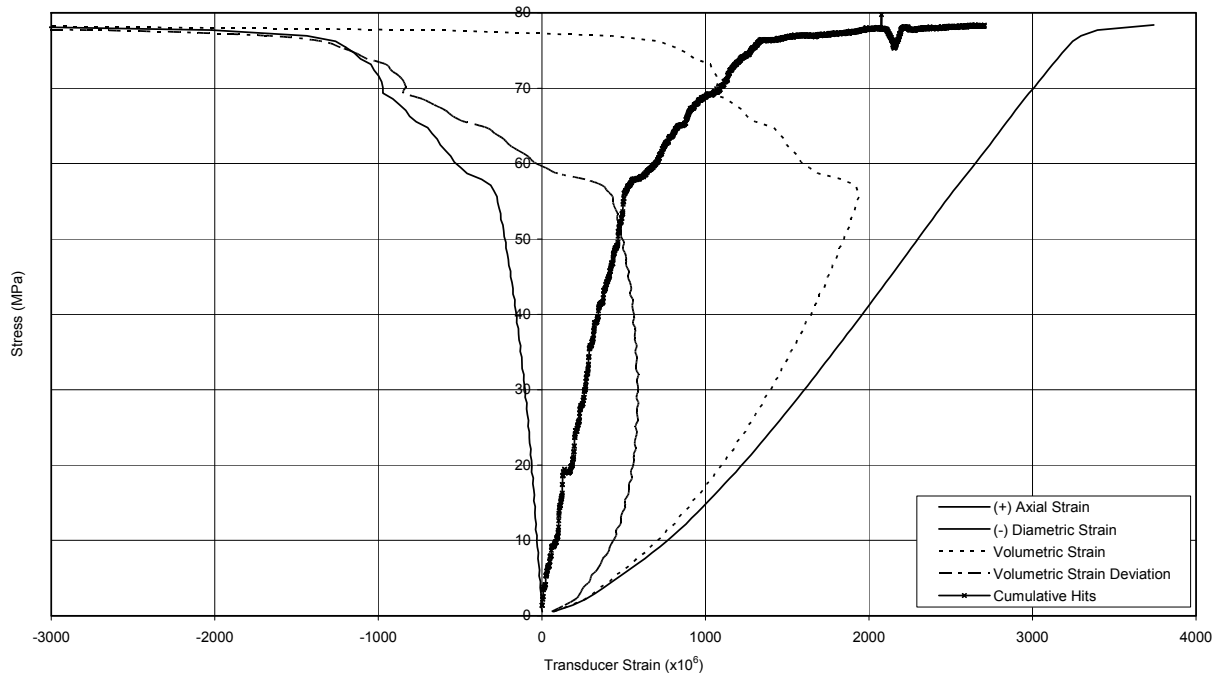
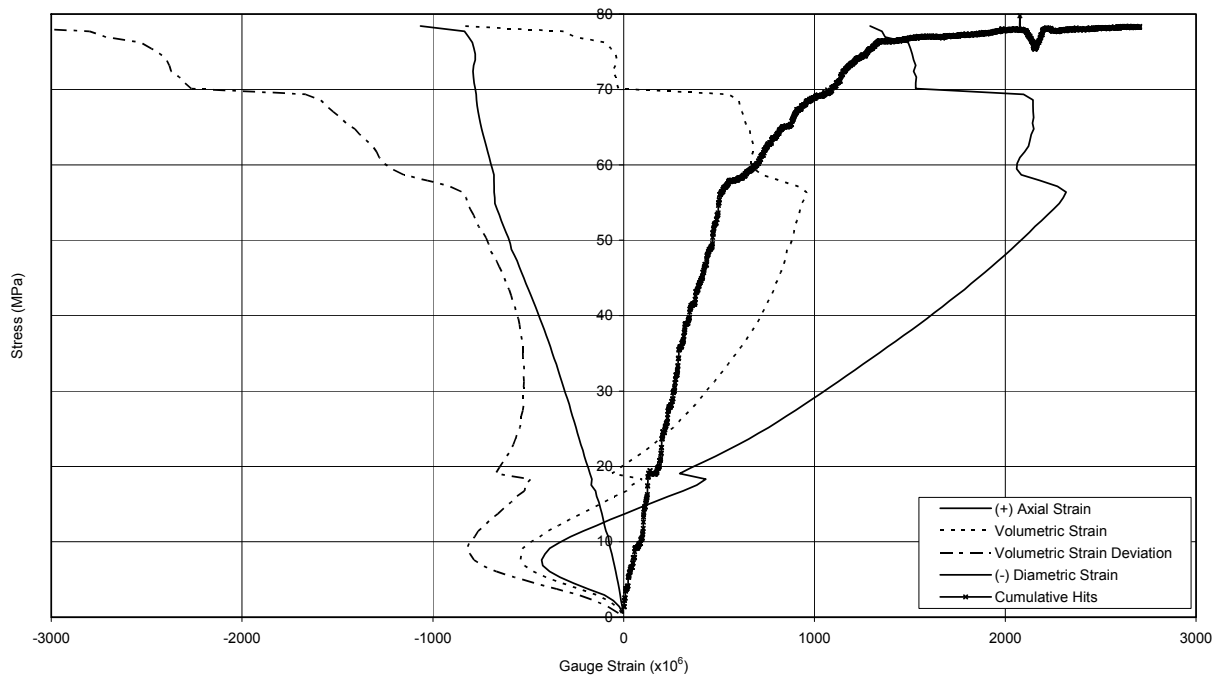


Figure B-35 Specimen DGR-2, 673.26 m

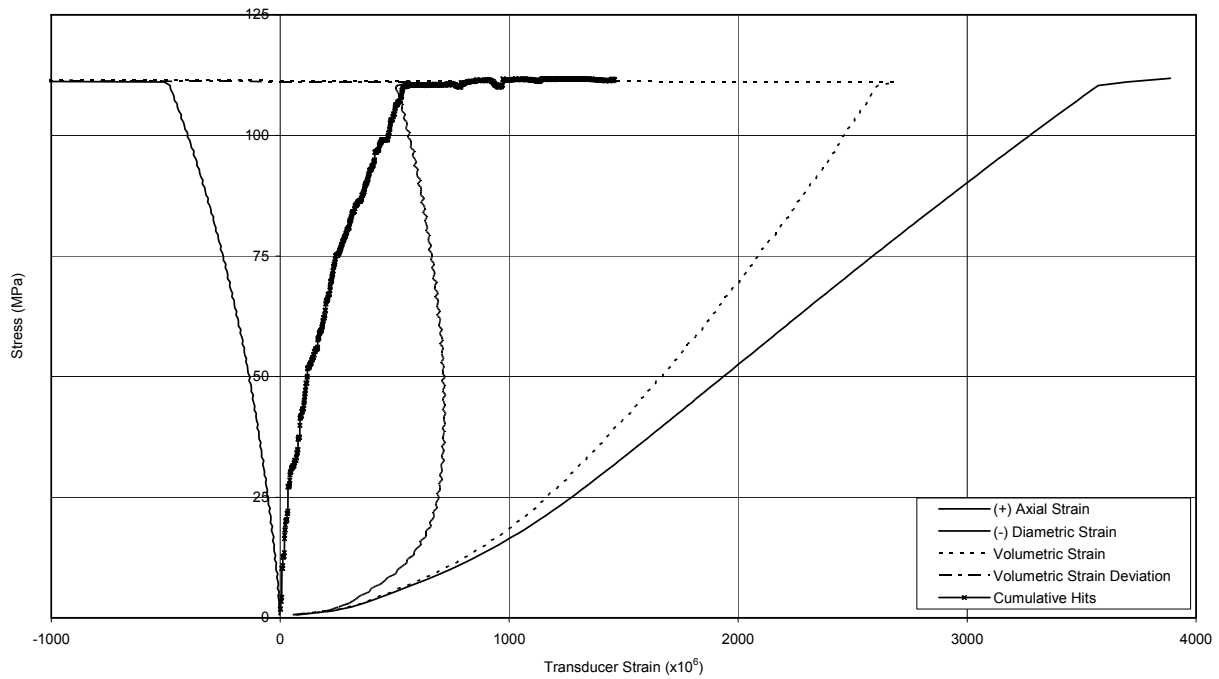
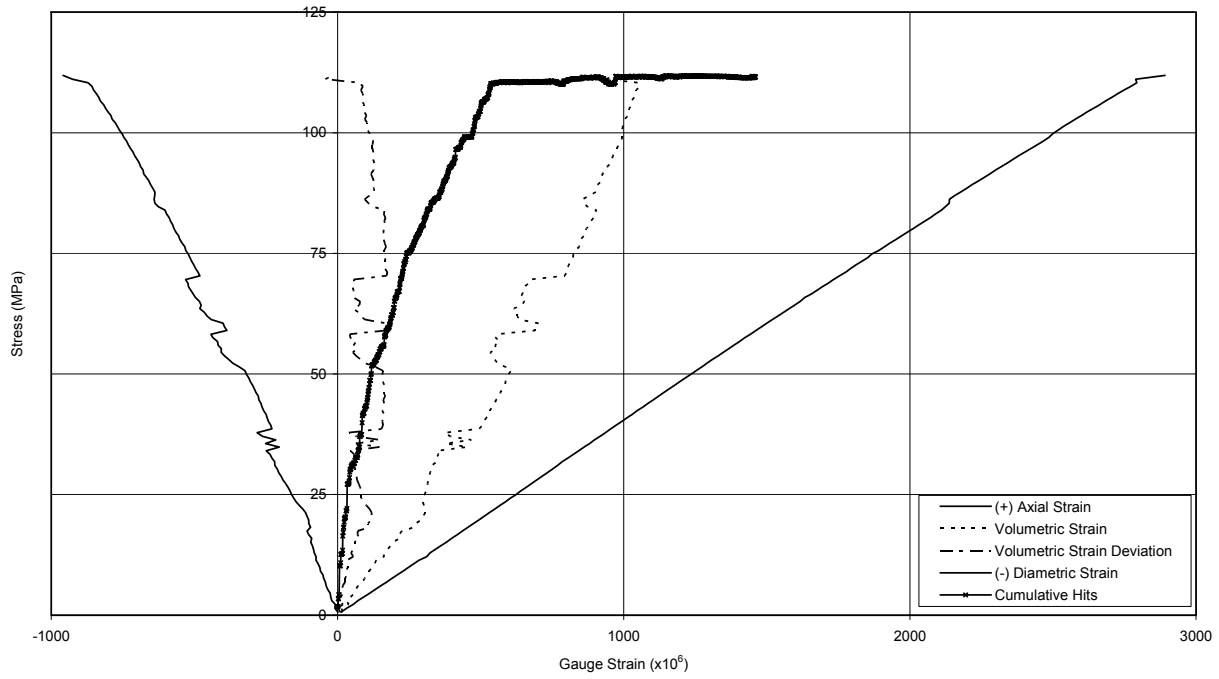


Figure B-36 Specimen DGR-2, 674.11 m

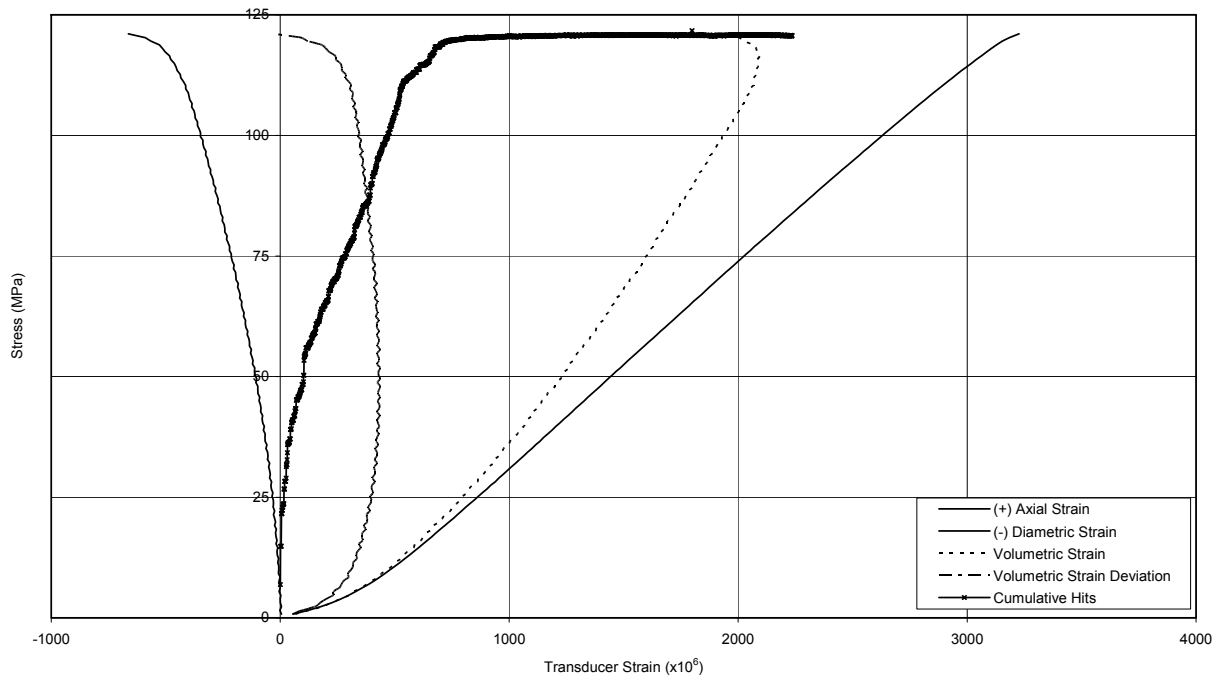
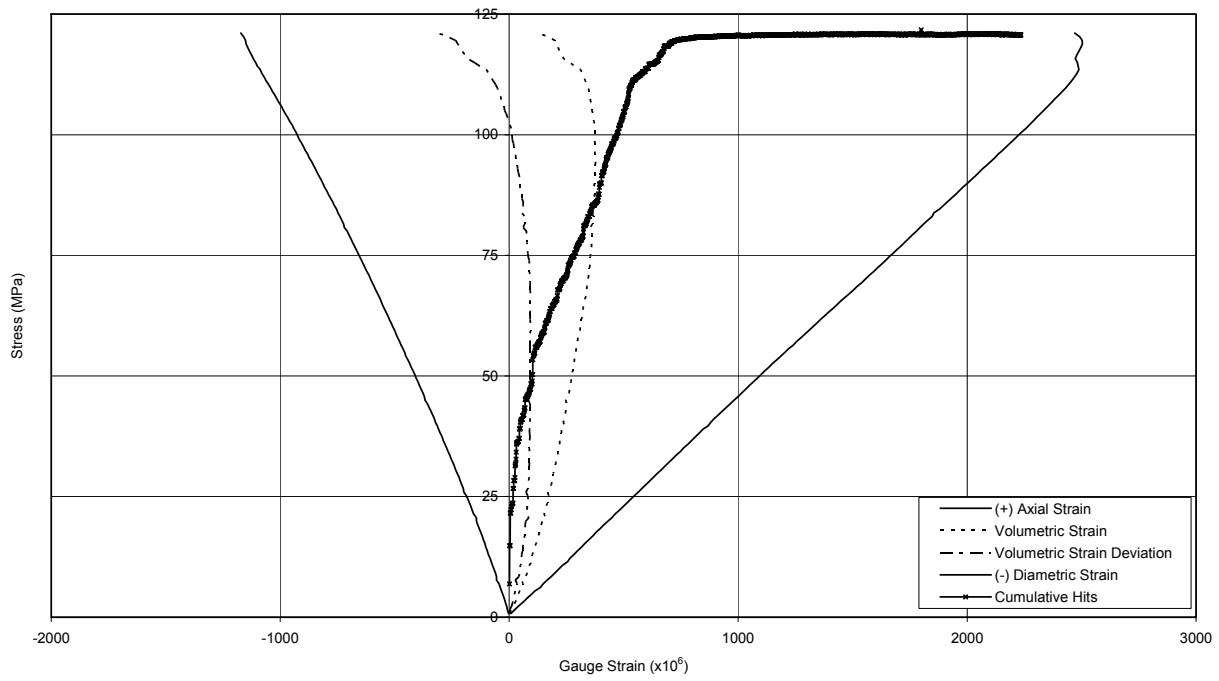


Figure B-37 Specimen DGR-2, 676.45 m

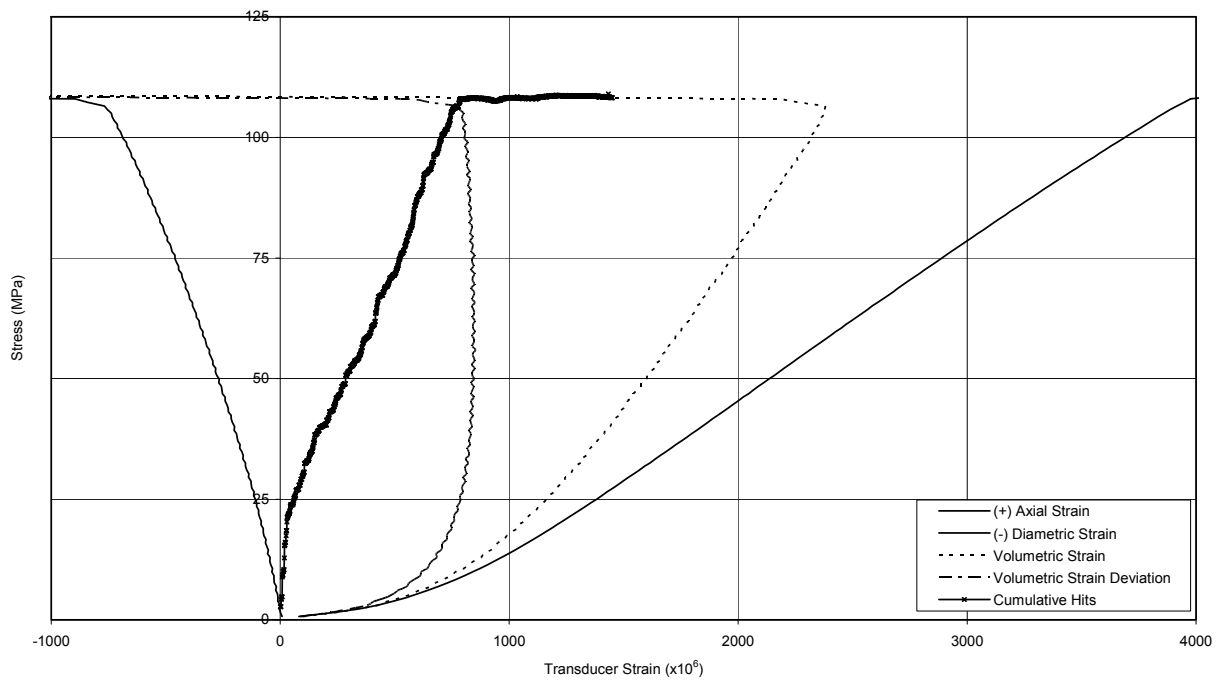
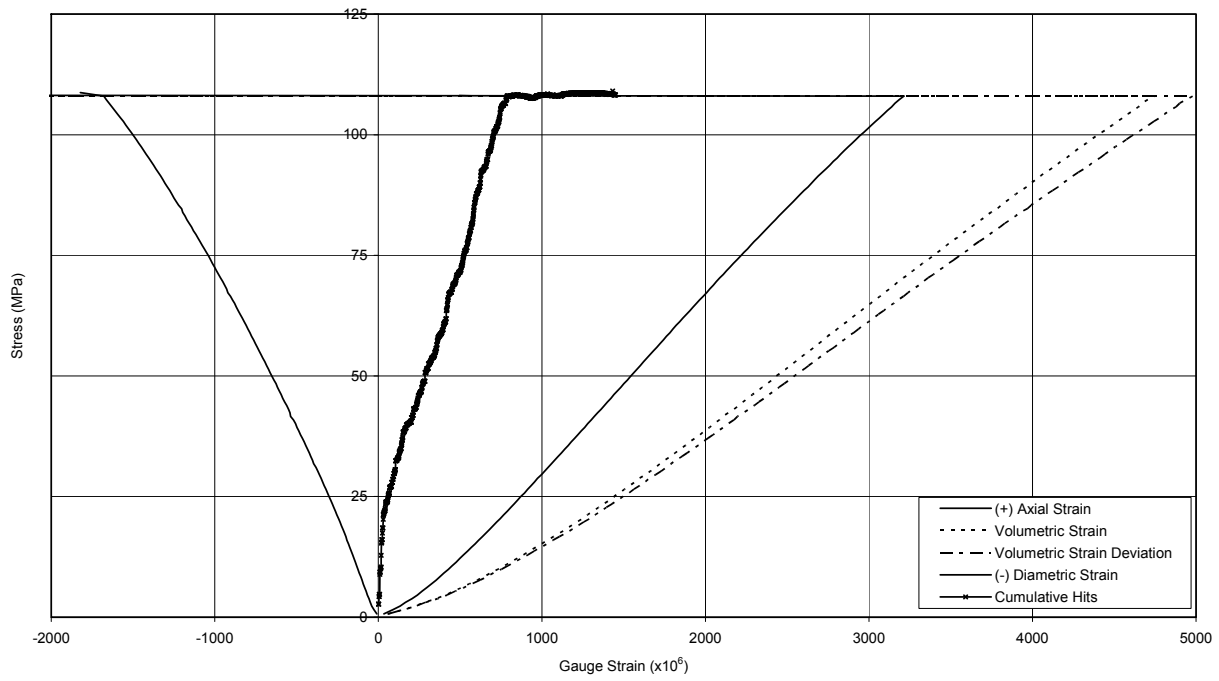


Figure B-38 Specimen DGR-2, 679.83 m

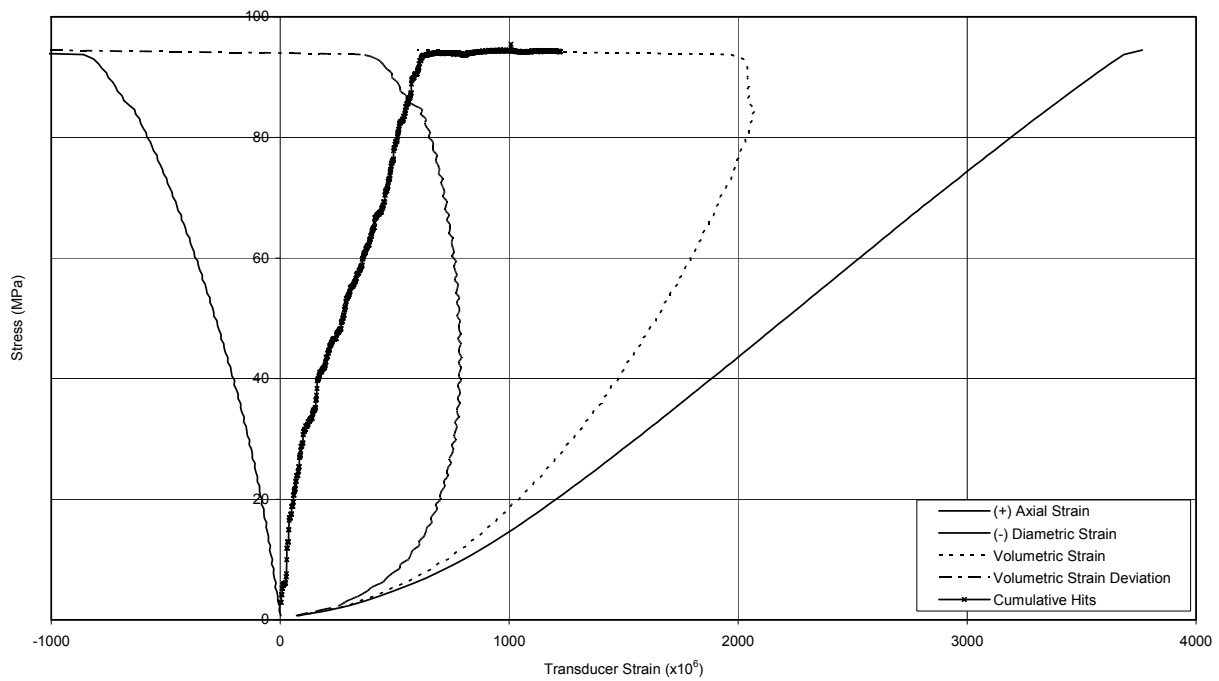
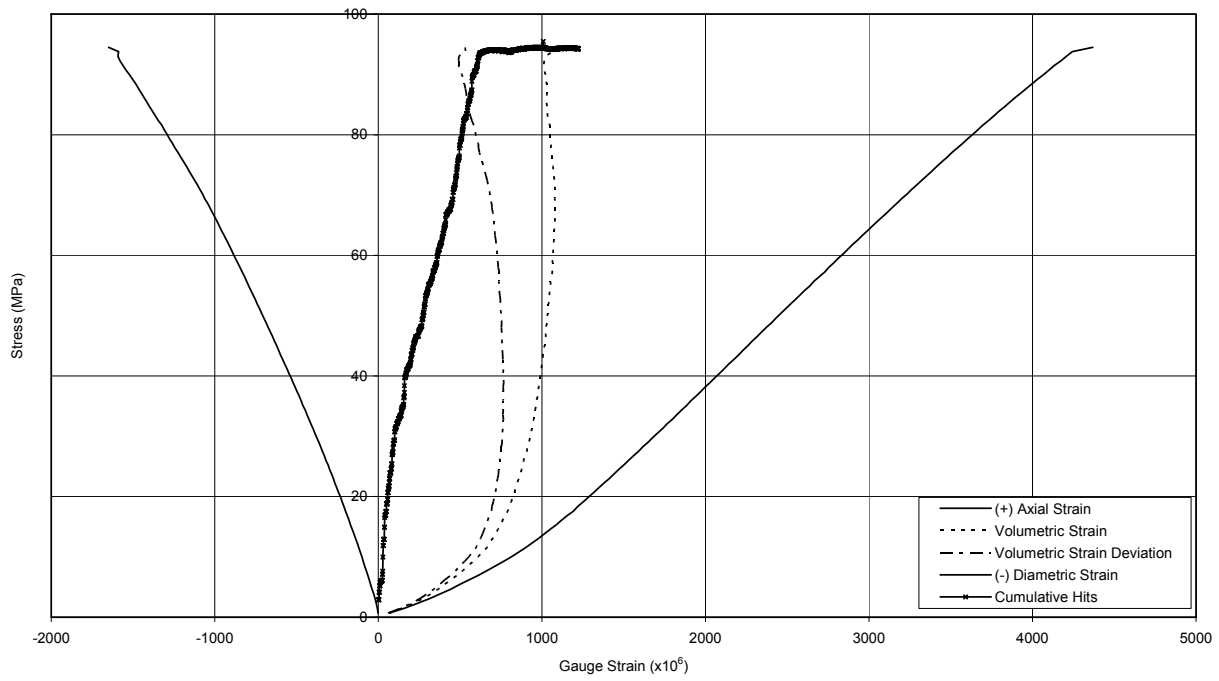


Figure B-39 Specimen DGR-2, 683.02 m

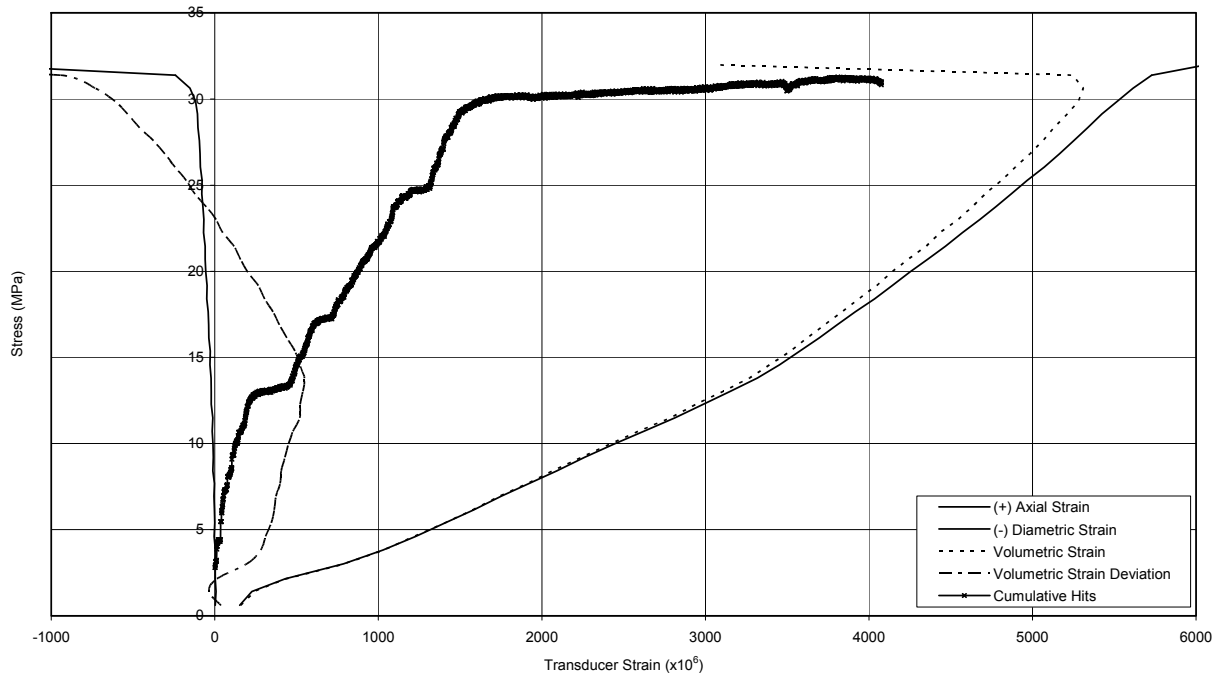
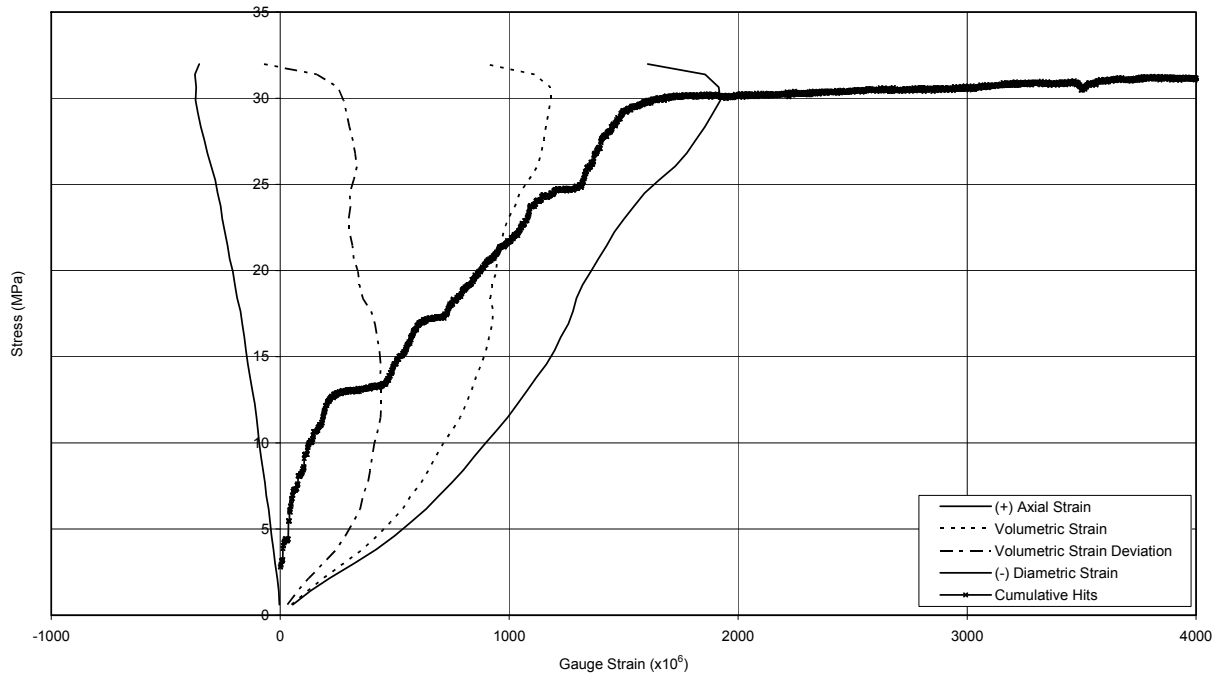


Figure B-40 Specimen DGR-2, 688.22 m

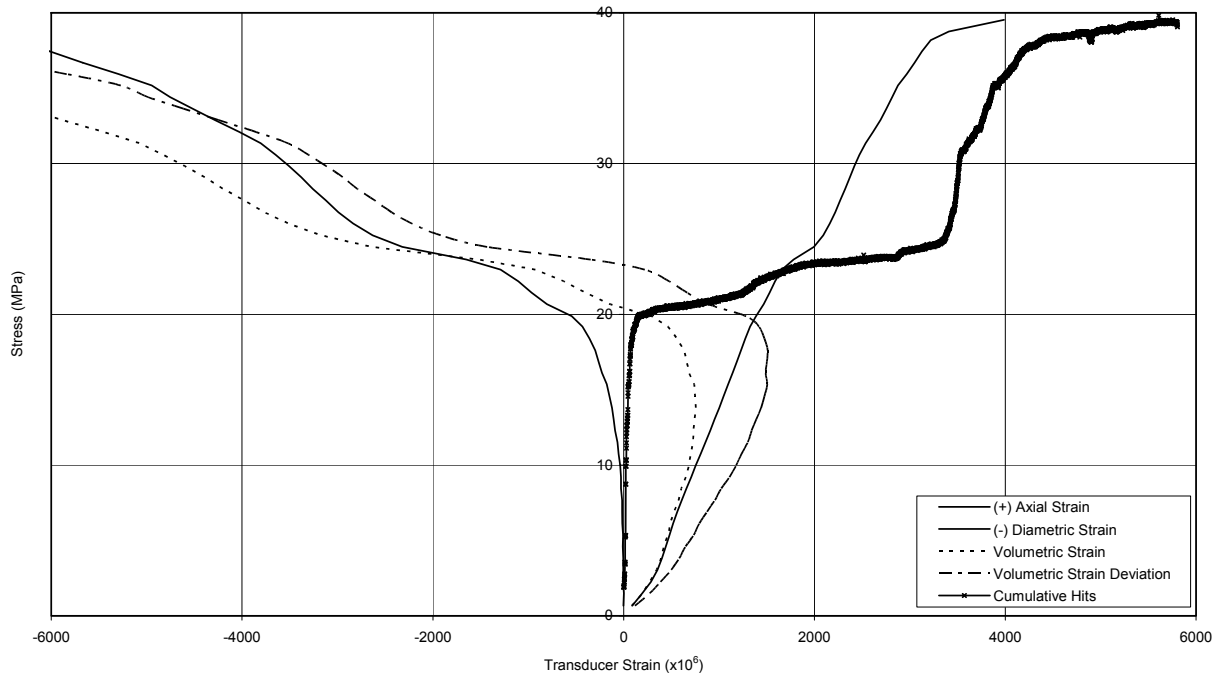
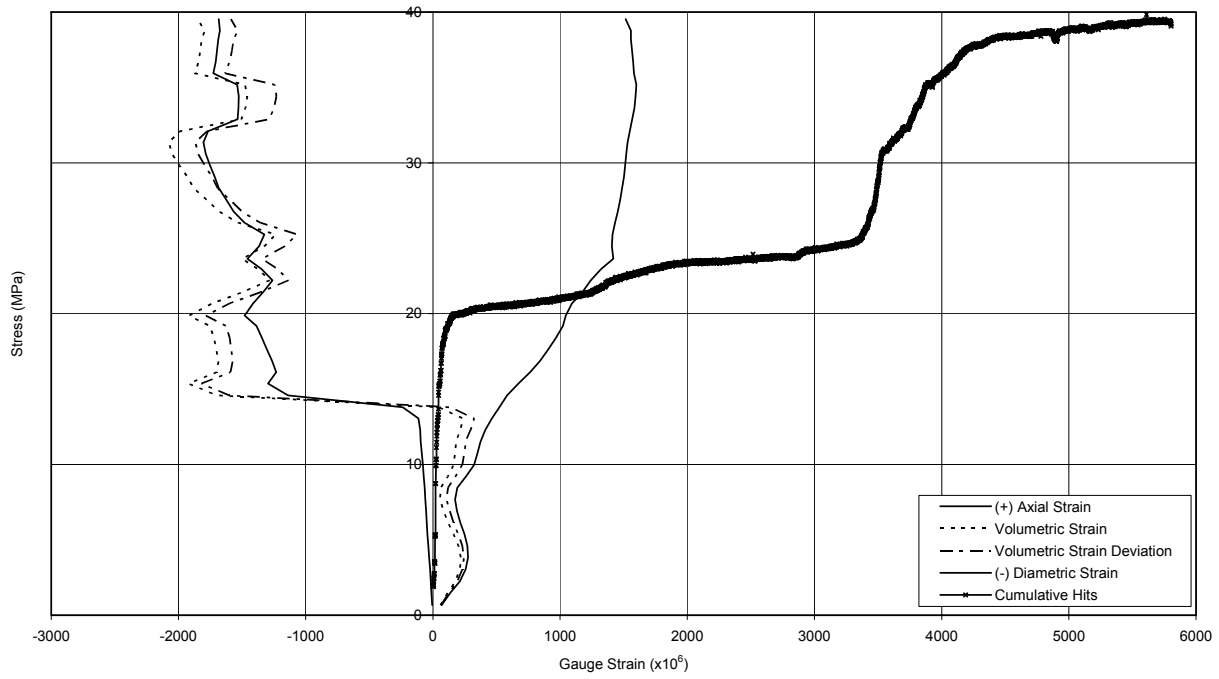


Figure B-41 Specimen DGR-2, 694.11 m

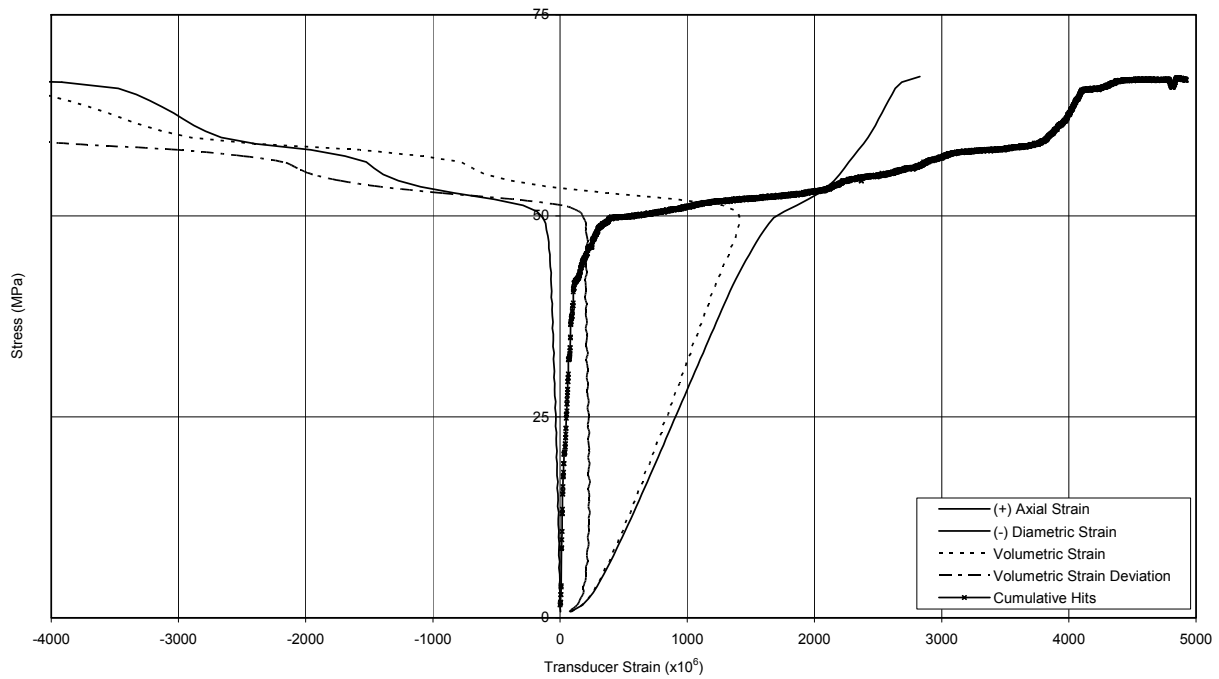
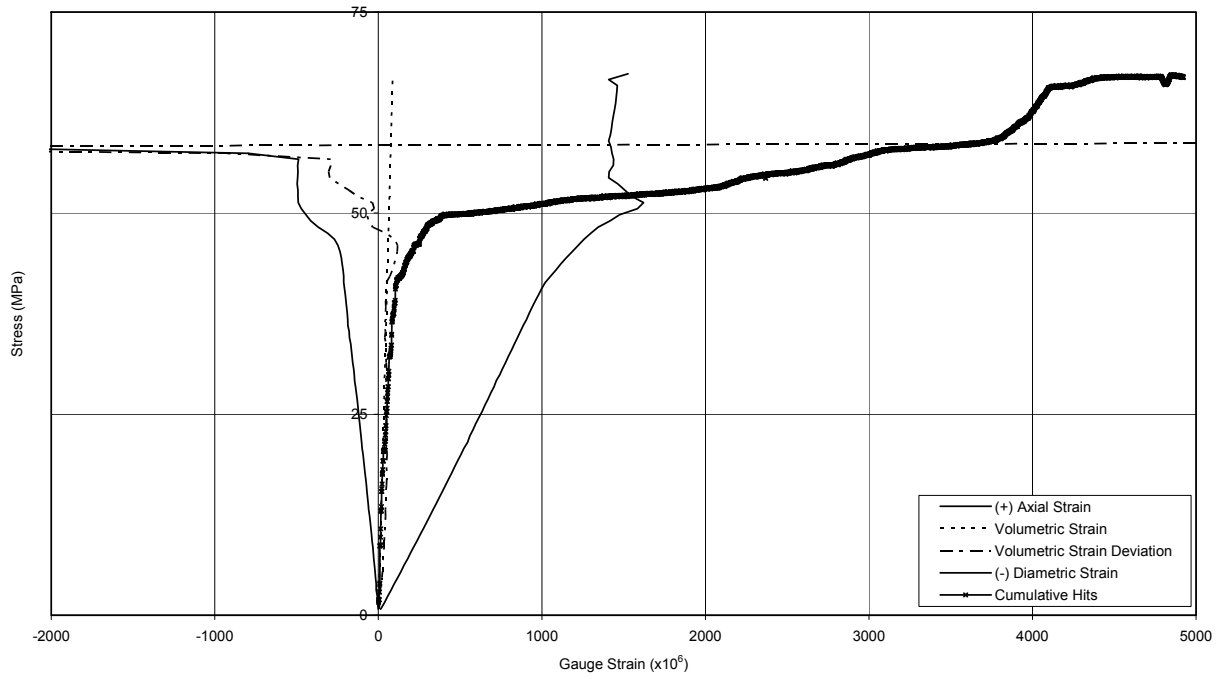


Figure B-42 Specimen DGR-2, 695.15 m

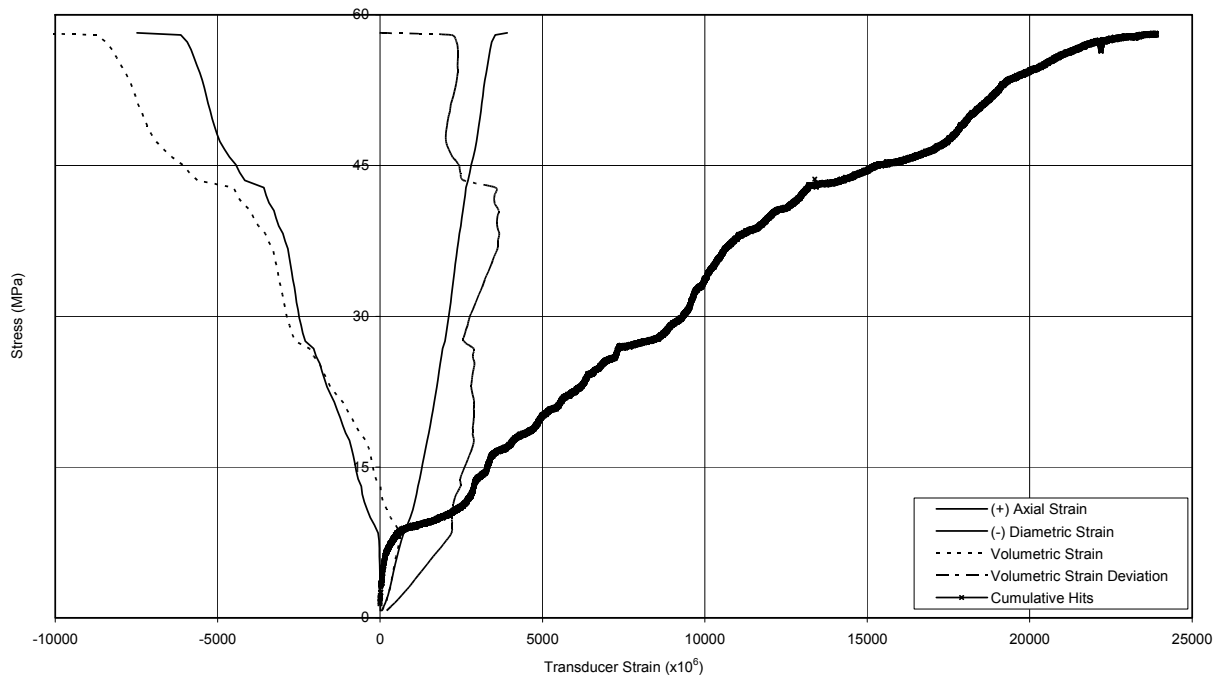
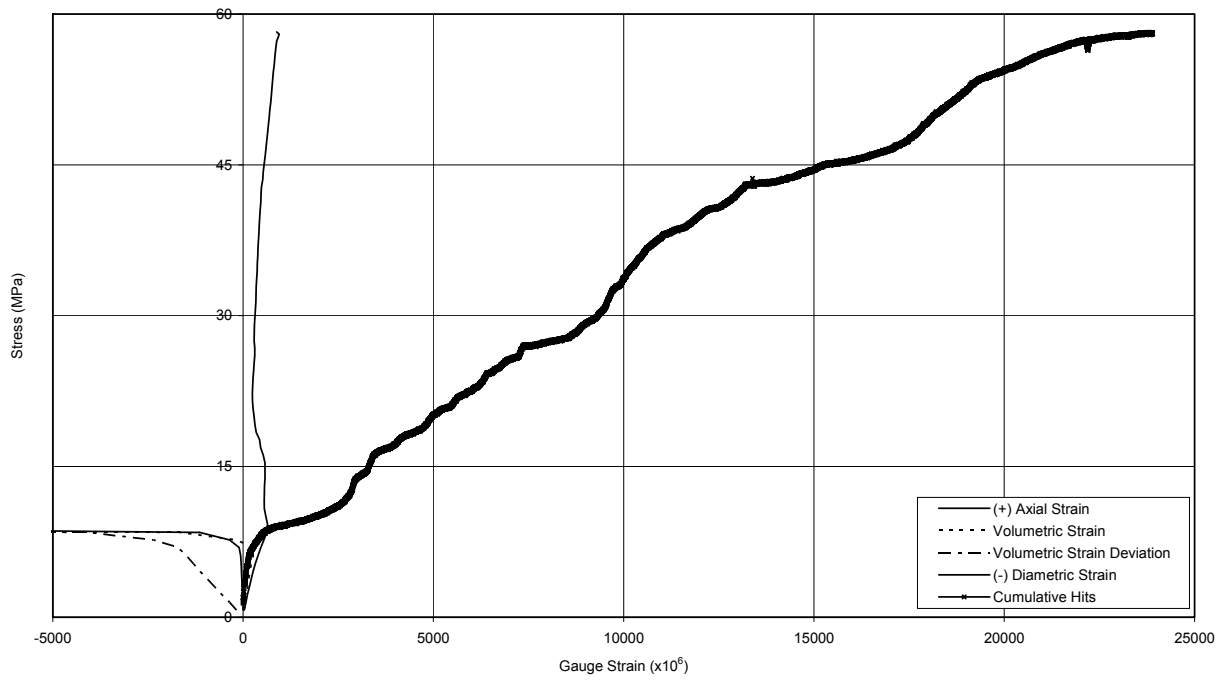


Figure B-43 Specimen DGR-2, 702.69 m

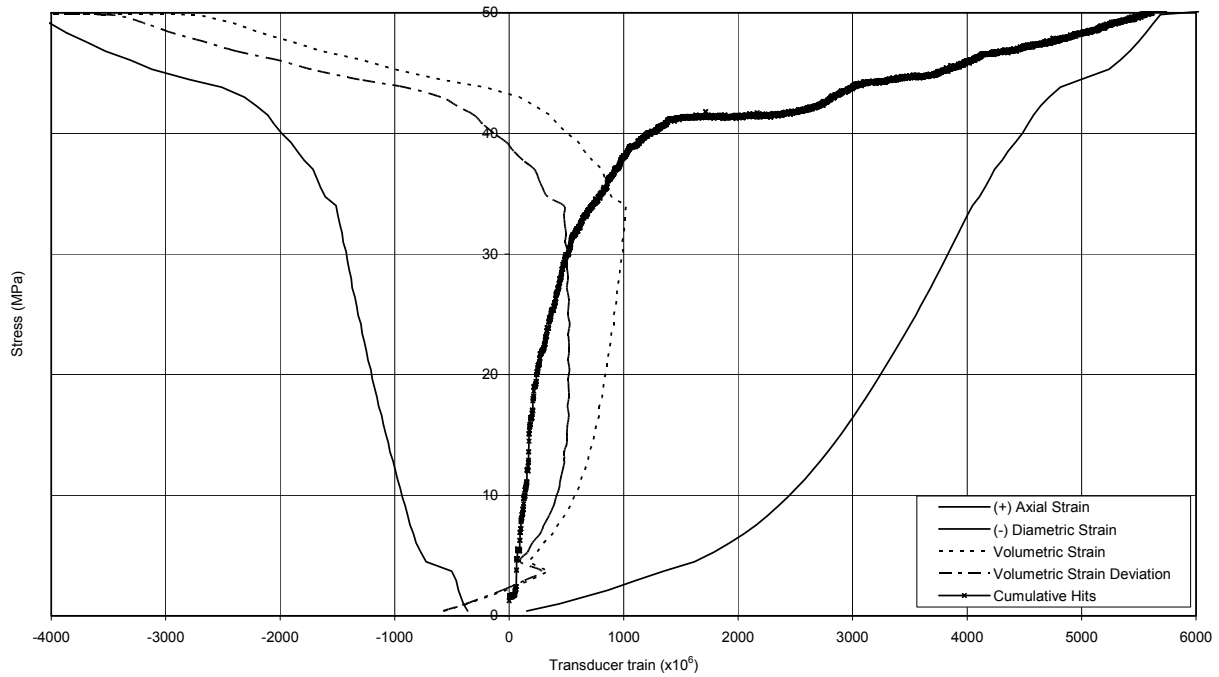
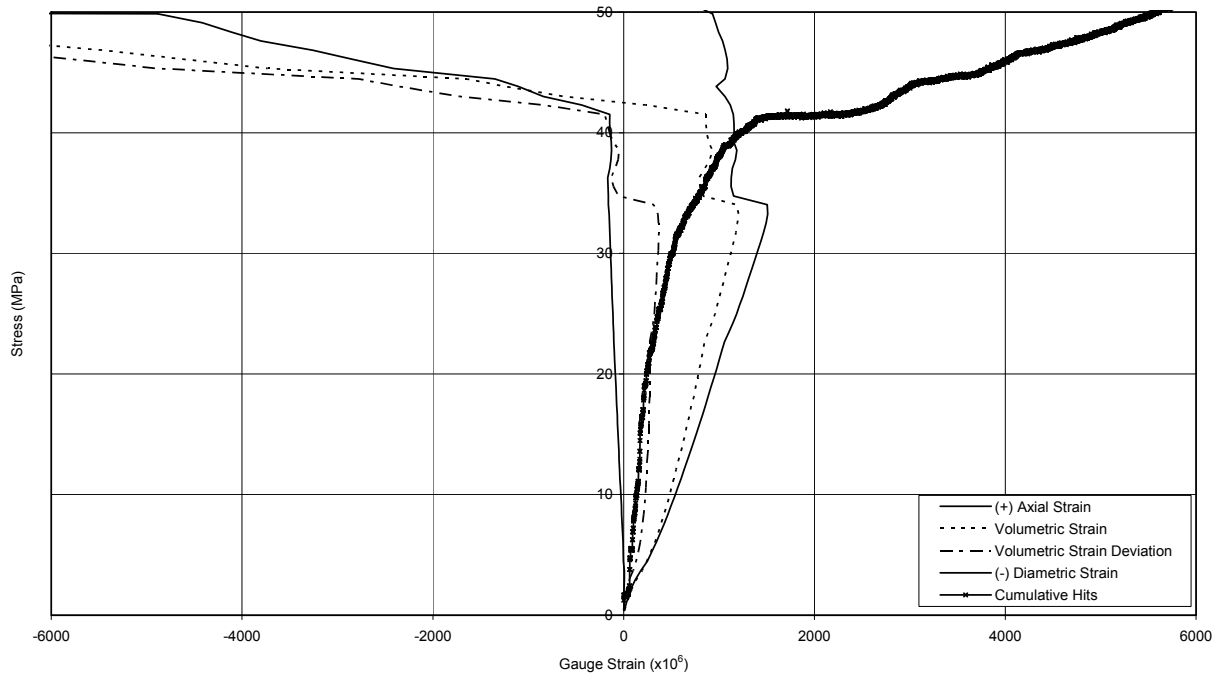


Figure B-44 Specimen DGR-2, 704.47 m

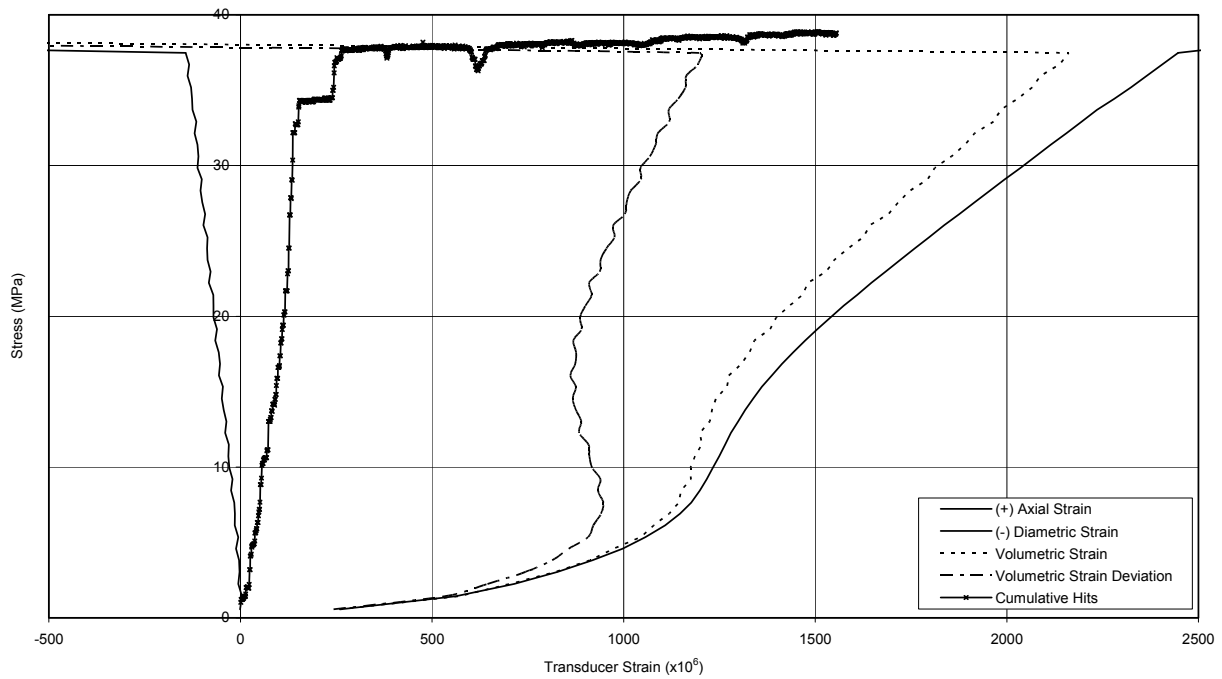
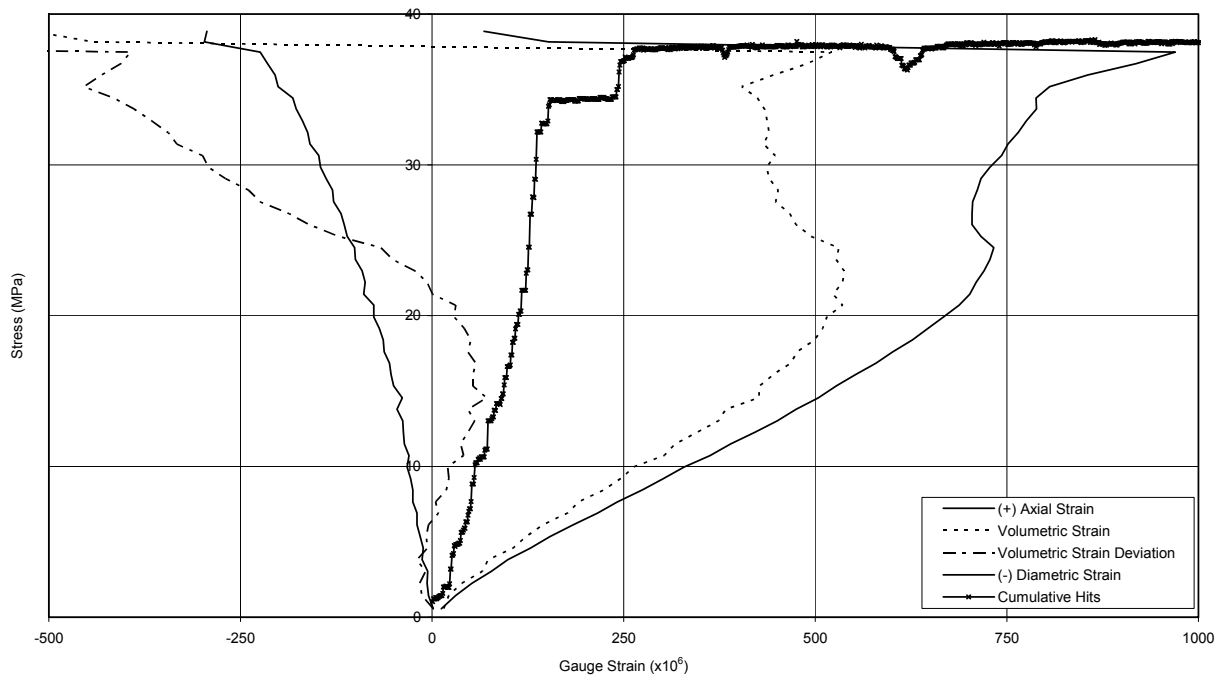


Figure B-45 Specimen DGR-2, 710.29 m

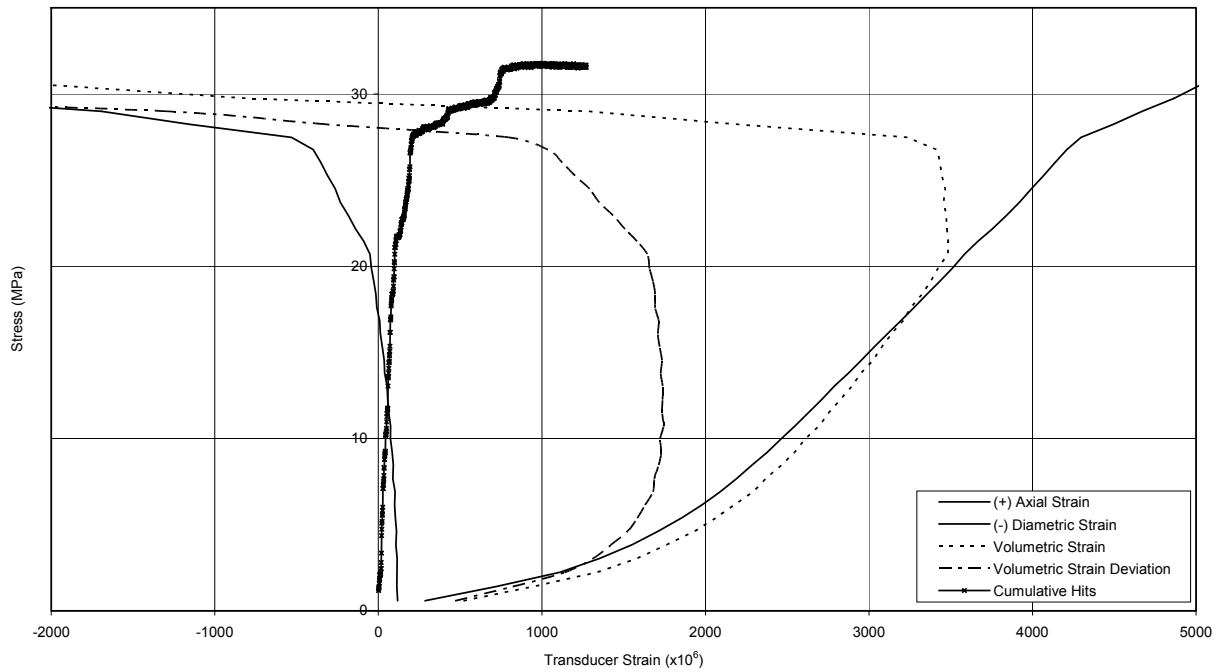
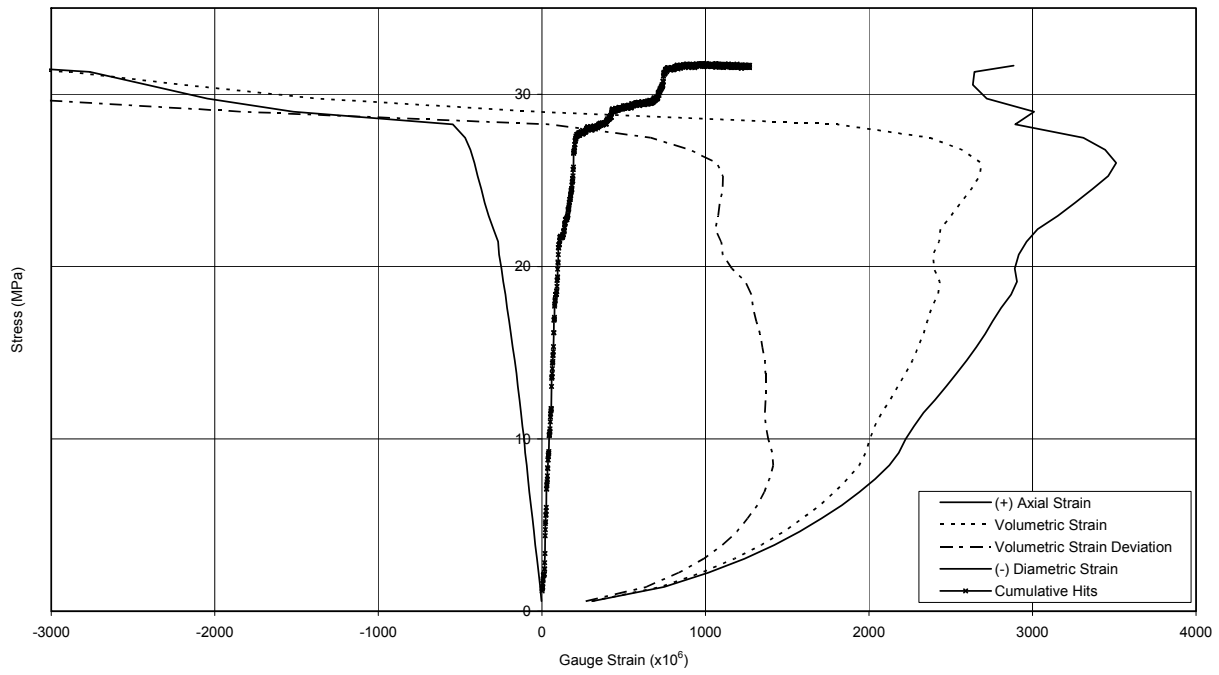


Figure B-46 Specimen DGR-2, 719.38 m

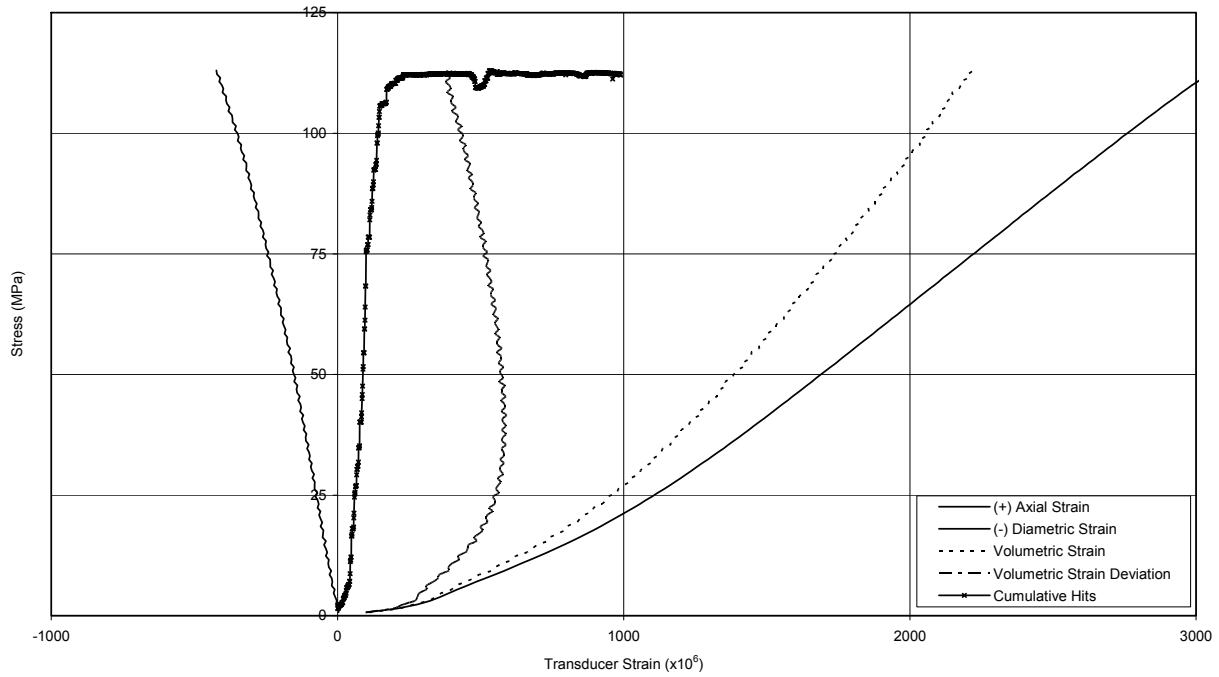
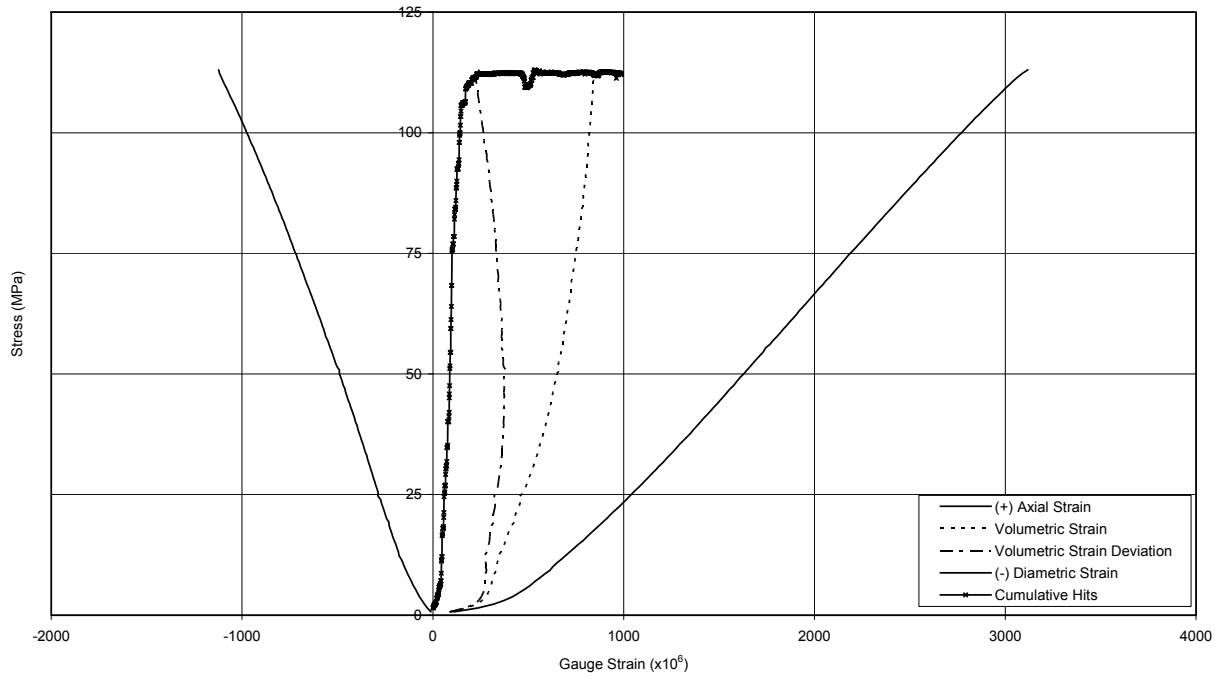


Figure B-47 Specimen DGR-2, 737.16 m

APPENDIX C

Failed Uniaxial Specimens and AE Source Locations

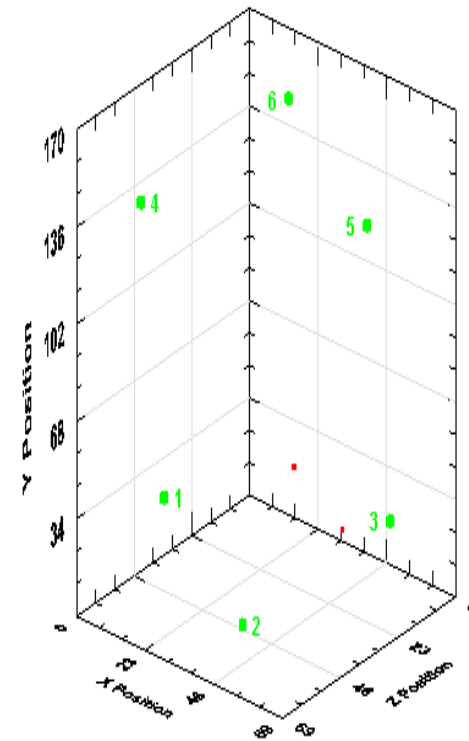


Figure C-1 Specimen DGR-1, 27.30 m

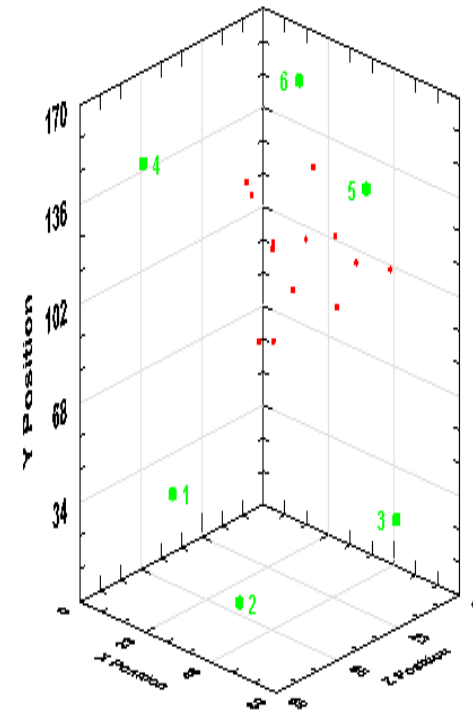
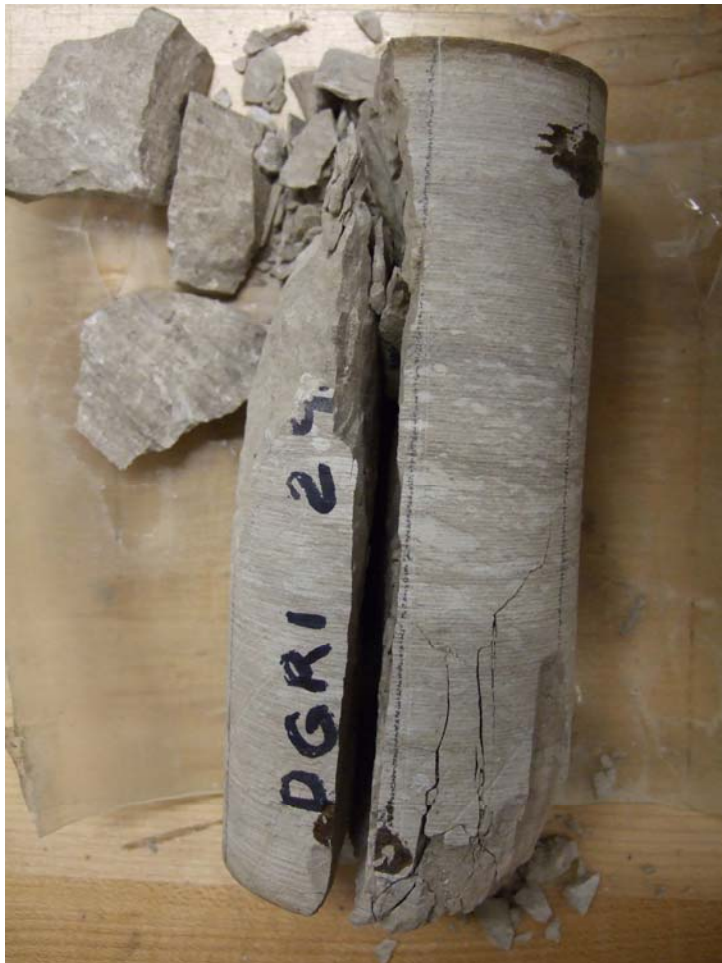


Figure C-2 Specimen DGR-1, 29.38 m

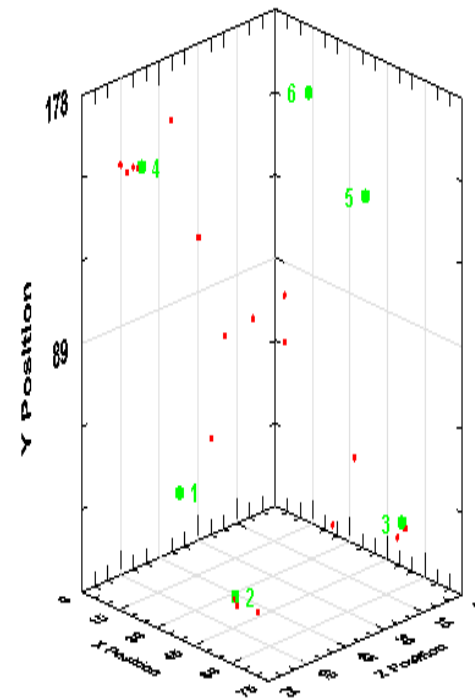


Figure C-4 Specimen DGR-1, 108.62 m

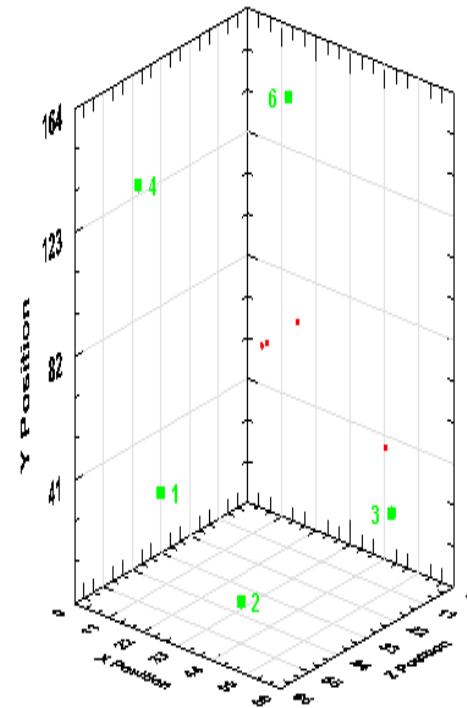


Figure C-5 Specimen DGR-1, 160.93 m

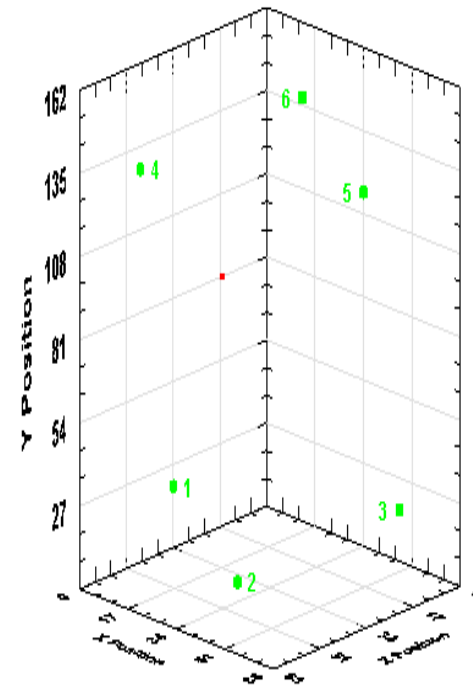


Figure C-6 Specimen DGR-1, 171.14 m

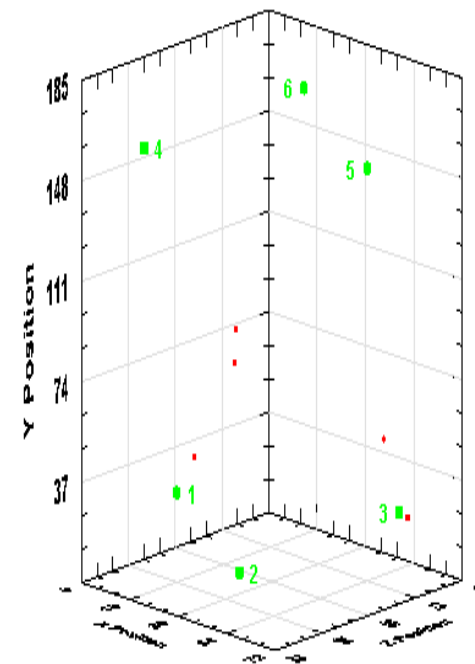


Figure C-7 Specimen DGR-1, 183.60 m

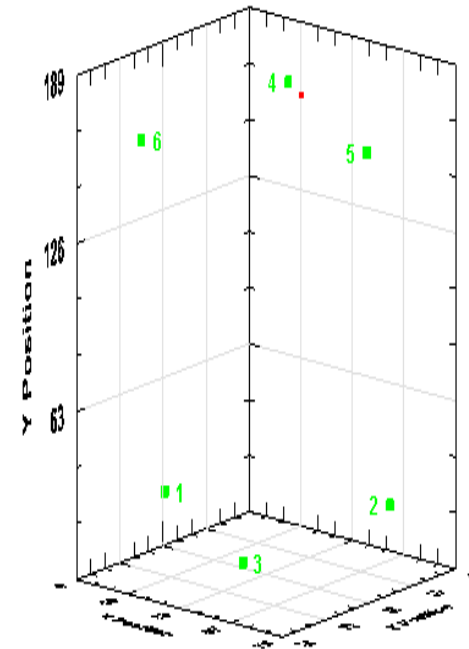


Figure C-8 Specimen DGR-1, 206.55 m

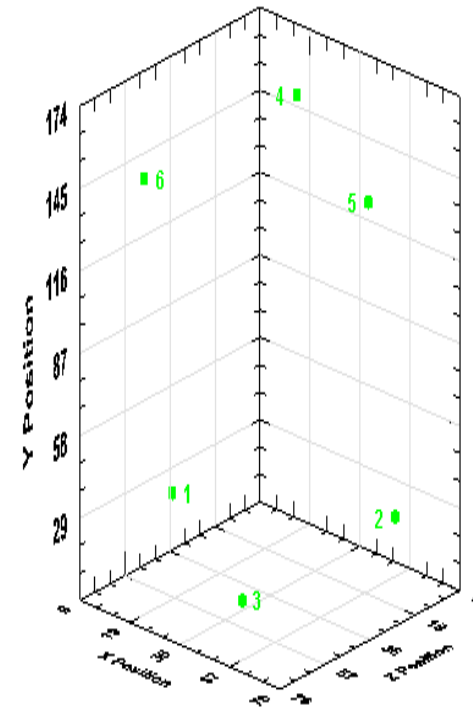


Figure C-9 Specimen DGR-1, 266.20 m

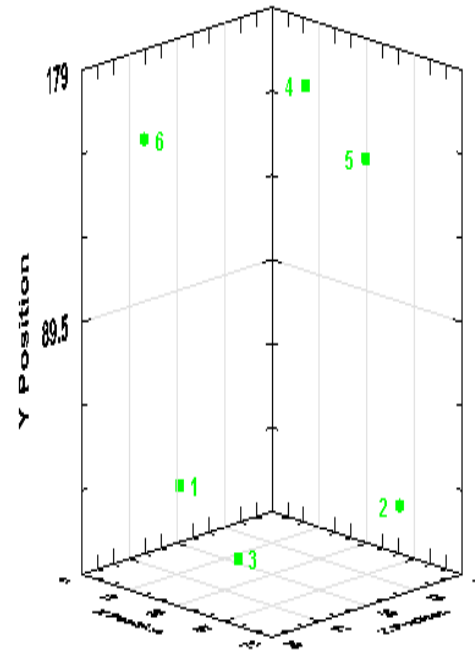


Figure C-10 Specimen DGR-1, 286.69 m

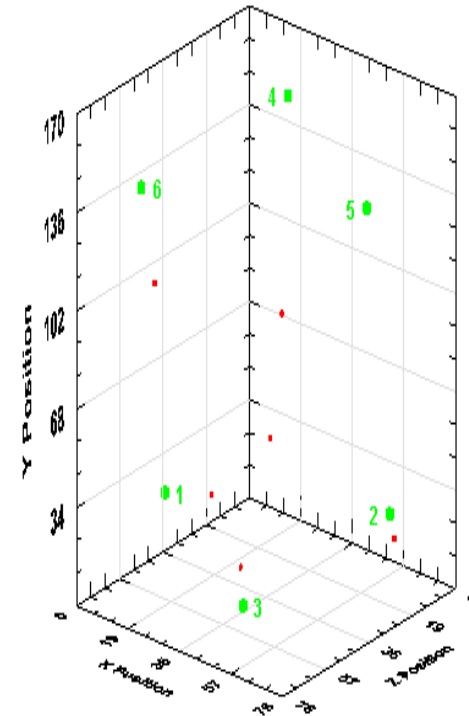


Figure C-11 Specimen DGR-1, 314.88 m

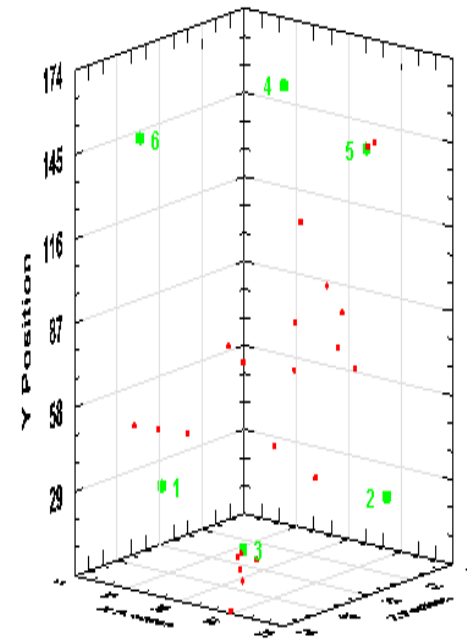


Figure C-12 Specimen DGR-1, 367.06 m

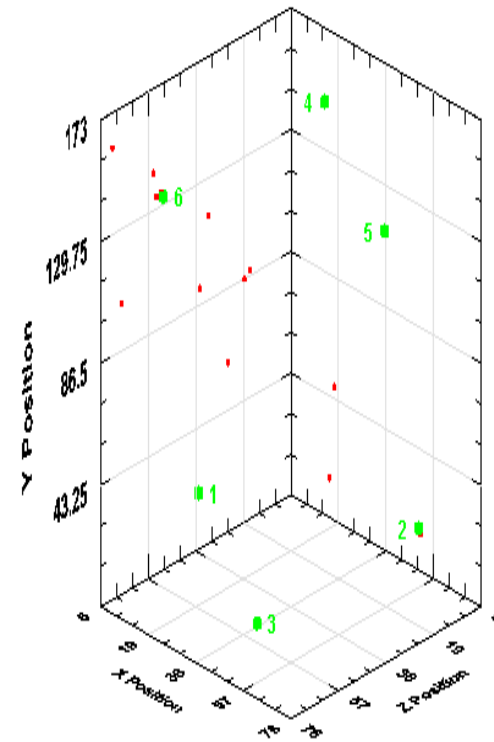


Figure C-13 Specimen DGR-1, 386.55 m

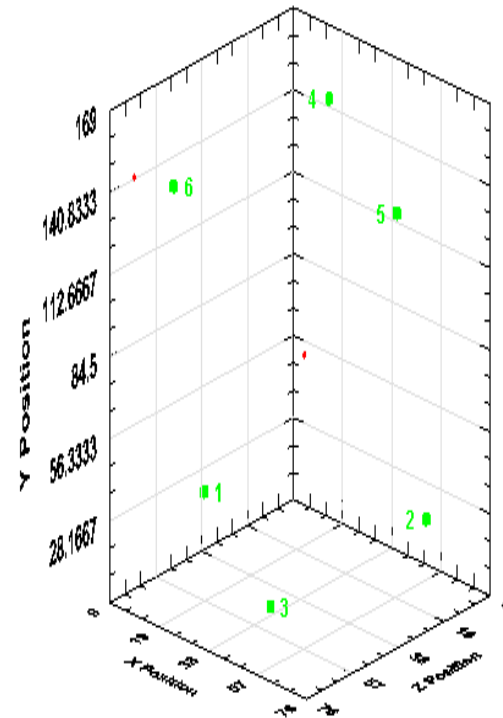


Figure C-14 Specimen DGR-1, 415.16 m

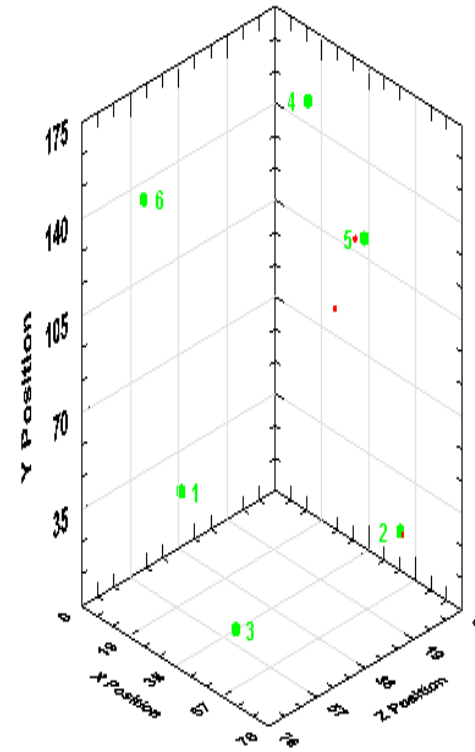


Figure C-15 Specimen DGR-1, 438.10 m

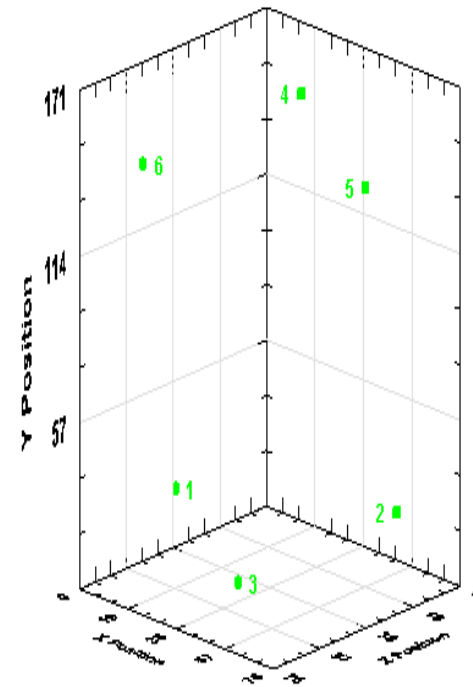


Figure C-16 Specimen DGR-1, 455.22 m

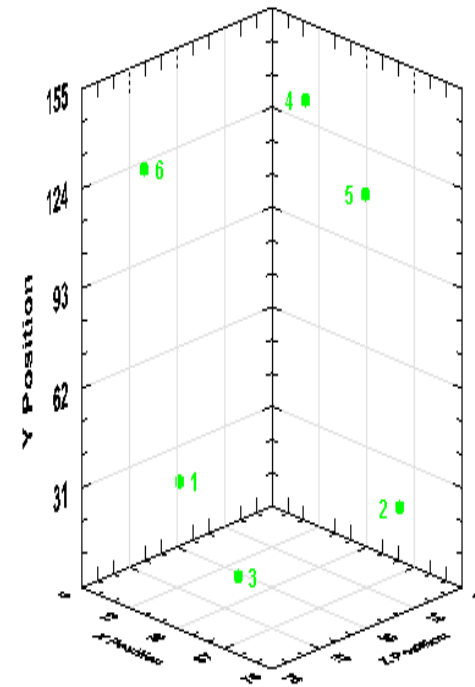


Figure C-17 Specimen DGR-1, 460.41 m

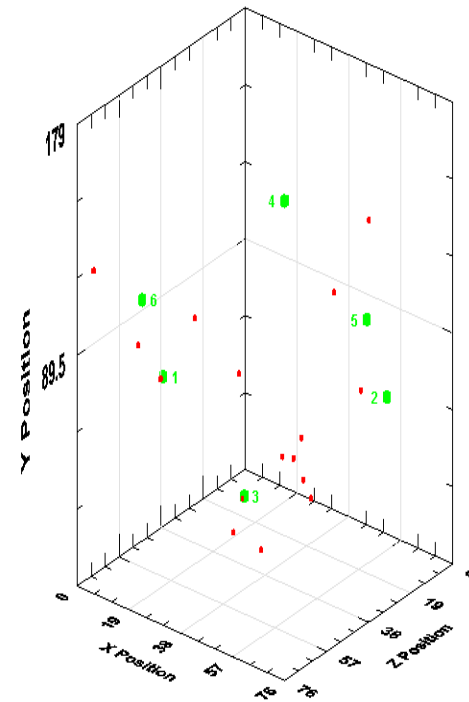


Figure C-18 Specimen DGR-2, 457.21 m

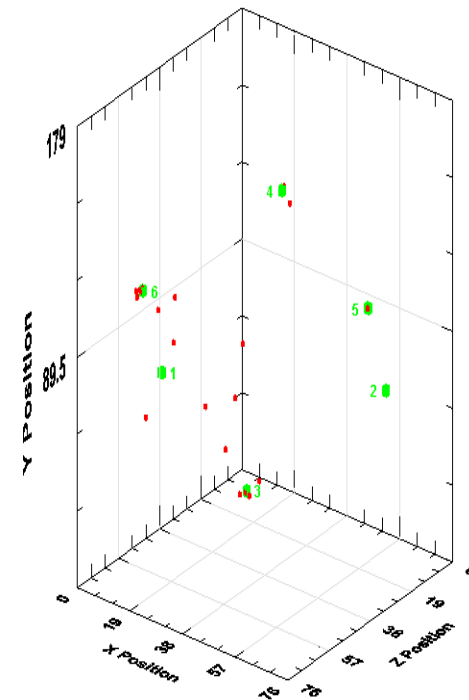


Figure C-19 Specimen DGR-2, 474.71 m

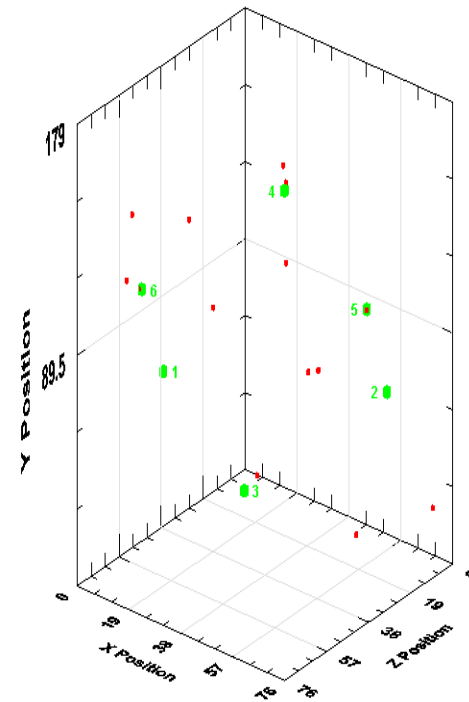


Figure C-20 Specimen DGR-2, 491.32 m

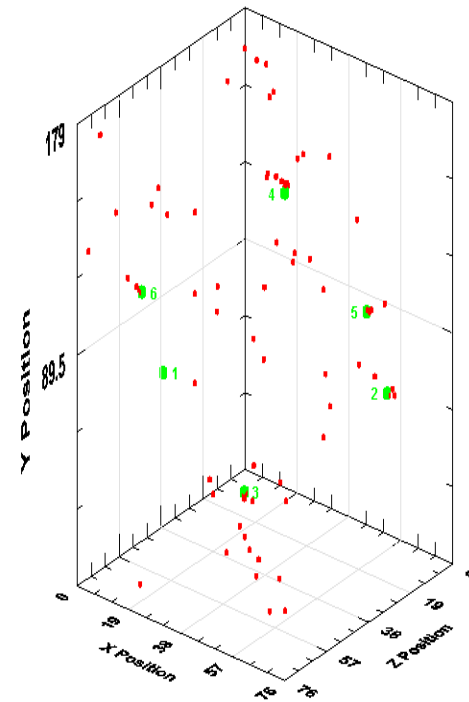


Figure C-21 Specimen DGR-2, 502.78 m

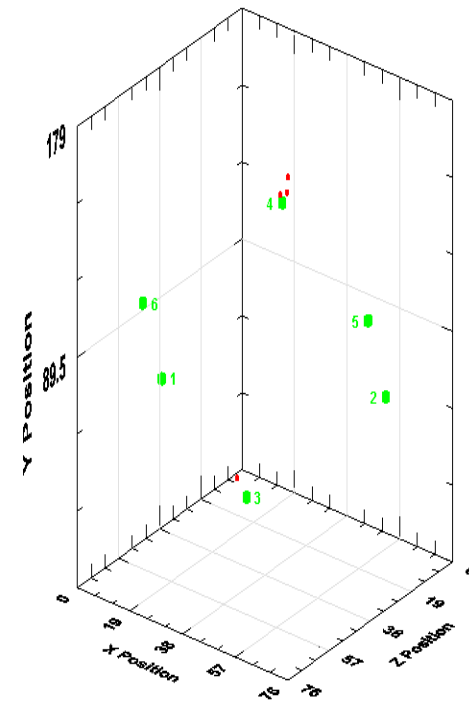


Figure C-22 Specimen DGR-2, 519.61 m

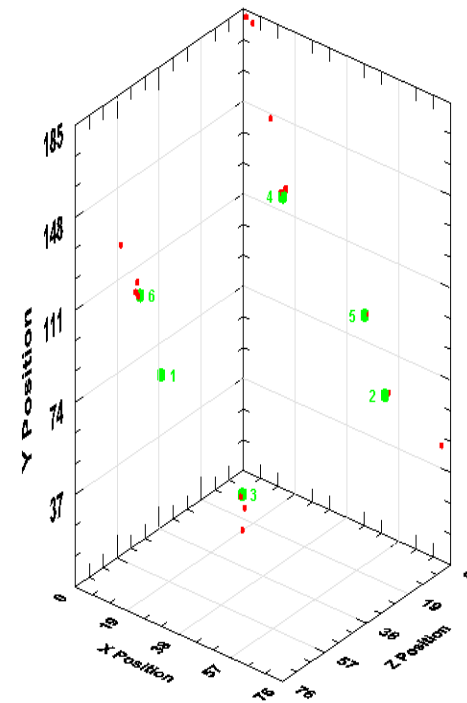


Figure C-23 Specimen DGR-2, 533.94 m

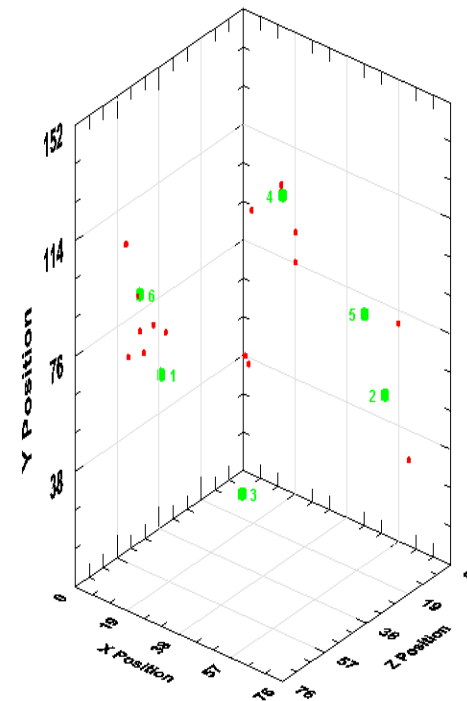


Figure C-24 Specimen DGR-2, 580.99 m

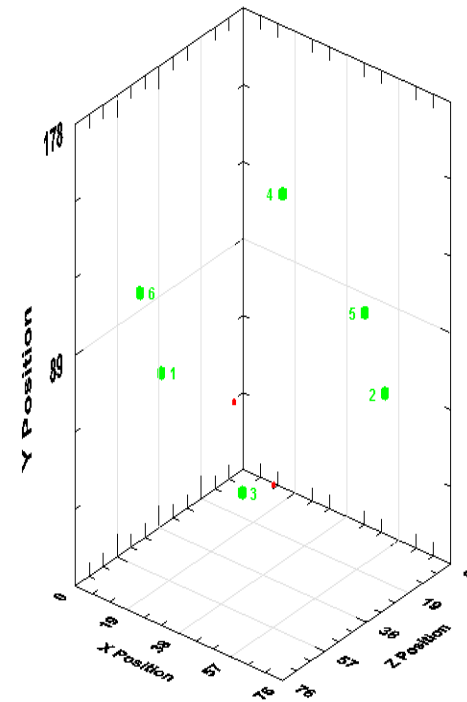


Figure C-25 Specimen DGR-2, 586.35 m

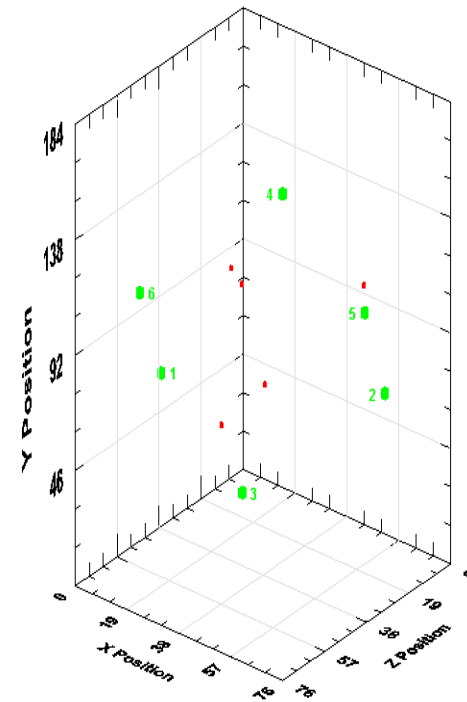


Figure C-26 Specimen DGR-2, 587.51 m

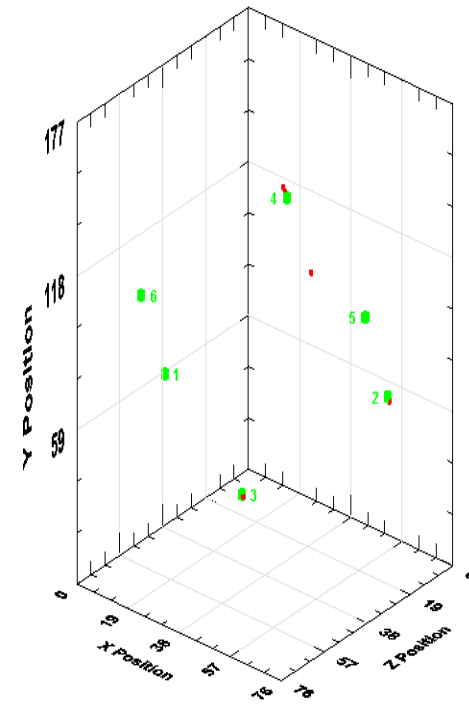


Figure C-27 Specimen DGR-2, 606.50 m

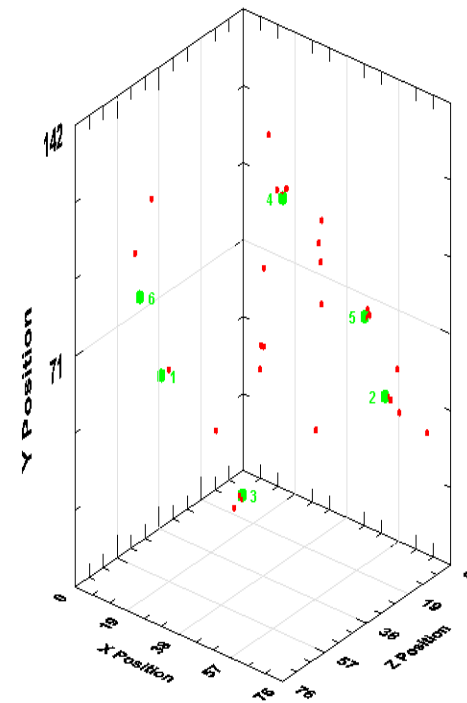


Figure C-28 Specimen DGR-2, 646.42 m

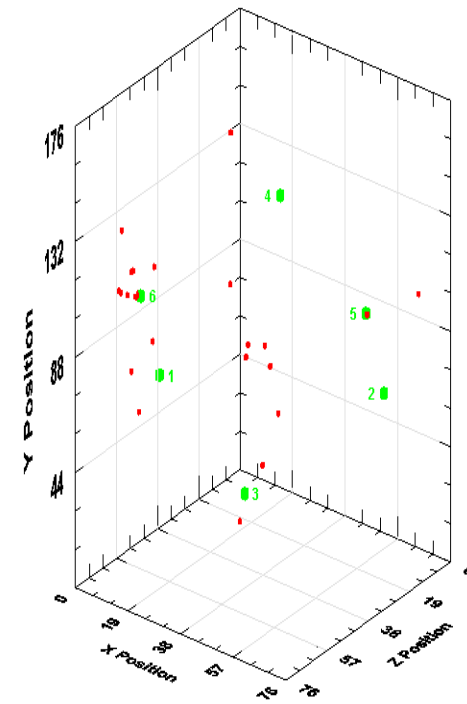


Figure C-29 Specimen DGR-2, 654.97 m

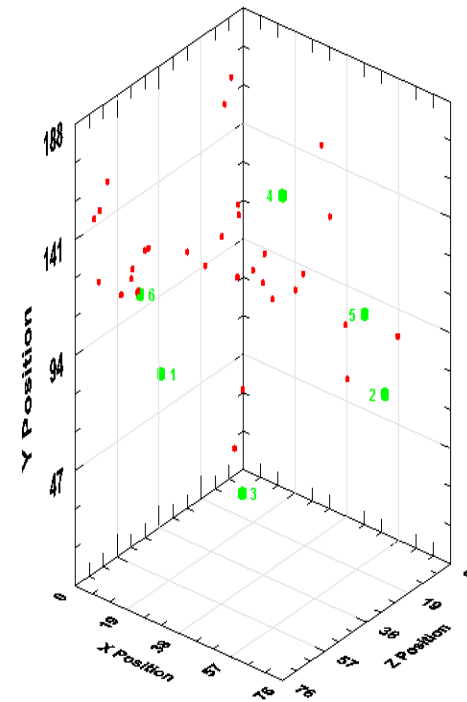


Figure C-30 Specimen DGR-2, 655.32 m

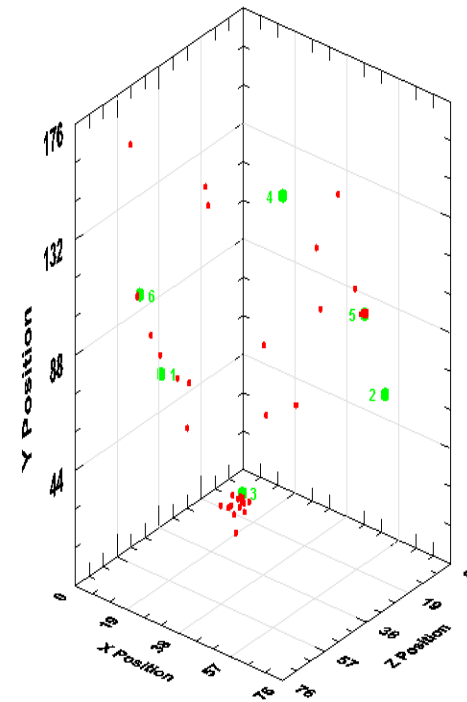


Figure C-31 Specimen DGR-2, 660.68 m

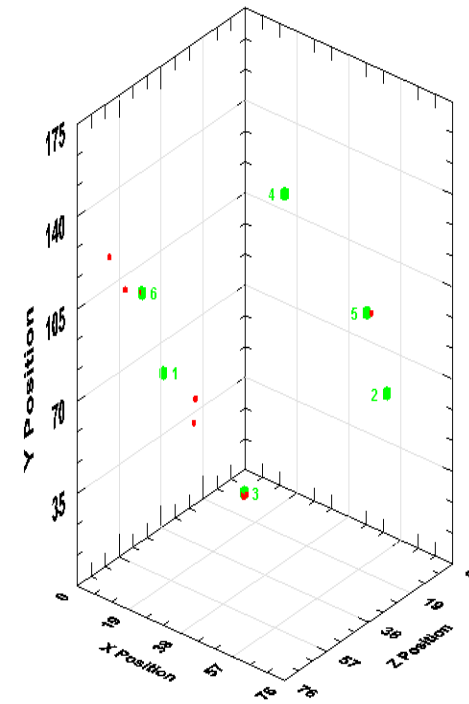


Figure C-32 Specimen DGR-2, 661.61 m

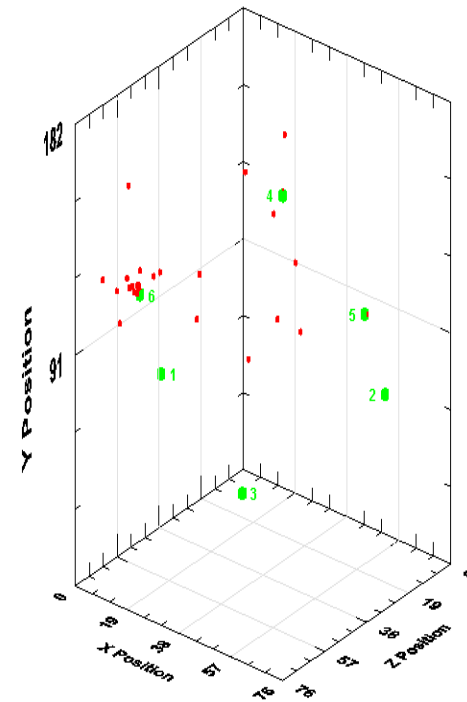


Figure C-33 Specimen DGR-2, 666.79 m

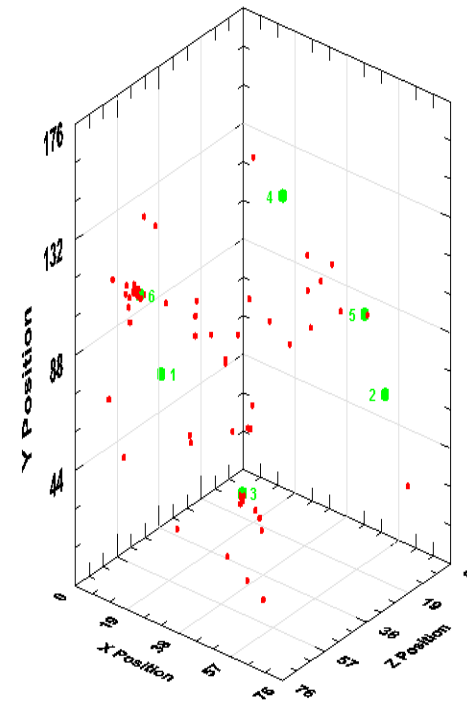
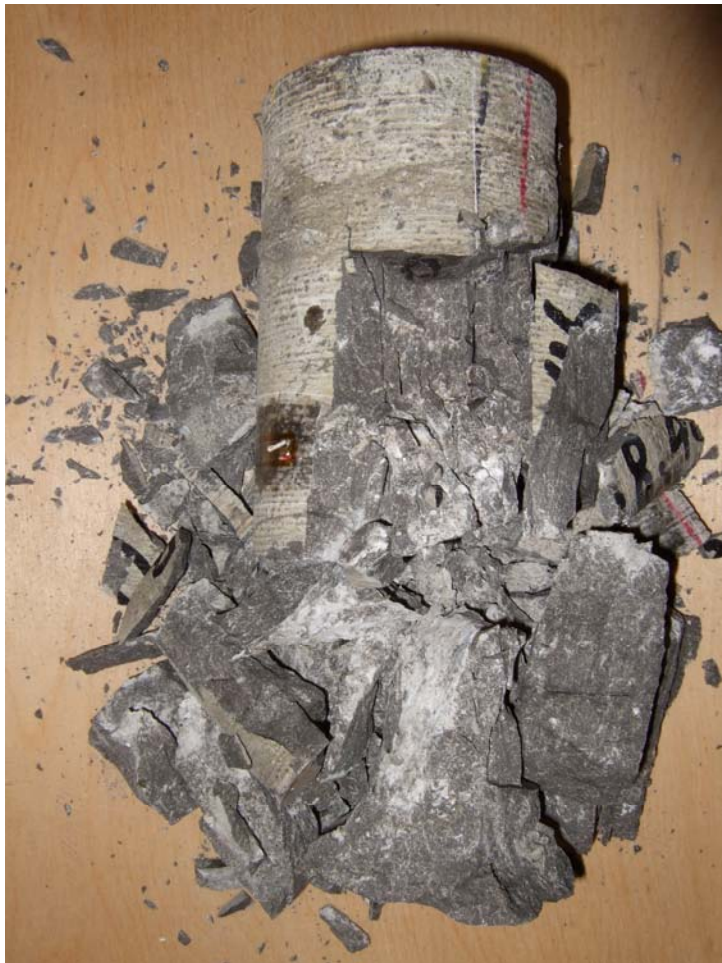


Figure C-34 Specimen DGR-2, 668.46 m

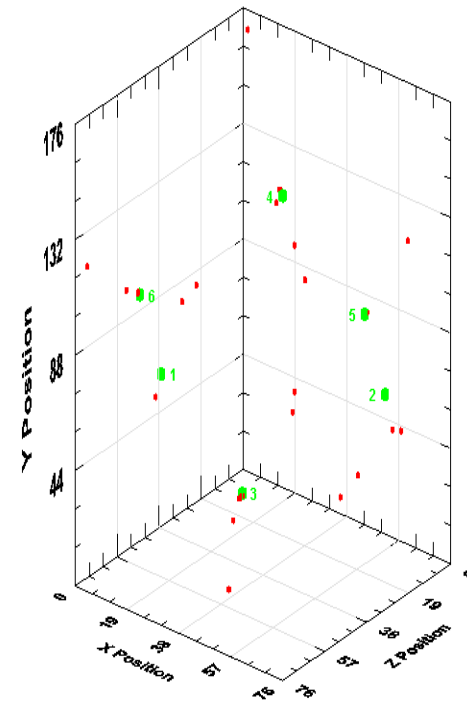


Figure C-35 Specimen DGR-2, 673.26 m

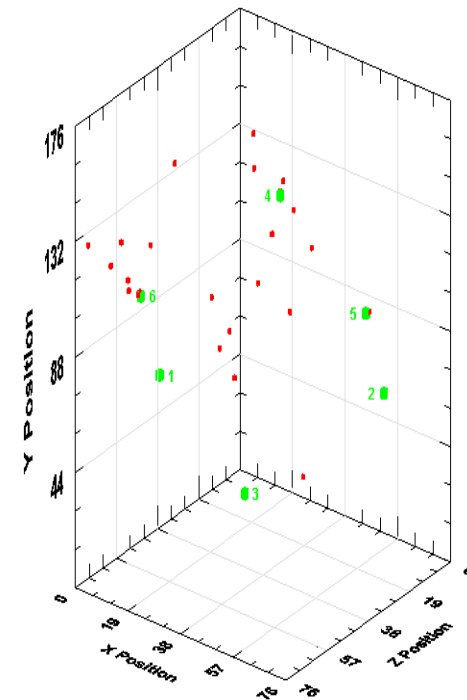


Figure C-36 Specimen DGR-2, 674.11 m

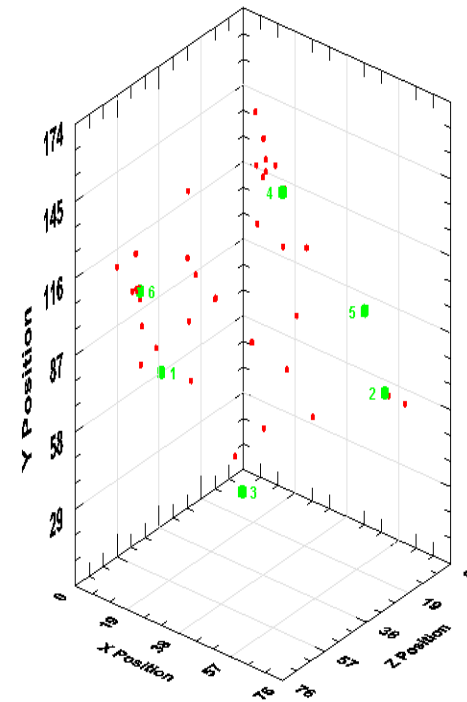


Figure C-37 Specimen DGR-2, 676.45 m

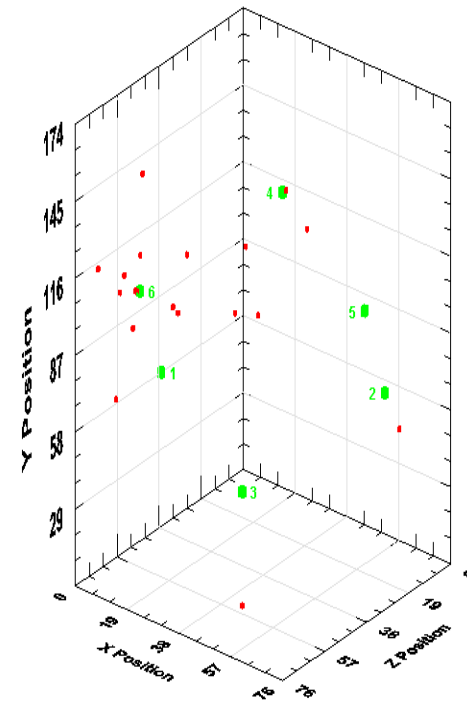


Figure C-38 Specimen DGR-2, 679.83 m

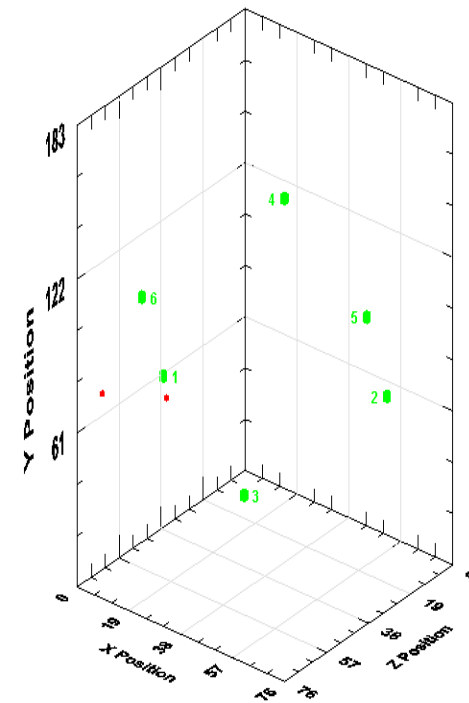


Figure C-39 Specimen DGR-2, 683.02 m

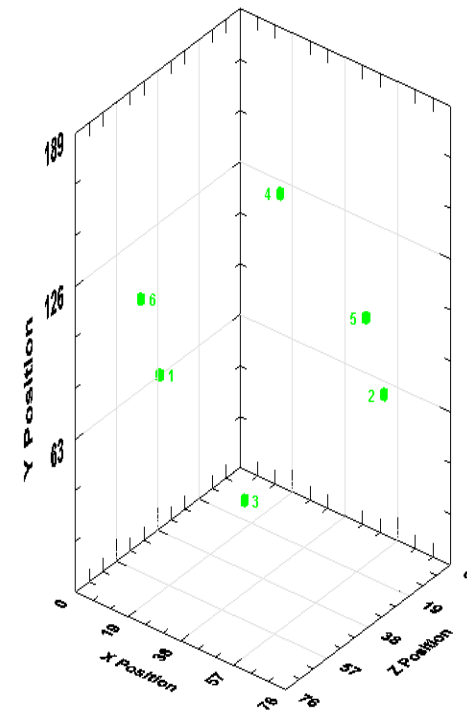


Figure C-40 Specimen DGR-2, 688.22 m

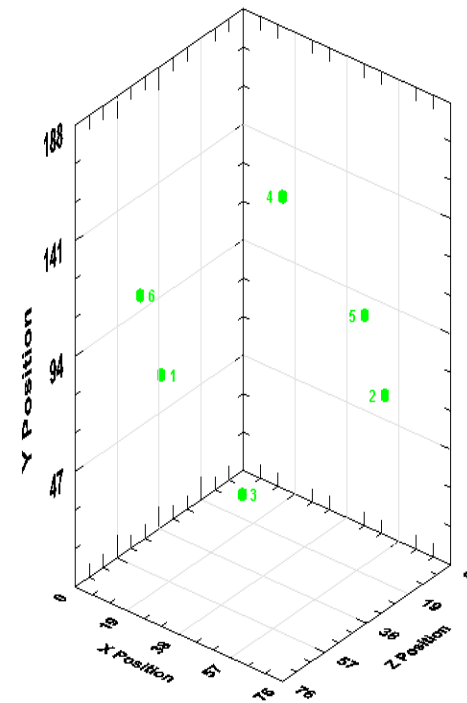


Figure C-41 Specimen DGR-2, 694.11 m

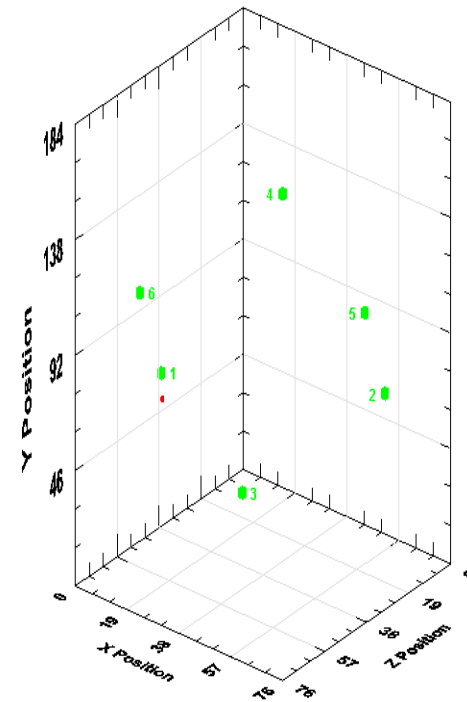


Figure C-42 Specimen DGR-2, 695.15 m

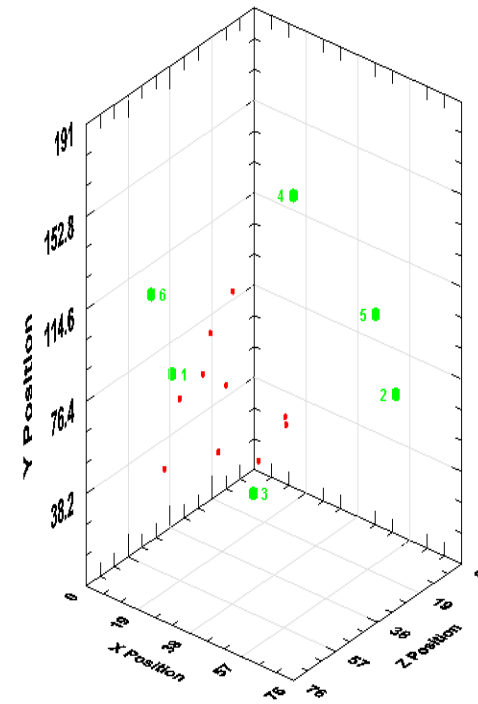


Figure C-43 Specimen DGR-2, 702.69 m

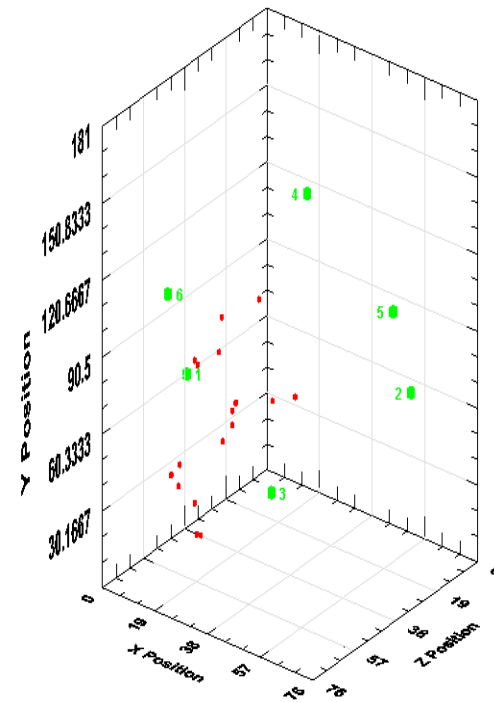


Figure C-44 Specimen DGR-2, 704.47 m

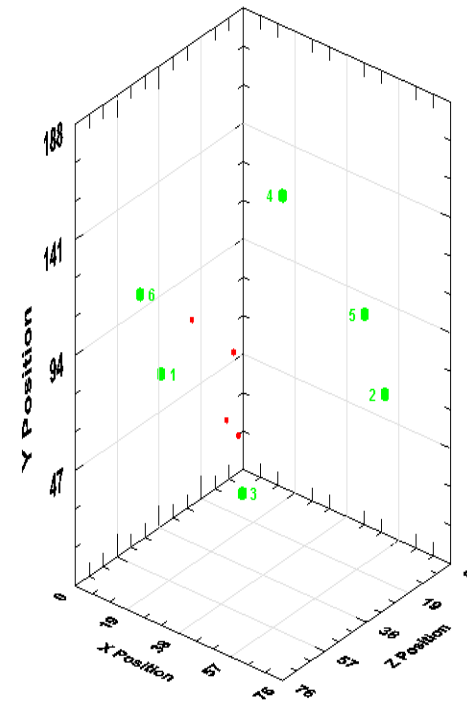


Figure C-45 Specimen DGR-2, 710.29 m

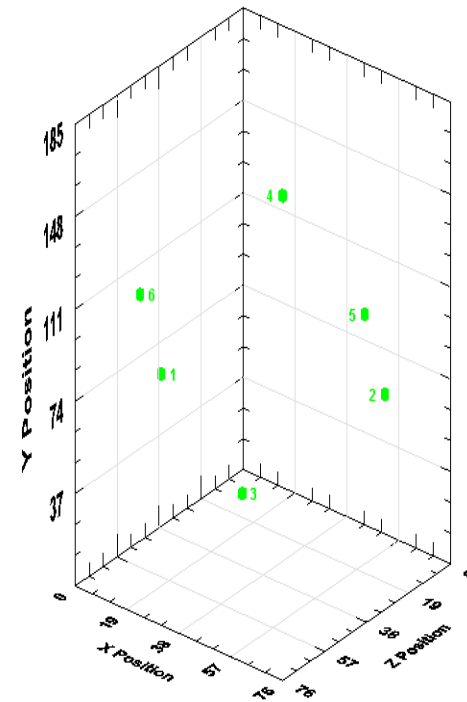


Figure C-46 Specimen DGR-2, 719.38 m

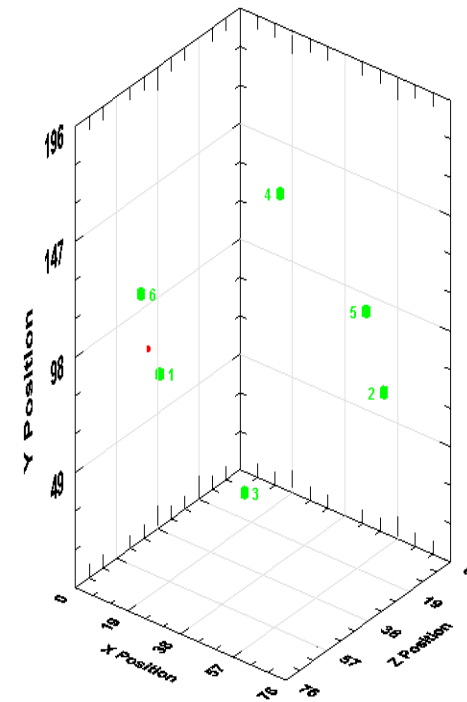


Figure C-47 Specimen DGR-2, 737.16 m

APPENDIX D

Shear Stress vs. Displacement and Shear Stress vs. Normal Stress

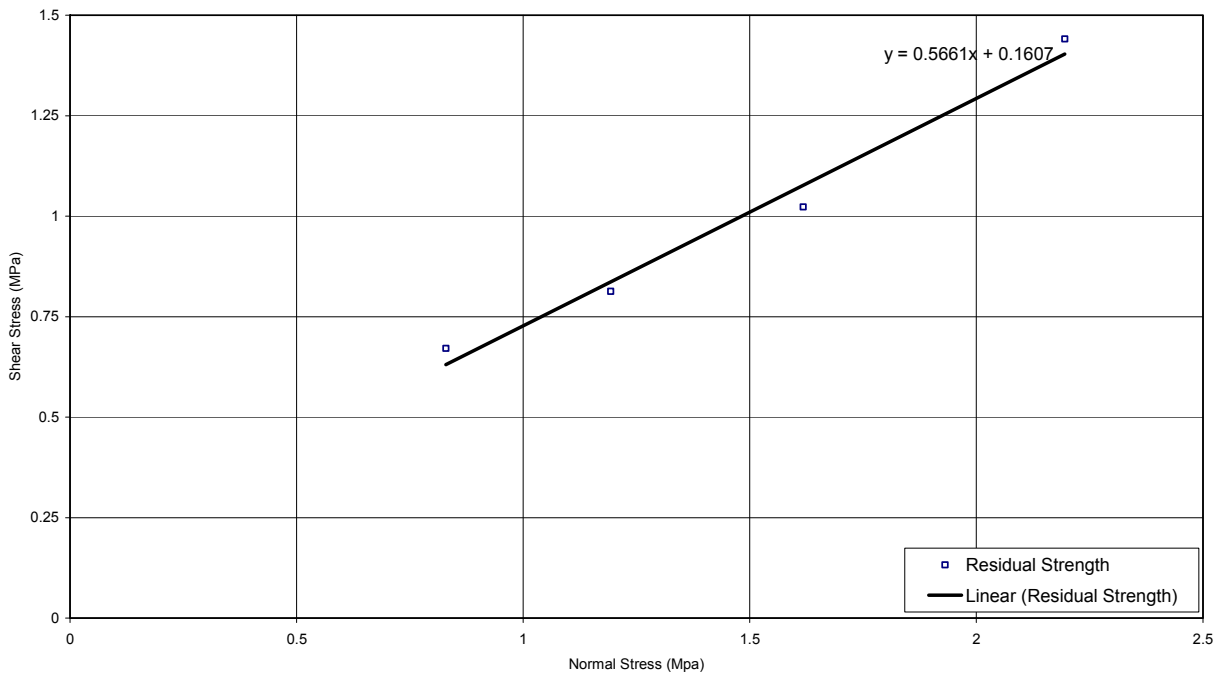
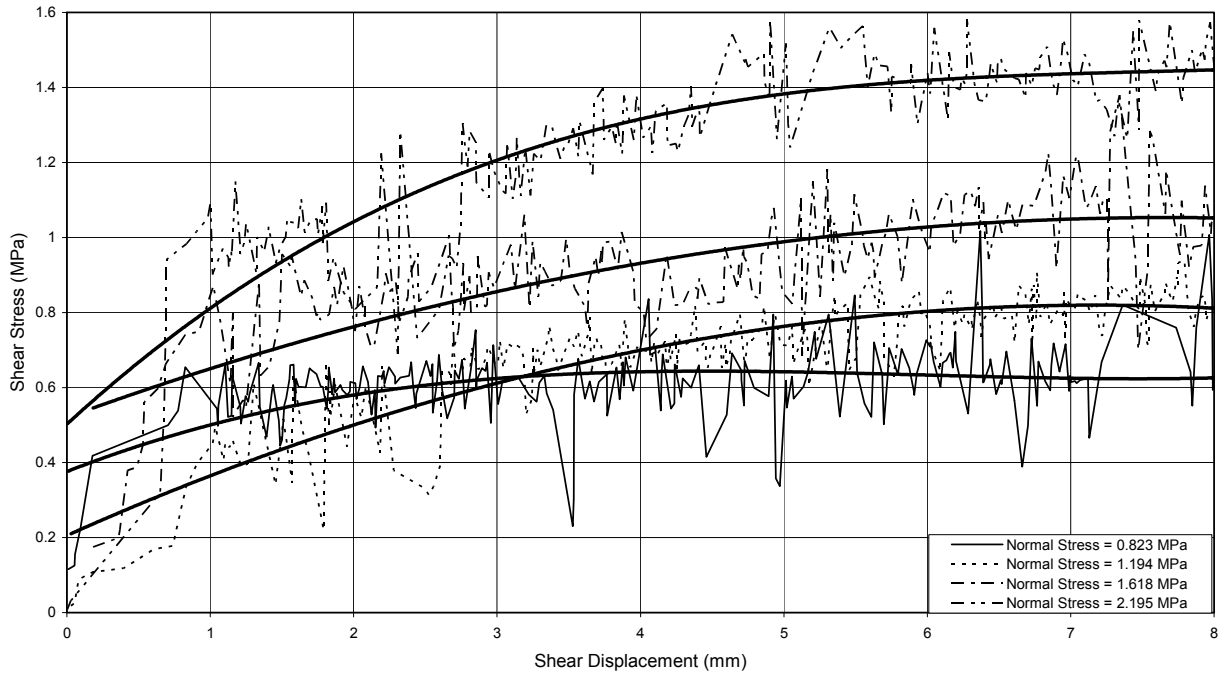


Figure D-1 Specimen DGR-2, 613.37 m

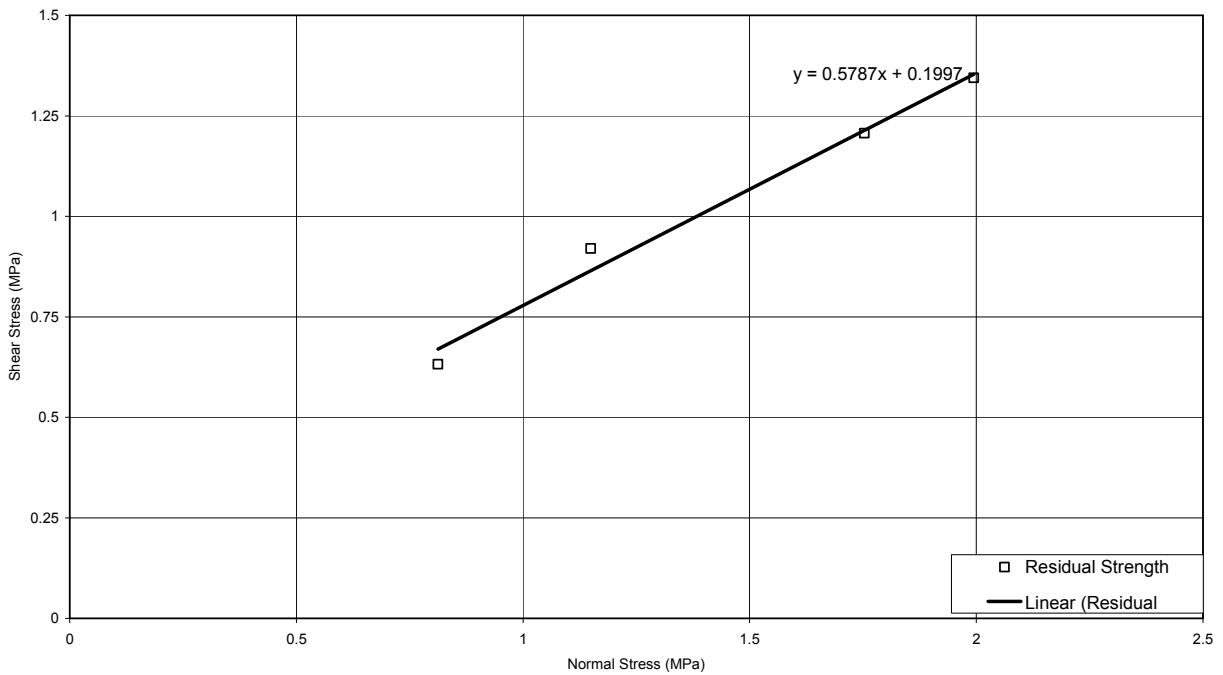
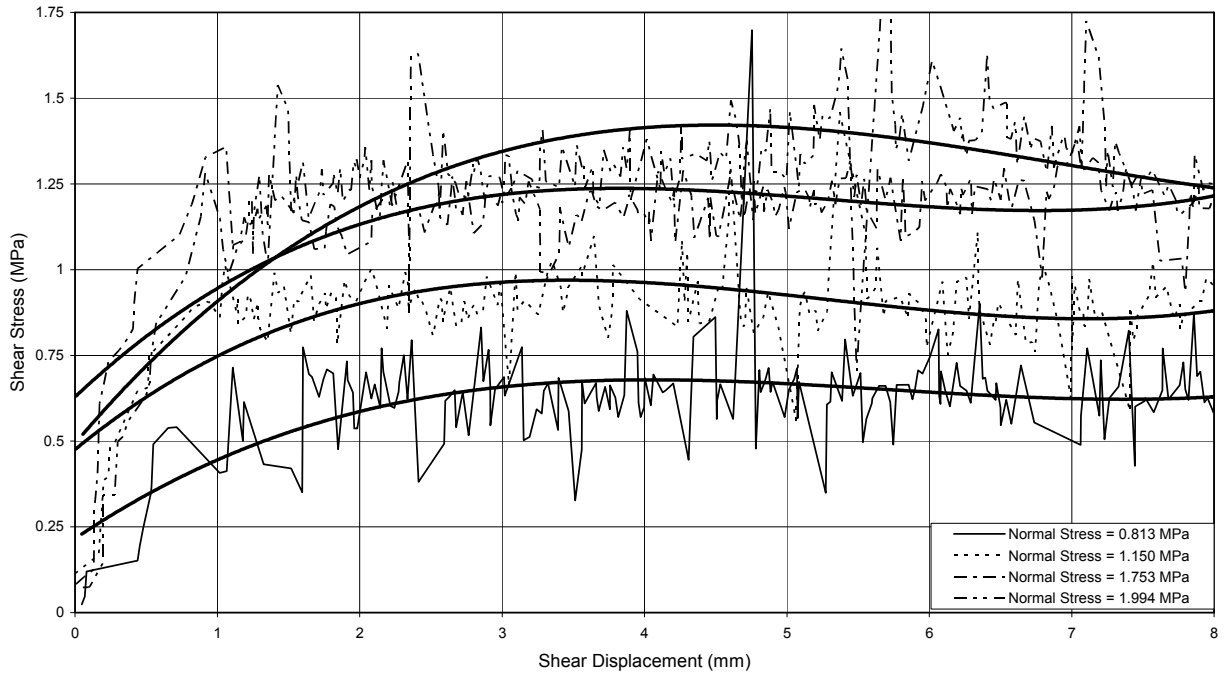


Figure D-2 Specimen DGR-2, 616.59 m

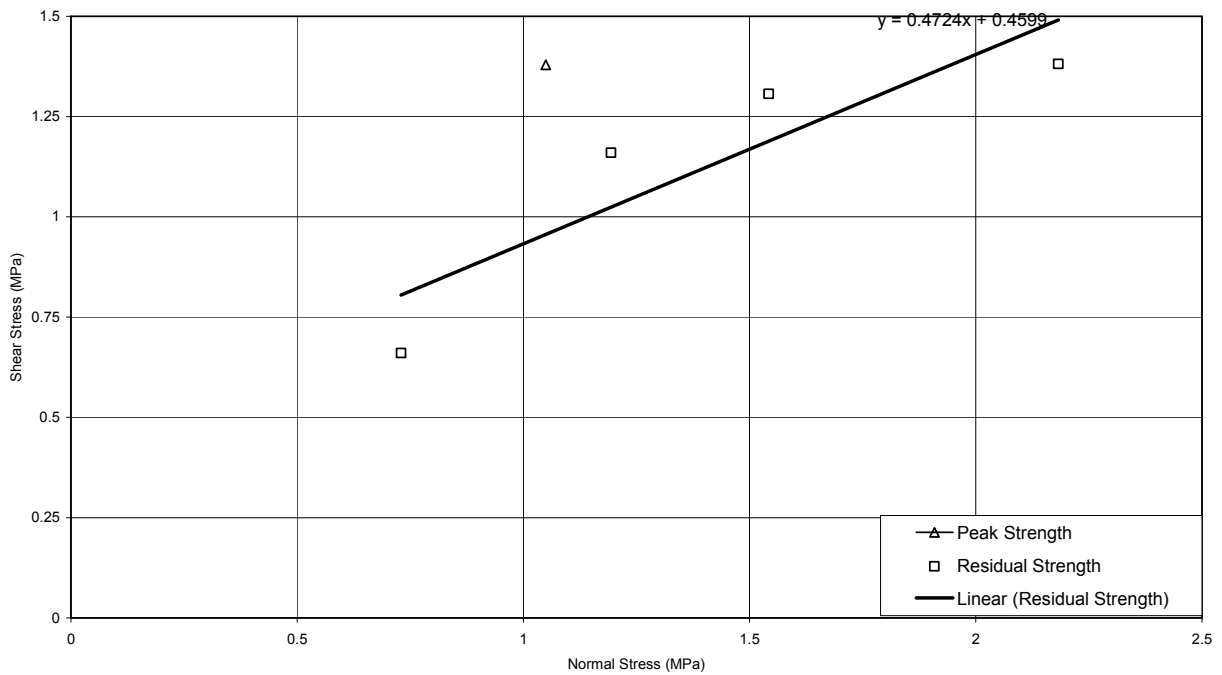
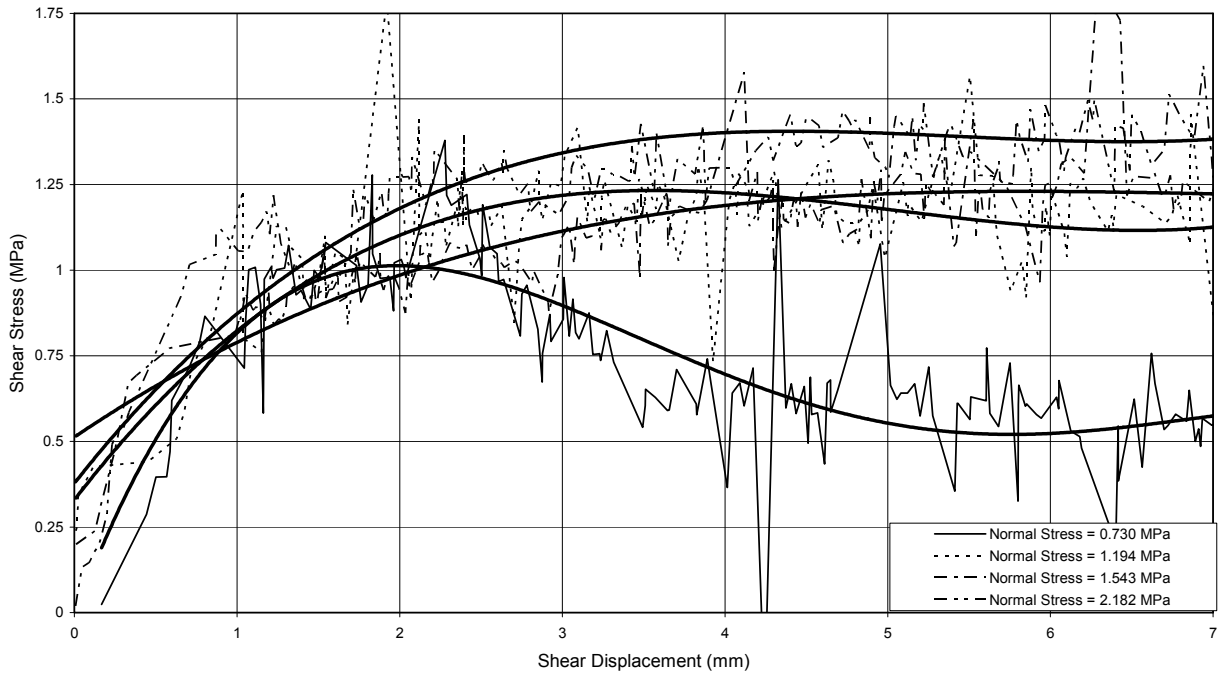


Figure D-3 Specimen DGR-2, 646.72 m

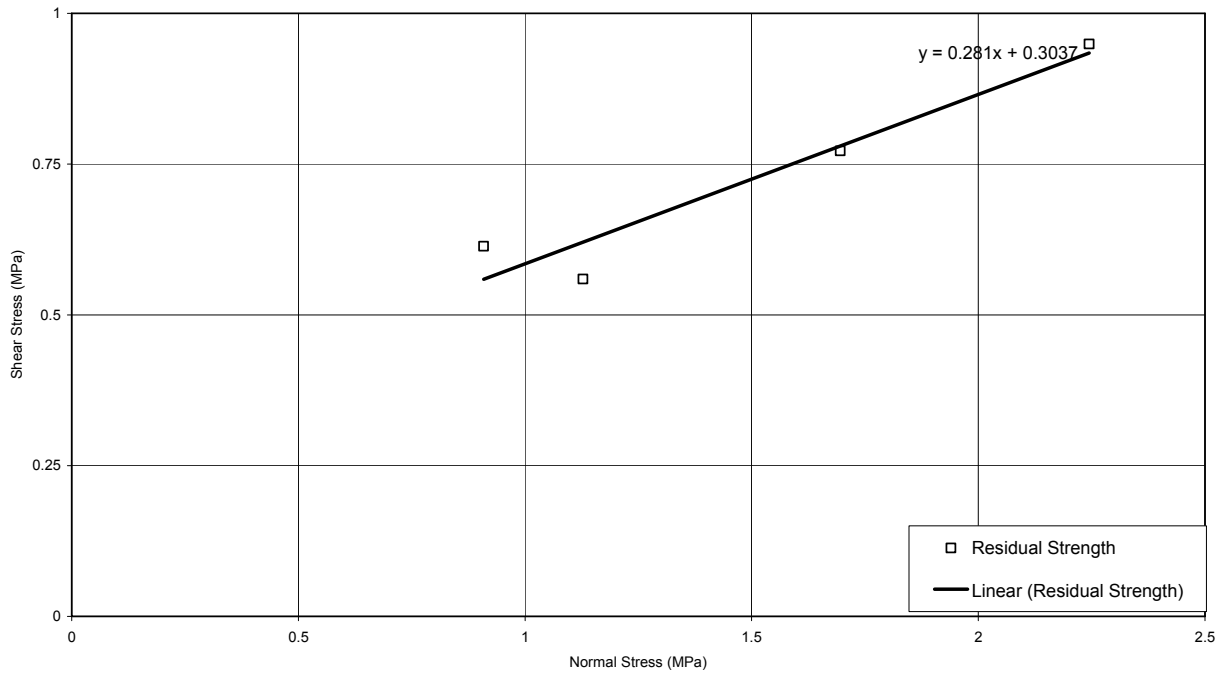
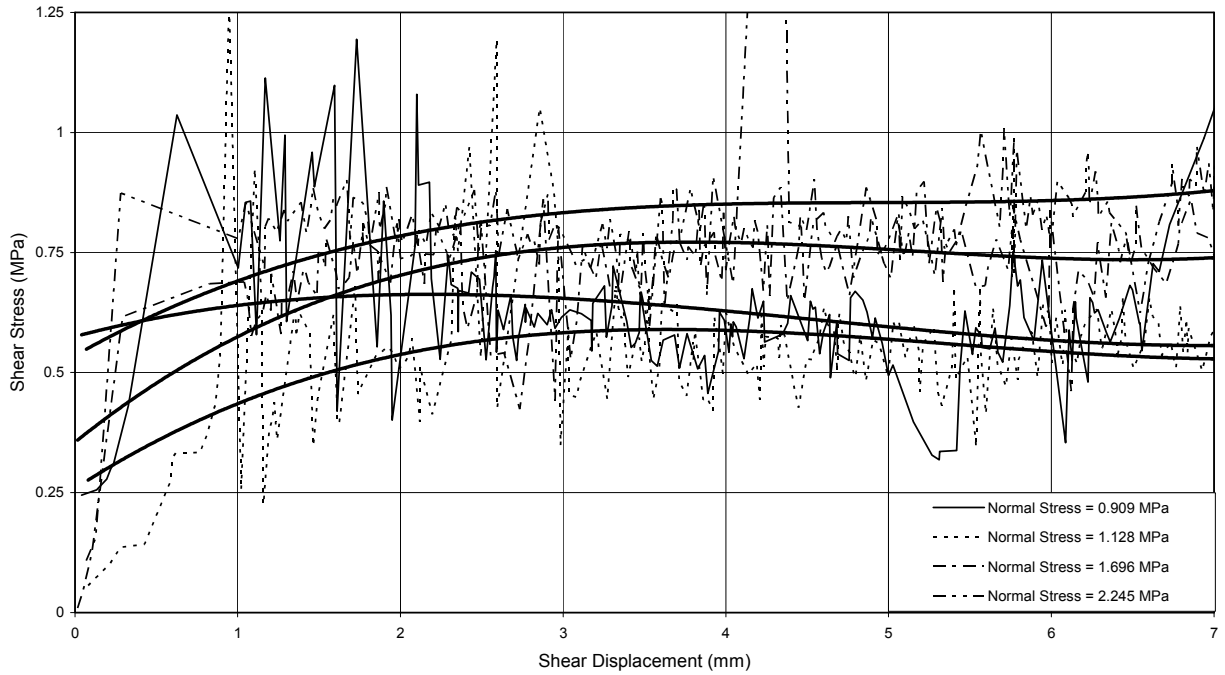


Figure D-4 Specimen DGR-2, 692.00 m

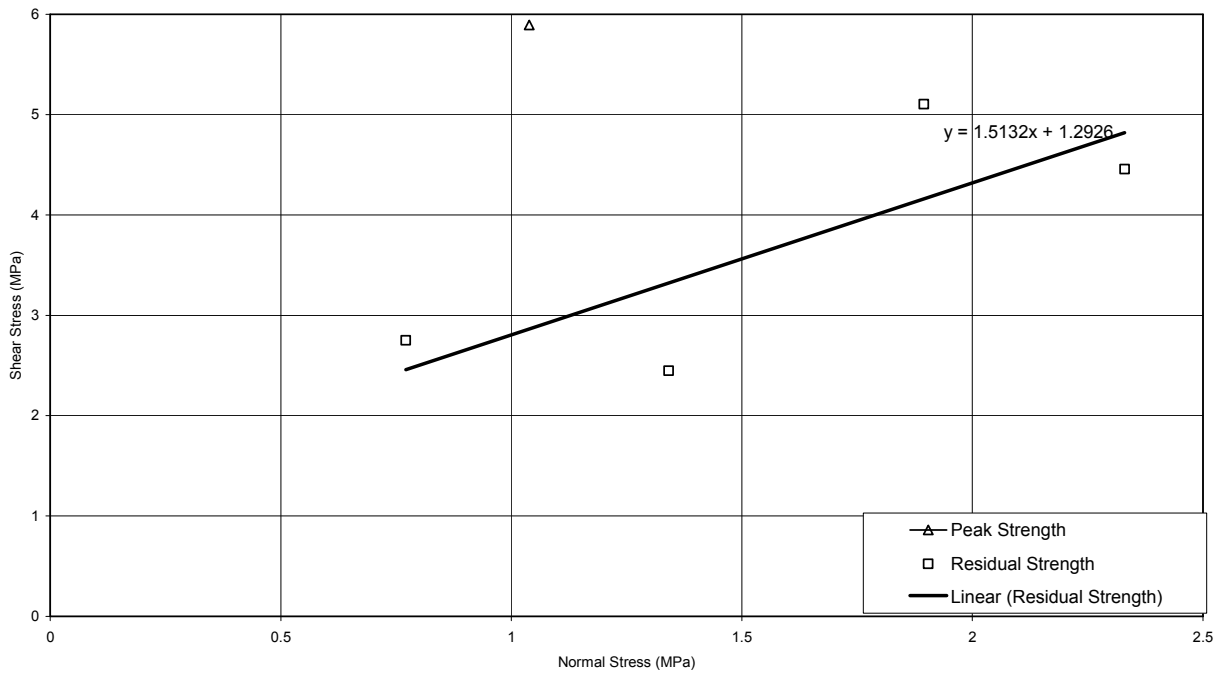
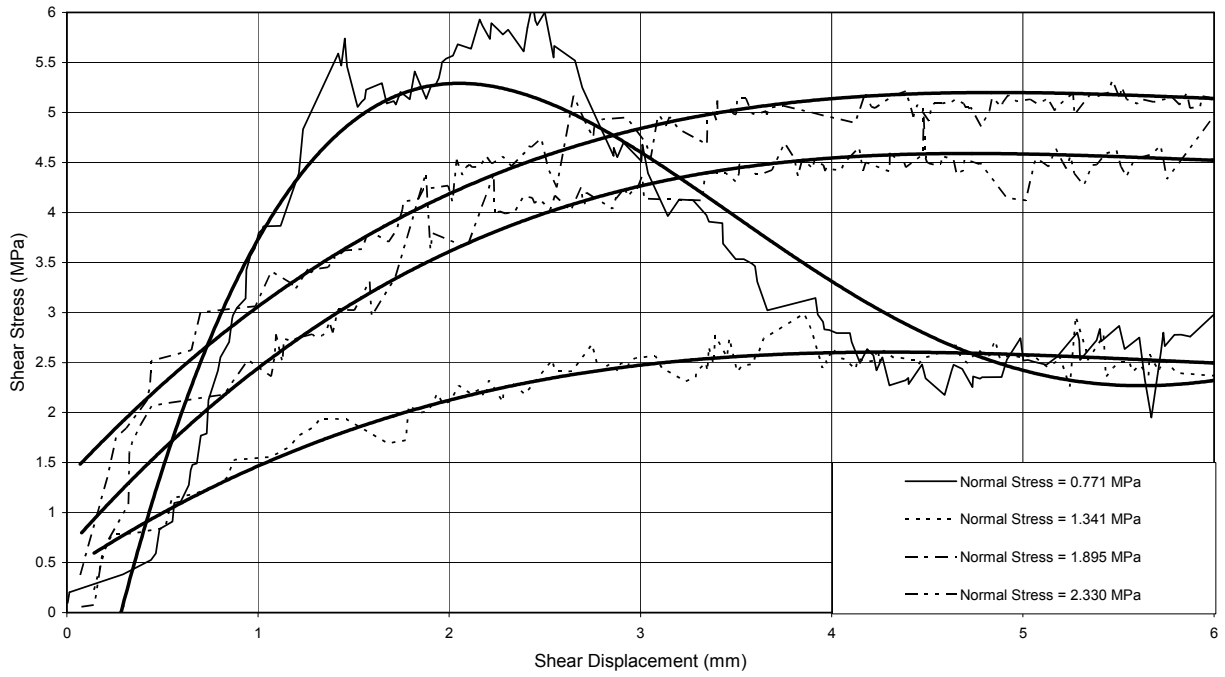


Figure D-5 Specimen DGR-2, 697.86 m

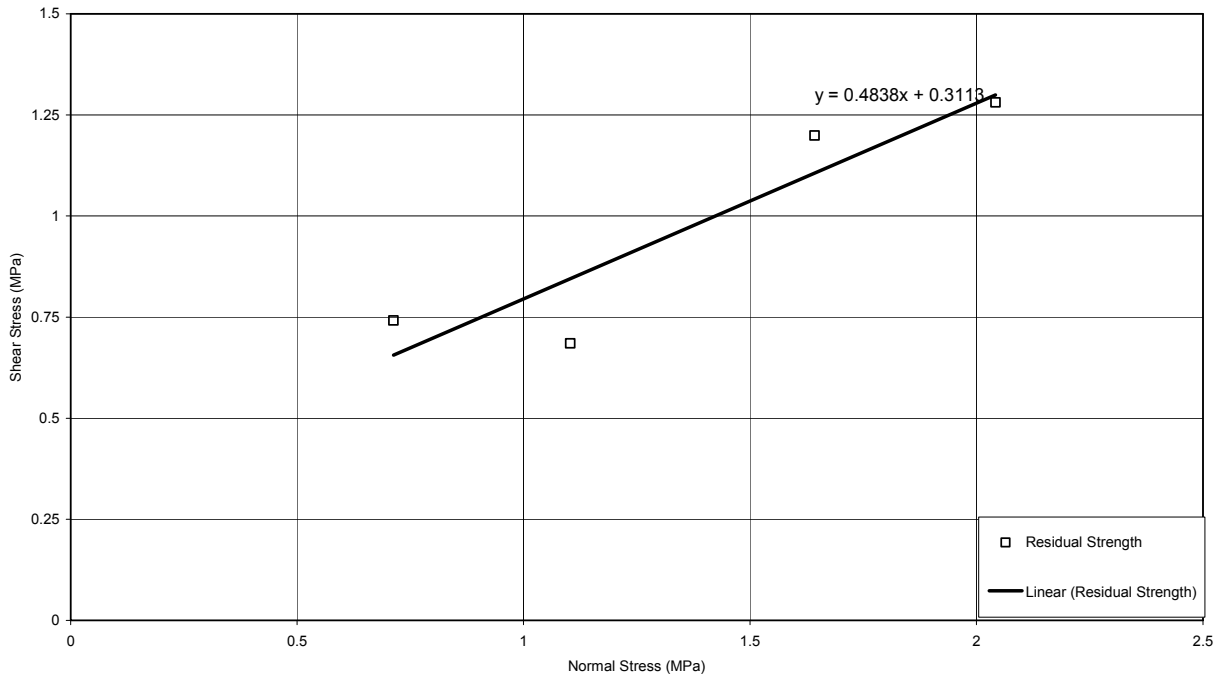
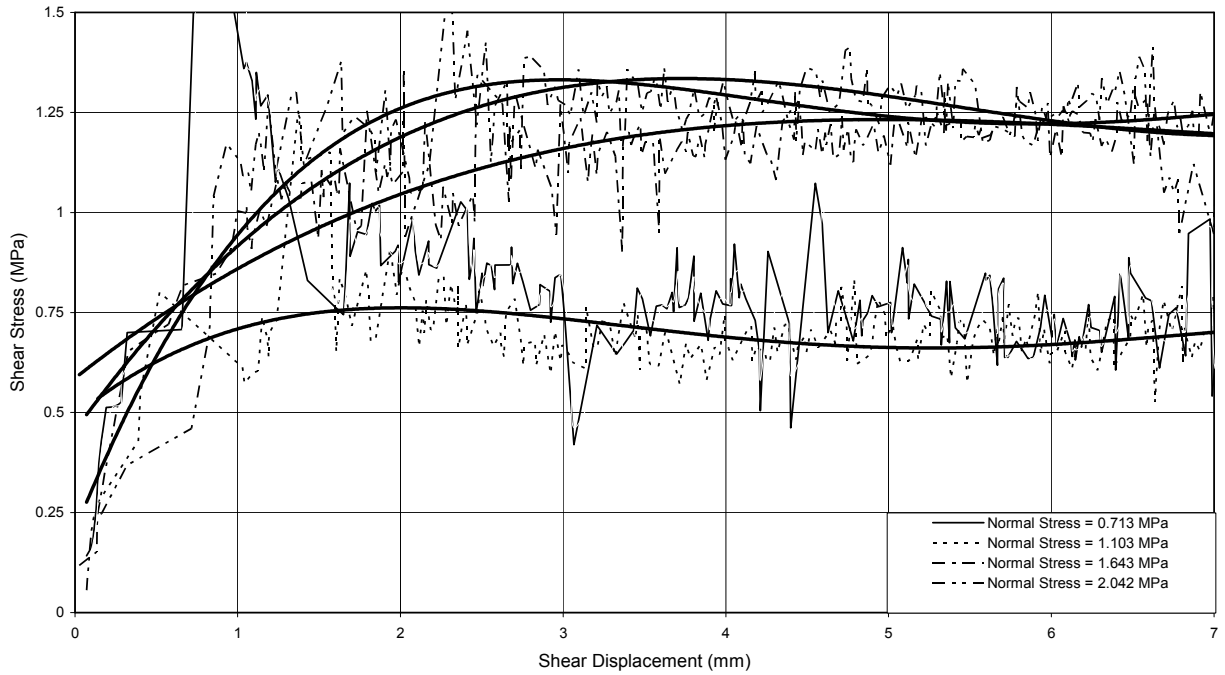


Figure D-6 Specimen DGR-2, 702.23 m

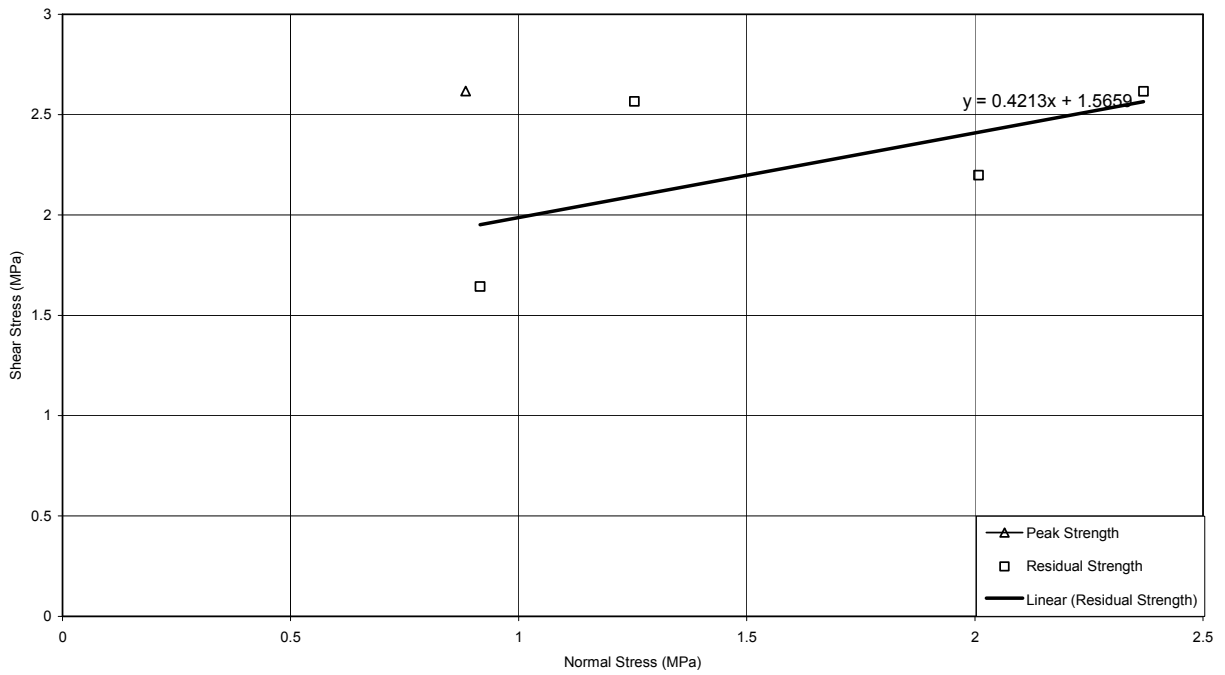
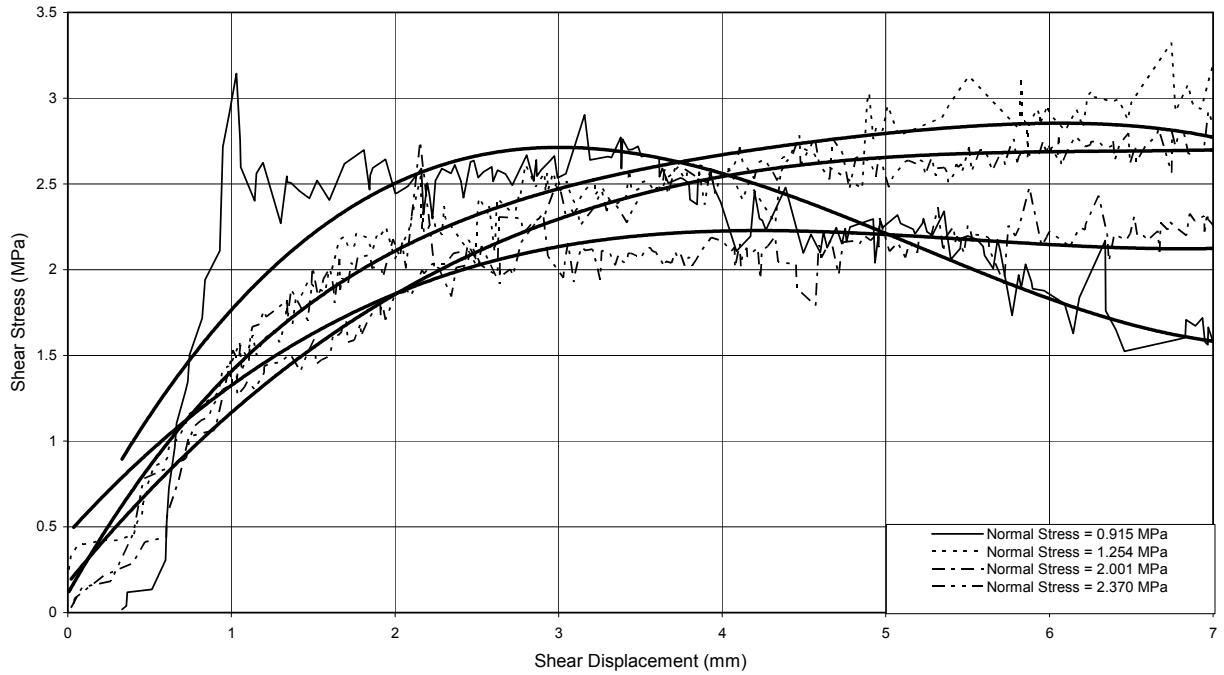


Figure D-7 Specimen DGR-2, 705.86 m

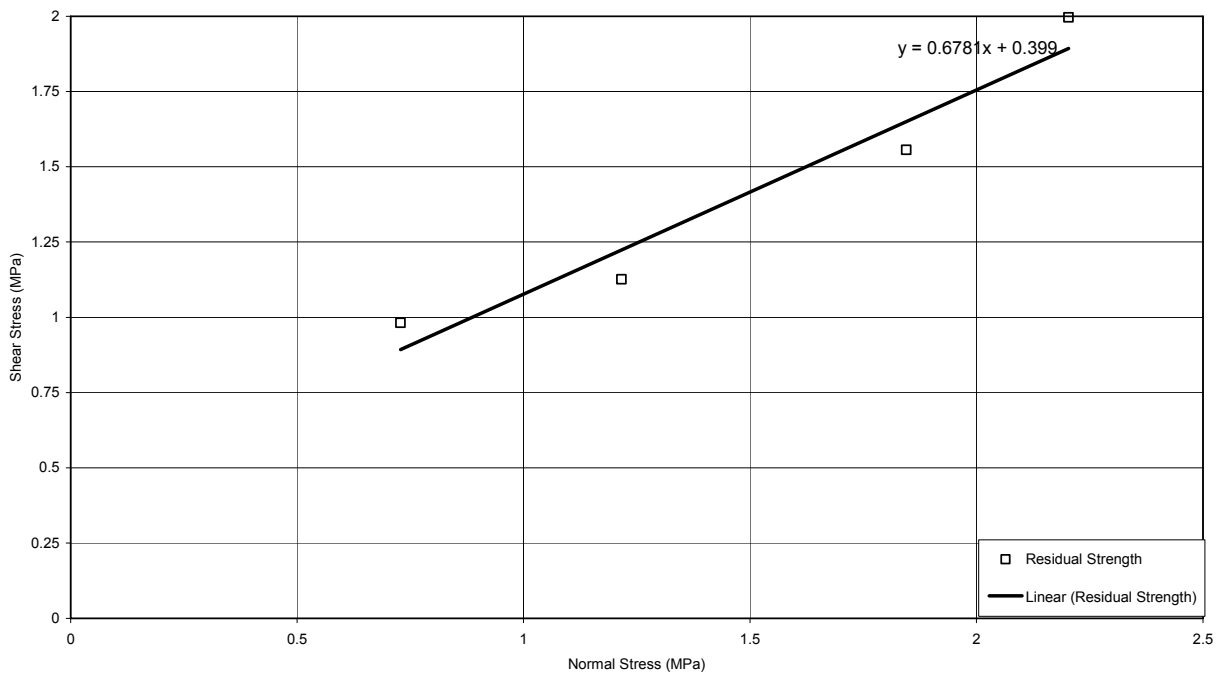
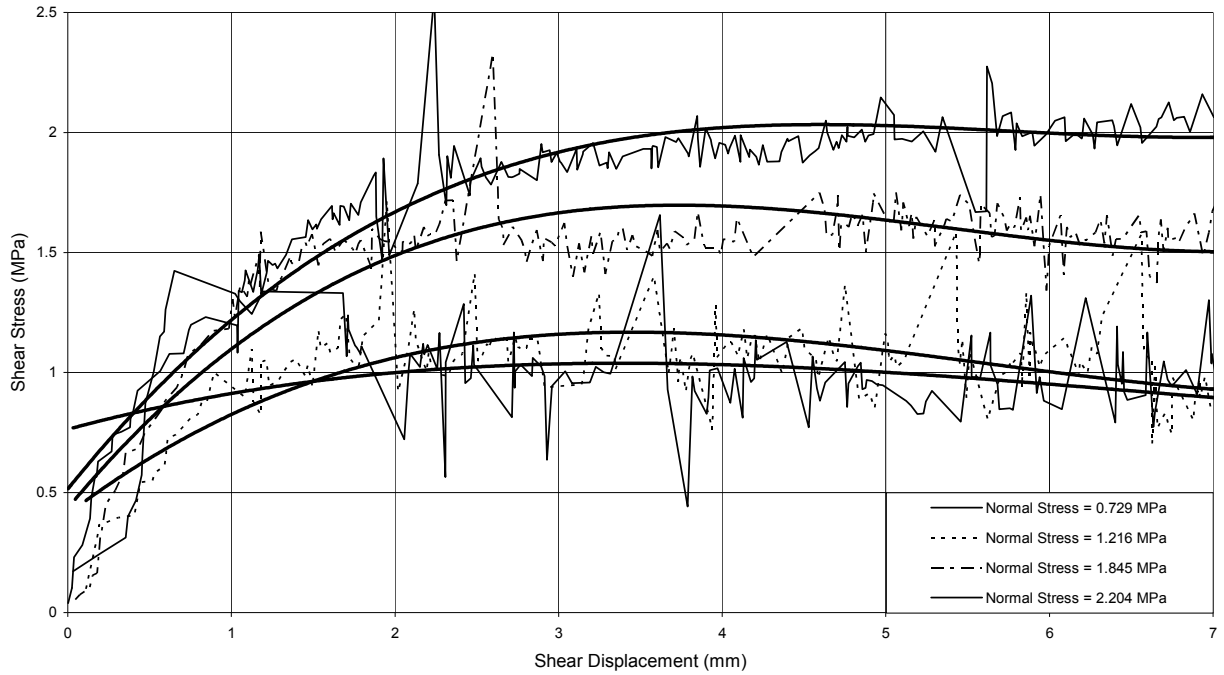


Figure D-8 Specimen DGR-2, 708.57 m

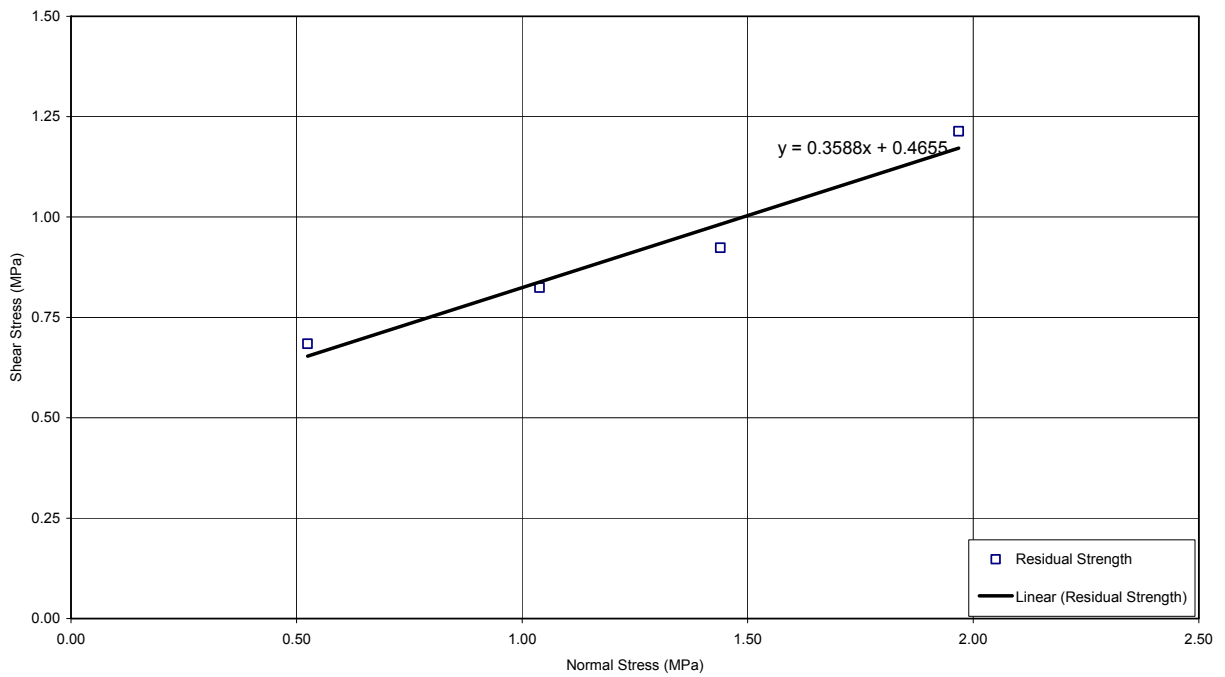
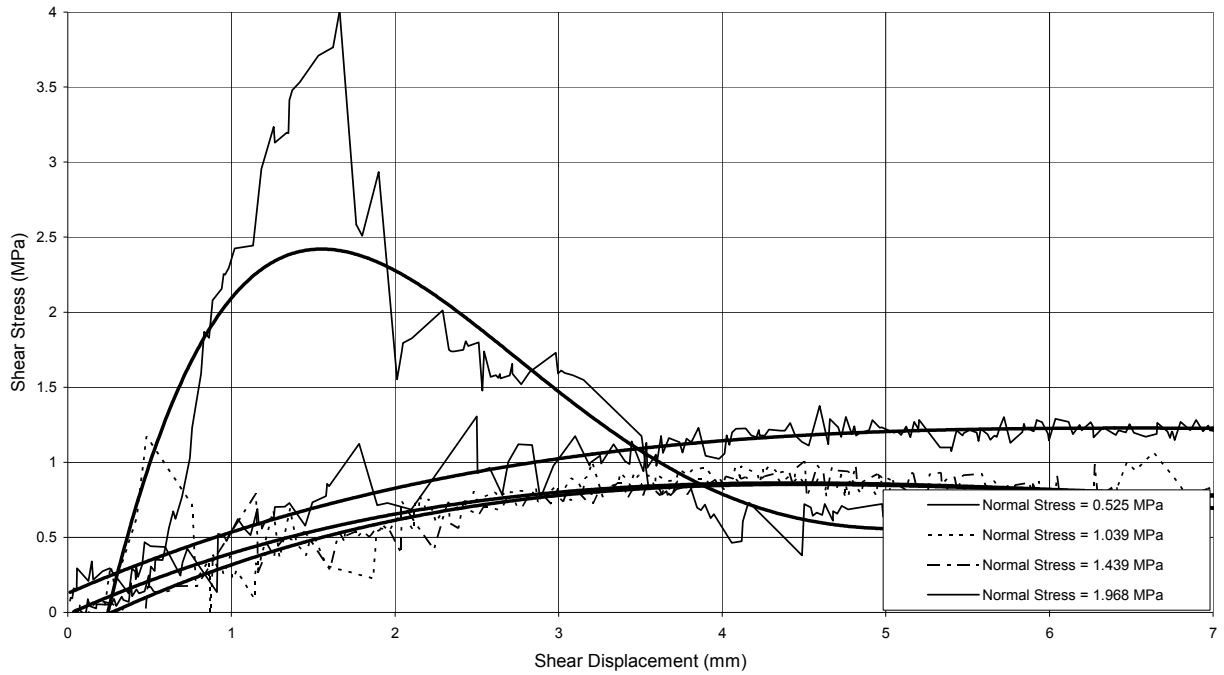


Figure D-9 Specimen DGR-2, 664.94 m

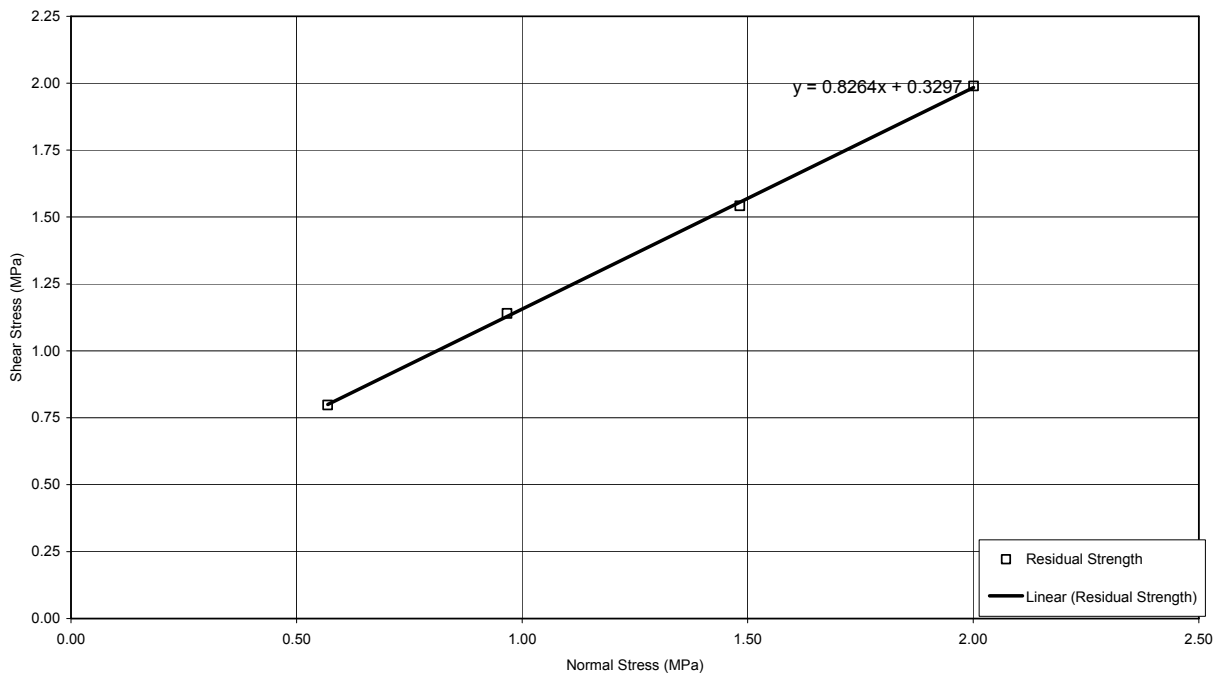
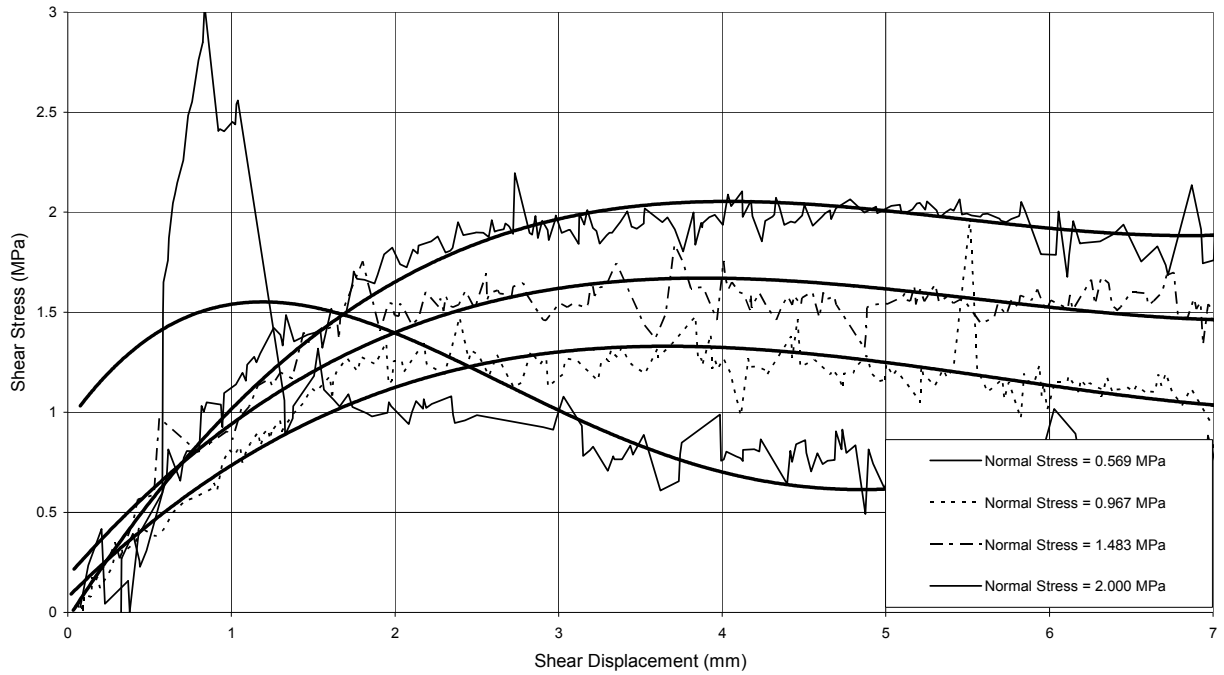


Figure D-10 Specimen DGR-2, 673.06 m

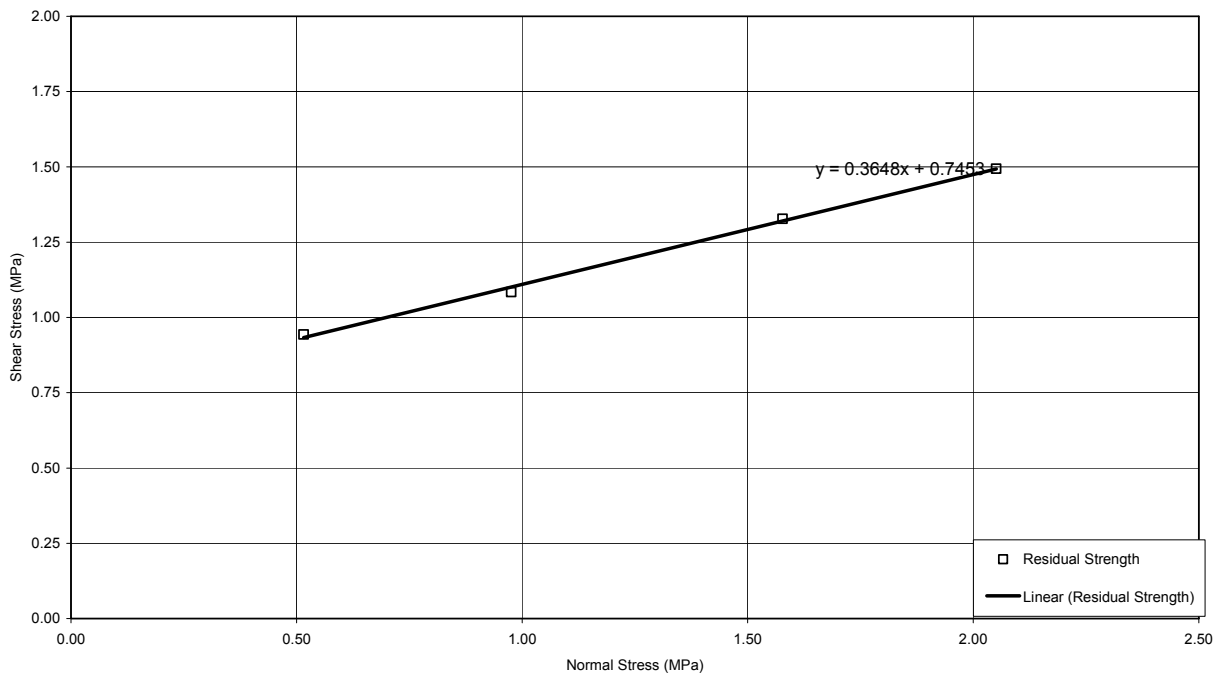
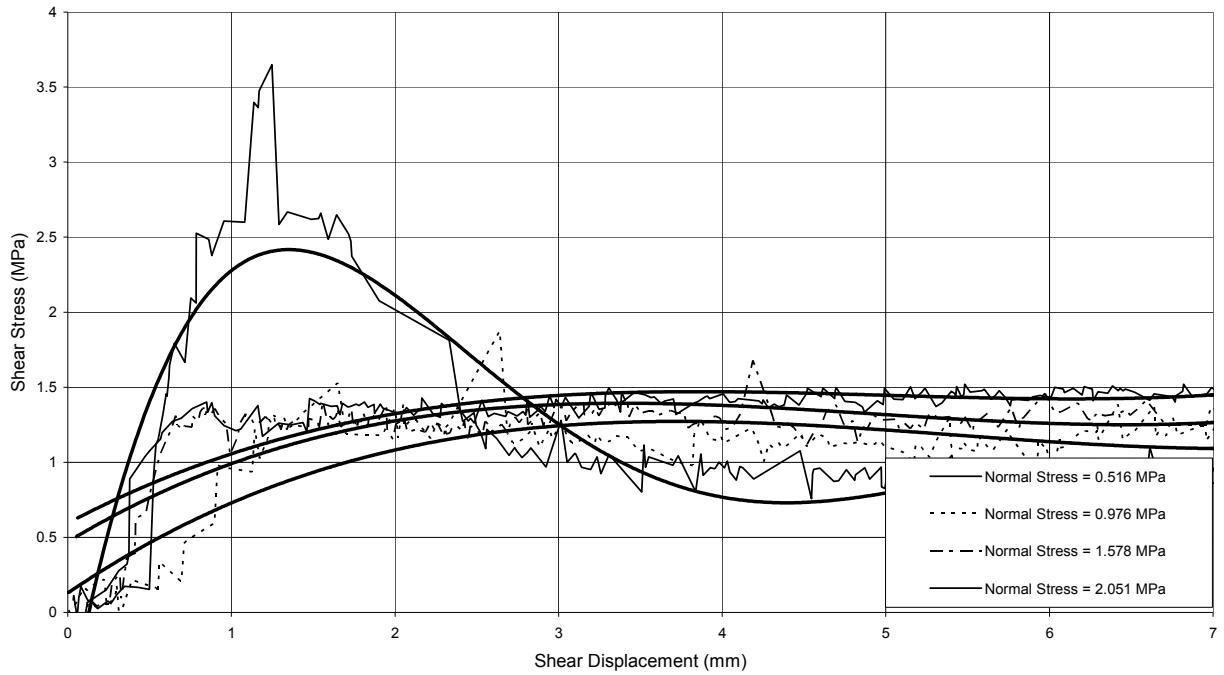


Figure D-11 Specimen DGR-2, 684.00 m

APPENDIX E
Failed Brazilian Specimens

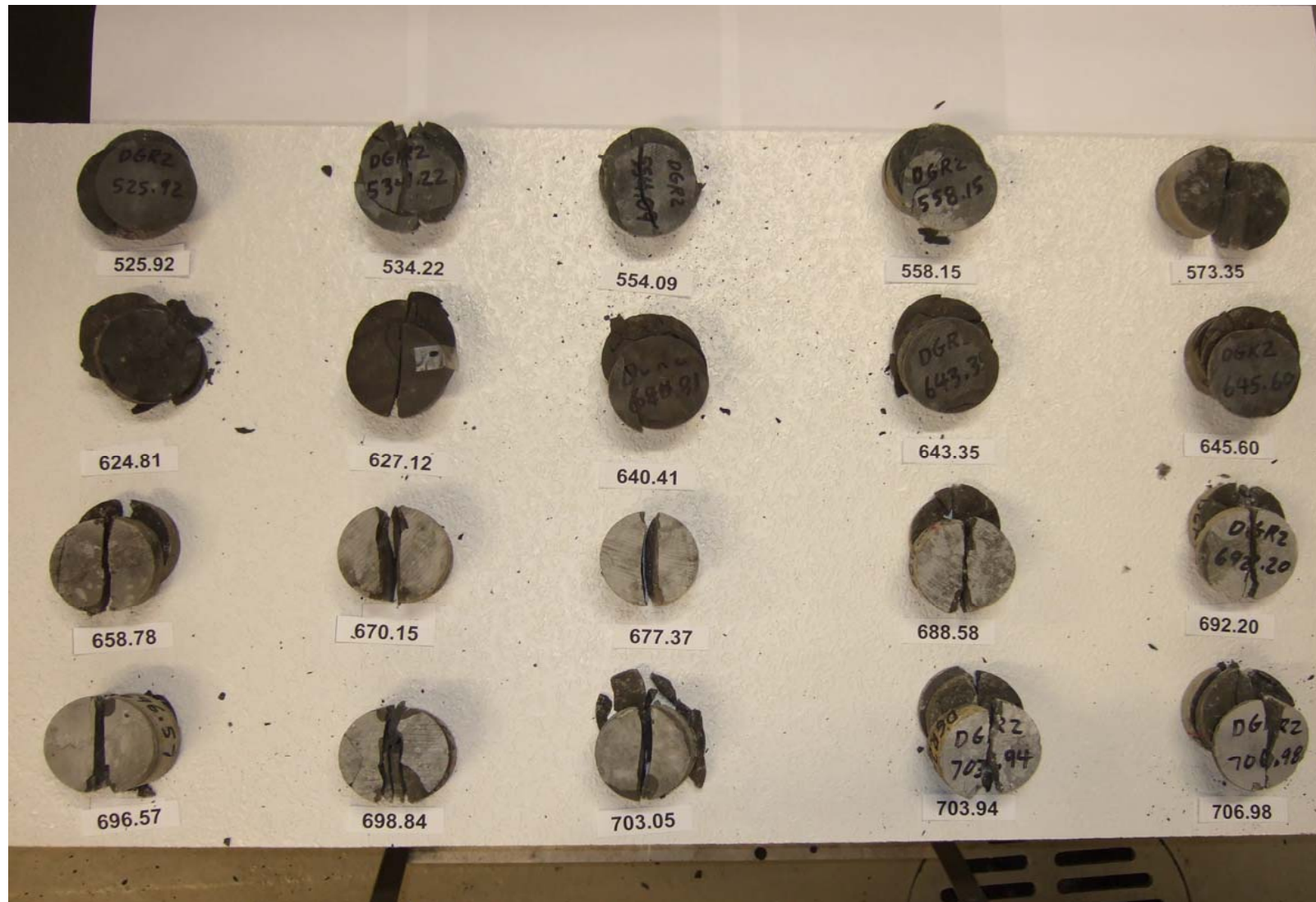


Figure E-1 Tested Brazilian Specimens (Samples Identified by Depth in m)

APPENDIX F

Geological Descriptions and Geological Formation of Intera DGR Specimens

Table F-1. Geological formations and descriptions of DGR-1 uniaxial specimens

Specimen ID	Formation	Specimen Description
DGR1-027.30	Lucas	light grey dolostone
DGR1-029.38	Lucas	light grey-tan dolostone
DGR1-070.84	Amherstburg	grey-brown dolostone
DGR1-108.62	Bois Blanc	grey-brown dolostone /w chert and mudstone clasts
DGR1-160.93	Bass Island	brown clastic dolostone
DGR1-171.14	Salina G-Unit	dolomitic shale /w anhydrite
DGR1-183.60	Salina, F-Unit	grey-green dolomudstone
DGR1-206.55	Salina, F-Unit	grey-green dolostone /w anhydrite
DGR1-266.20	Salina, B-Unit	brecciated dolostone
DGR1-286.69	Salina, B-Unit	brecciated dolostone
DGR1-314.88	Salina, A2 Unit	tan-grey dolostone
DGR1-367.06	Salina, A0 Unit	grey crystalline dolostone
DGR1-386.55	Goat Island	grey crystalline dolostone
DGR1-415.16	Cabot Head	massive non-calcareous red shale
DGR1-438.10	Manitoulin	grey dolostone /w shale layers
DGR1-455.22	Queenston	red shale
DGR1-460.41	Queenston	red shale

Note: Source data compiled and provided by Intera Engineering Limited

Table F-2. Geological formations and descriptions of DGR-2 uniaxial specimens

Specimen ID	Formation	Specimen Description
DGR2-457.21	Queenston	red shale
DGR2-474.71	Queenston	red shale
DGR2-491.32	Queenston	argillaceous limestone with interbedded green shale
DGR2-502.78	Queenston	argillaceous limestone with interbedded green shale
DGR2-519.61	Georgian Bay	argillaceous limestone with interbedded green shale
DGR2-533.94	Georgian Bay	argillaceous grey siltstone
DGR2-580.99	Georgian Bay	grey shale with siltstone layers
DGR2-586.35	Georgian Bay	greenish grey shale with limestone/siltstone interbeds
DGR2-587.51	Georgian Bay	greenish grey shale with argillaceous limestone/siltstone interbeds
DGR2-606.50	Georgian Bay	greenish grey shale with coarse grained sandstone/siltstone interbeds
DGR2-646.42	Blue Mountain	dark grey shale
DGR2-654.97	Collingwood Member, Cobourg	argillaceous grey-brown limestone
DGR2-655.32	Collingwood Member, Cobourg	argillaceous light grey-tan limestone and shale
DGR2-660.68	Cobourg	argillaceous light grey-tan limestone
DGR2-661.61	Cobourg	argillaceous light grey-tan limestone
DGR2-666.79	Cobourg	argillaceous light grey-tan limestone
DGR2-668.46	Cobourg	argillaceous light grey-tan limestone
DGR2-673.26	Cobourg	argillaceous light grey-tan limestone
DGR2-674.11	Cobourg	argillaceous light grey-tan limestone
DGR2-676.75	Cobourg	argillaceous grey limestone with thin shale stringers
DGR2-679.83	Cobourg	argillaceous grey limestone
DGR2-683.02	Cobourg	argillaceous grey limestone
DGR2-688.22	Sherman Fall	argillaceous grey limestone
DGR2-694.11	Sherman Fall	argillaceous grey limestone
DGR2-695.15	Sherman Fall	argillaceous light grey limestone
DGR2-702.69	Sherman Fall	argillaceous grey limestone with shale interbeds
DGR2-704.47	Sherman Fall	argillaceous grey limestone with shale interbeds
DGR2-710.29	Sherman Fall	argillaceous grey-tan limestone with shale interbeds
DGR2-719.38	Kirkfield	argillaceous grey limestone
DGR2-737.16	Kirkfield	argillaceous grey limestone

Note: Source data compiled and provided by Intera Engineering Limited

Table F-3. Geological formations and descriptions of DGR-2 Brazilian specimens

Specimen ID	Formation	Specimen Description
DGR2-525.92	Georgian Bay	argillaceous grey siltstone and shale
DGR2-534.22	Georgian Bay	greenish grey shale
DGR2-554.09	Georgian Bay	grey shale
DGR2-558.15	Georgian Bay	greenish grey shale with limestone/siltstone interbeds
DGR2-573.35	Georgian Bay	grey siltstone and shale
DGR2-624.81	Blue Mountain	dark grey shale
DGR2-627.12	Blue Mountain	dark grey shale
DGR2-640.41	Blue Mountain	dark grey to black shale
DGR2-643.35	Blue Mountain	dark grey to black shale
DGR2-645.60	Blue Mountain	dark grey shale
DGR2-658.78	Collingwood Member, Cobourg	argillaceous light grey limestone and shale
DGR2-670.15	Cobourg	argillaceous light grey-tan limestone
DGR2-677.37	Cobourg	argillaceous grey limestone
DGR2-688.58	Sherman Fall	mottled argillaceous grey limestone
DGR2-692.20	Sherman Fall	argillaceous grey limestone with stylolites
DGR2-696.57	Sherman Fall	argillaceous grey limestone with shale partings
DGR2-698.84	Sherman Fall	argillaceous grey limestone with shale interbeds
DGR2-703.05	Sherman Fall	argillaceous grey limestone with shale interbeds
DGR2-703.94	Sherman Fall	argillaceous grey limestone with shale interbeds
DGR2-706.98	Sherman Fall	argillaceous grey-tan limestone with shale interbeds

Note: Source data compiled and provided by Intera Engineering Limited

Table F-4. Geological formations and descriptions of DGR-2 shear specimens

Specimen ID	Formation	Specimen Description
DGR2-613.37	Blue Mountain	dark grey shale
DGR2-616.59	Blue Mountain	dark grey shale
DGR2-646.72	Blue Mountain	dark grey shale
DGR2-692.00	Sherman Fall	argillaceous grey limestone
DGR2-697.86	Sherman Fall	argillaceous grey limestone with shale interbeds
DGR2-702.23	Sherman Fall	argillaceous grey limestone with shale interbeds
DGR2-705.86	Sherman Fall	mottled bioclastic argillaceous grey limestone
DGR2-708.57	Sherman Fall	argillaceous grey-tan limestone with shale interbeds
DGR2-664.94	Cobourg	argillaceous light grey-tan limestone
DGR2-673.06	Cobourg	argillaceous light grey-tan limestone
DGR2-684.00	Cobourg	argillaceous grey limestone

Note: Source data compiled and provided by Intera Engineering Limited